THE DEVELOPMENT OF A NEW COMPACT MODEL FOR PREDICTION OF FORCED FLOW BEHAVIOUR IN LONGITUDINAL FIN HEAT SINKS WITH TIP BYPASS

by

C.B. Coetzer
9300406

Presented as partial fulfilment of the requirements for the degree of

MEng (Mechanical)

University of Pretoria
Faculty engineering
Department Mechanical Engineering

May 2000

Promoter: **Prof. J.A. Visser**

ABSTRACT

Increasing power dissipation and chip densities in the rapidly evolving electronics cooling industry are causing an ever increasing need for the tools and methods necessary for electronic systems design and optimisation. Modern electronic systems have the capacity to produce significant amounts of heat which, if not removed efficiently, could lead to component failure.

The most common technique of heat removal is by making use of a heat spreader, or so-called heat sink. These devices are excellent heat conductors with a large surface area to volume ratio, and cooled through either natural or forced convection. Despite the advantages of these devices, there are serious consequences involved in the application of heat sinks. The required size of a heat sink may limit the miniaturisation of a product, while inadequate design, due to a lack of understanding of the flow physics, may lead to premature component failure. It is therefore crucial that an optimal heat sink design is achieved for every particular application.

In the past, both heat sink design and optimisation have occurred mostly through experimental characterisation of heat sinks, which was not always particularly successful or accurate. Recent rapid developments in computer technology have led to the availability of various computational fluid dynamics or CFD software packages, with the capability of solving the discretized form of the conservation equations for mass, momentum, and energy to provide a solution of the flow and heat fields in the domain of interest. This method of using the fundamental flow physics is currently the most complete way to determine the solution to the heat sink design and optimisation problem. It does unfortunately have the drawback of being computationally expensive and excessively time consuming, with commercial software prices being financially restrictive to the average designer.

The electronics cooling community has subsequently identified the need for so-called "compact models" to assist in the design of electronic enclosures. Compact models use available empirical relations to solve the flow field around a typical heat sink. Current models require significantly less computational power and time compared to CFD analysis, but have the drawback of reduced accuracy over a wide range of heat sink geometries and Reynolds numbers. This is one of the reasons that compact modelling of heat sinks remain an international research topic today.

This study has focused on the CFD modelling of a variety of forced flow longitudinal fin heat sinks with tip clearance. Tip clearance allows the flow to bypass the heat sink and downgrade its thermal performance. The flow bypass phenomenon, general flow behaviour, and pressure loss characteristics were investigated in detail. Thermal modelling of the heat sinks was left for future study.

The flow information provided by the CFD analysis was combined with data available from literature to develop an improved compact flow model for use in a variety of practical longitudinal fin heat sinks. The new compact model leads to a 4.6 % improvement in accuracy compared to another leading compact model in the industry, and also provides more localised flow information than was previously available from compact modelling.

The study therefore contributed significantly towards the general understanding and prediction of forced flow behaviour in longitudinal fin heat sinks with tip bypass, using both CFD analysis and the compact modelling approach.

The new improved compact model may now be extended and incorporated together with the relevant flow details from the CFD analysis in a total package, solving for the flow and heat fields of forced flow longitudinal fin heat sinks. The study therefore assists in the global effort of making the confident and accurate use of compact modelling in modern electronic systems design and optimisation a practical reality.

UITTREKSEL

Moderne elektroniese stelsels het die eienskap om substansiële hitte te genereer. Hierdie hitte kan, as dit nie verwyder word nie, lei tot vroegtydige faling van elektroniese komponente.

Die mees algemene tegniek om hierdie hitte te verwyder is deur gebruik te maak van 'n sogenaamde hittesink. 'n Hittesink is 'n voorwerp met 'n groot area tot volume verhouding, en word vervaardig van goeie geleidende materiale. Die hittesink word dan verkoel deur middel van natuurlike of geforseerde konveksie. Ten spyte van die voordele van die gebruik van 'n hittesink, het dit ook verskeie nadele. 'n Te groot hittesink beperk die verkleining van die elektroniese komponent, terwyl 'n swak ontwerp as gevolg van gebrekkige begrip van die vloei gedrag tot faling mag lei. Dit is dus baie belangrik dat 'n optimale ontwerp telkens gedoen word.

In die verlede het die ontwerp en optimering van 'n hittesink meestal deur eksperimentele tegnieke plaasgevind. Met die vinnige ontwikkeling van rekenaartegnologie het die tegniek van numeriese vloei analises veral na vore getree. Numeriese analises maak gebruik van die gelyktydige oplossing van die vergelykings van massa, momentum, en energie om vloei gedrag te simuleer. Hierdie tegniek is tans die beste beskikbaar vir die besproke applikasie. Numeriese simulasie het egter die nadeel dat dit hoogs rekenaar en tyd intensief is, en die sagteware se prys plaas dit ook buite bereik van die gemiddelde ontwerper.

Die elektroniese verkoelings gemeenskap het dus die noodsaaklikheid van 'n sogenaamde kompakte model geïdentifiseer om te assisteer met die ontwerp van elektroniese stelsels. Kompakte modelle maak gebruik van beskikbare empiriese vergelykings om op te los vir die vloei en hitteveld rondom 'n tipiese hittesink. Die kompakte model is baie minder berekenings en tyds intensief, maar het probleme met akkuraatheid in die modellering van 'n verskeidenheid geometrieë en Reynoldsgetalle. Laasgenoemde is die hoofrede waarom die ontwikkeling van kompakte modelle vandag steeds internasionale aandag geniet.

Hierdie studie het gefokus op die numeriese modellering van vloei vir 'n verskeidenheid longitudinale vin hittesinke met bopunt gapings onder geforseerde konveksie toestande. Die gapings veroorsaak dat vloei verby die hittesink beweeg, en veroorsaak dus 'n degradering in die termiese eienskappe van die hittesink. Die modellering van termiese eienskappe is gelaat vir latere studie.

Die numeriese vloei resultate is gekombineer met data beskikbaar uit die praktyk, om sodoende 'n verbeterde kompakte model te skep. Die nuwe kompakte model het gelei tot 'n gemiddelde verbetering van 4.6 % in akkuraatheid in vergelyking met toonaangewende bestaande kompakte modelle, en verskaf ook aansienlik meer inligting aangaande die lokale vloeigedrag as bestaande kompakte modelle.

Hierdie studie het dus bygedra tot die algemene begrip en voorspelling van vloeigedrag in longitudinale vin hittesinke met top gapings, deur gebruik te maak van beide CFD analise en kompakte modellering.

Die verbeterde kompakte model mag nou verder uitgebrei word vir finale gebruik in 'n totale pakket vir die oplossing van vloei en hittevelde van longitudinale vin hittesinke onder geforseerde konveksie toestande. Dit sal die gebruik van kompakte modelle met vertroue 'n werklikheid maak in die ontwerp en optimering van moderne elektroniese sisteme.

ACKNOWLEDGEMENTS

The author would like to acknowledge the following persons for their valuable contributions and assistance, and without whom the study would not have been possible.

Promoter: Prof. J. A. Visser, for his time, help and assistance throughout the project.

Mr. P Gauche, for his valuable advice and help with FLOTHERM.

Mr. A.C. Loots, for allowing the time to conduct this study.

Prof. H. N. Dreyer, for his time and advice on a variety of matters during the course of the study.

Prof. S. Heyns, for his assistance in the difficulties related to part time studies.

Prof. J. L. Steyn, for the opportunity to do this project and for the use of the facilities of the University of Pretoria.

My wife Miranda, without whose patience, love, and assistance the project might never have been completed.

TABLE OF CONTENTS

CHAPTER 5: CONCLUSIONS AND RECOMMENDATIONS

NOMENCLATURE

C_d	Dimensionless pressure loss coefficient.	
$\bar{d}$	Turbulent flow length scale	[m]
D_f	Fin density.	
D_h	Hydraulic diameter.	
f	Fanning friction factor.	
g	Gravitational constant	[m/s^2]
H	Total heat sink assembly height	[m]
h	Heat sink height	[m]
H_b	Heat sink tip bypass height	[m]
h_b	Heat sink base height	[m]
h_f	Heat sink fin height	[m]
K_c	Kays contraction pressure loss coefficient.	
K_e	Kays expansion pressure loss coefficient.	
L	Heat sink length	[m]
N	Heat sink number of fins	
P	Pressure	[Pa]
ΔP_{hi}	Heat sink entrance pressure loss	[Pa]
ΔP_{he}	Heat sink exit pressure loss	[Pa]
ΔP_{hf}	Heat sink frictional pressure loss	[Pa]
ΔP_{ti}	Tip bypass entrance pressure loss	[Pa]
ΔP_{te}	Tip bypass exit pressure loss	[Pa]
ΔP_{tf}	Tip bypass frictional pressure loss	[Pa]
ΔP_{hs}	Blunt body entrance pressure loss	[Pa]
ΔP_{hb}	Blunt body exit pressure loss	[Pa]
P_0	Freestream pressure	[Pa]
Q_h	Heat sink average volume flow	[m^3/s]
Q_l	Lateral bypass average volume flow	[m^3/s]
Q_t	Tip bypass average volume flow	[m^3/s]
R	Thermal resistance.	
Rjc	Junction to case thermal resistance.	
Rcs	Case to sink thermal resistance.	
Rsa	Sink to ambient thermal resistance.	
Re	Reynolds number.	
s	Heat sink interfin space	[m]
S_h	Blockage ratio.	
t	Heat sink fin thickness	[m]
$\bar{u}$	Turbulent flow velocity scale	[m/s]
U_h	Heat sink average interfin velocity	[m/s]
U_l	Average lateral bypass velocity	[m/s]
U_{lk}	Heat sink leakage velocity	[m/s]
U_0	Channel freestream velocity	[m/s]
U_t	Average tip bypass velocity	[m/s]
W_h	Heat sink width	[m]
W_l	Lateral bypass width	[m]
x	General progressive distance	[m]

GREEK SYMBOLS

ρ	Density of air	[kg/m^3]
μ	Static viscosity of air	[kg/m s]
τ	Shear force	[Pa]

SUBSCRIPTS

b	Bypass
e	Exit
f	Friction losses
h	Heat sink section
i	Entrance
l	Lateral bypass section
lam	Laminar flow
O	Freestream or bulk value
t	Tip bypass section
turb	Turbulent flow

ABBREVIATIONS

CFD	Computational fluid dynamics
U.P.	University Pretoria

Chapter 1

INTRODUCTION

1.1 THE PROBLEM CONSIDERED

The trend in modern electronic systems design is to increase the speed and power of processing, while at the same time reducing the size and weight of the electronic device [1]. The electronic systems can however produce a significant amount of heat, which may cause failures due to overheating of the individual components if no steps are taken to prevent excessive temperatures [2]. One way of achieving this, is by utilising a forced flow heat sink, which operates as a convection device with small outer dimensions but large surface area, in order to promote convective heat transfer. The continuous increase in power dissipation from electronic systems is currently driving many systems to the limit of heat removal capacity. Therefore, the heat removal capacity of cooling air should be utilised to its fullest extent and must be expanded through design optimisation [3].

In the quest for the design of an optimal heat sink for a given electronic enclosure, it is necessary to accurately and efficiently determine the thermal and flow characteristics of the heat sink. This is no trivial exercise, as there are a huge amount of variables to be considered. This is one of the reasons why heat sink characterisation and performance optimisation remain an international research topic today.

In the past, experimental methods were mostly used for the characterisation of forced flow heat sinks [4]. The experimental results were used to develop design graphs for typical heat sinks. These graphs were unfortunately limited in application since they were only applicable to geometrically similar devices [5].

Rapid developments in modern computer technology have resulted in the use of three-dimensional numerical solutions to these complex heat sink characterisation problems. Computerised fluid dynamics or CFD analysis provides a cost effective alternative to experimental investigation, and allows for both analysis and optimisation of the variables in question [6,7]. Although CFD analysis has proven to be very accurate in this application, it can be extremely time consuming, with expensive computer hardware and occasional mainframe access necessary. The cost implications of the software necessary for these solutions can also be financially restrictive, with the result that CFD analysis is not always readily available to the average designer.

The electronics cooling industry has subsequently identified the need for lumped parameter models, which have been termed "compact models" in order to assist in the thermal design of electronic enclosures [8]. These models should be readily usable on a standard personal computer, they should neither be excessively time consuming nor should it be necessary to purchase overly expensive software. It should also allow the user to determine both flow and thermal characterisation of the heat sink in question with reasonable accuracy. It should finally provide a very real alternative to CFD simulation, especially in system level analysis where large computational requirements are necessary.

This thesis will contribute towards the development of such a compact model for heat sink analysis in practical electronic enclosures.

1.2 BACKGROUND

There are a wide variety of different heat sink configurations in existence today. Geometries vary from pin fins and stacked fin arrays to the more conventional longitudinal fin heat sink arrangement [9]. As only longitudinal fin heat sinks will be studied in this document, only the background on longitudinal fin heat sinks will be considered here, although many of the flow and thermal characteristics discussed are equally relevant to other configurations. More detail on other heat sink configurations may be found in the literature review of section 1.3, and available literature from Lee [10], and Chapman [9].

The two ways in which cooling of electronic enclosures utilising heat sinks may be achieved are the following:

- Natural convection.
- Forced convection.

In the instance of natural convection, the flow of air is buoyancy driven due to density differences arising from the heat transfer from the heat sink to the air [11]. The internal design and layout of the PCB's play an important role in this type of cooling [12]. In the case of forced convection, the air is forced through the heat sink using a fan. Forced convection is obviously the more efficient cooling method, at the expense of adding an additional cooling fan to the electronic enclosure. Only forced flow heat sinks will be discussed in this document.

There are several geometric variables associated with a forced convection longitudinal fin heat sink, as depicted in figure 1.1. Each of these variables influences the flow and heat transfer characteristics in a different manner. The cooling performance of the heat sink therefore depends on the entire combination of the variables in question [8].

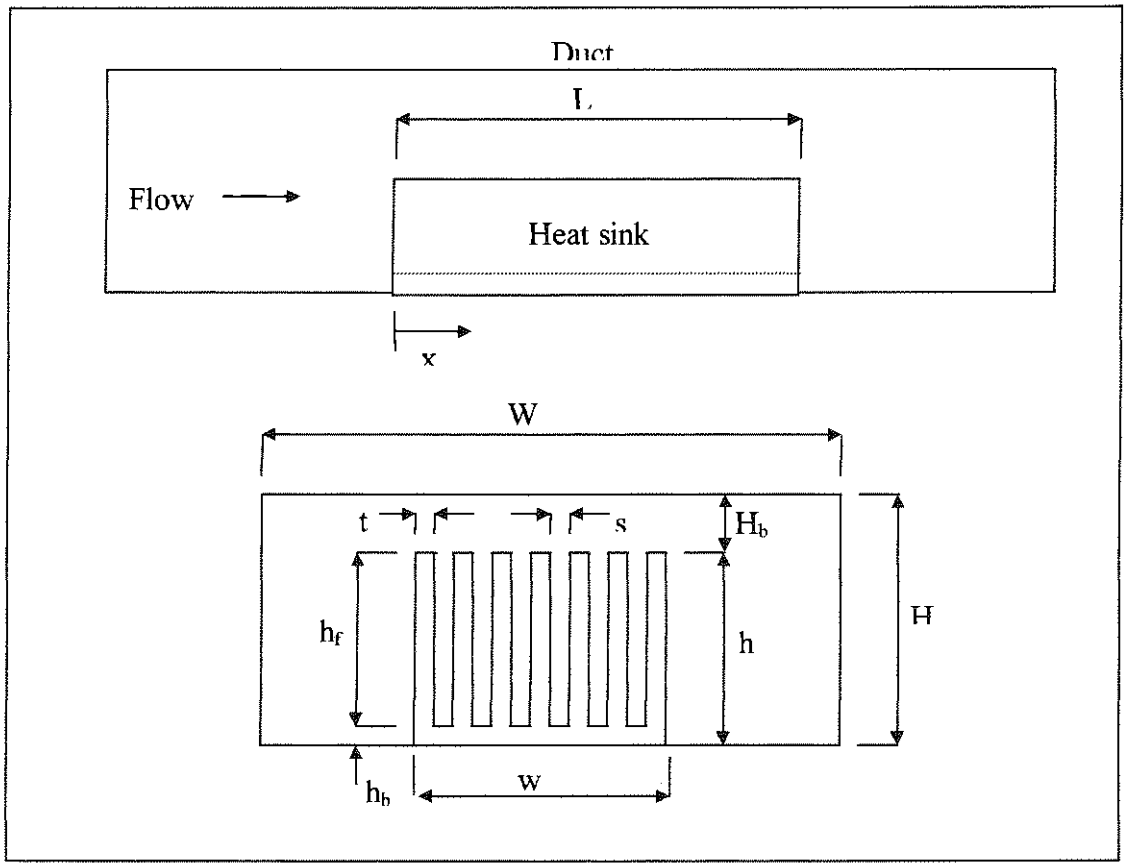

Figure 1.1 Ducted longitudinal fin heat sink geometry.

Briefly summarised the geometric variables are:

- W : Channel width.
- H : Channel height.
- L : Heat sink length.
- t : Fin thickness.
- s : Fin gap.
- h : Heat sink height.
- w : Heat sink width.
- h_f : Fin height.
- h_b : Base height.
- H_b : Bypass height.
- N : Number of fins.

The blockage ratio of the channel heat sink assembly is defined as

$$S_h = \frac{wh_f}{WH} \qquad [1.1]$$

and is a function of the fin height, gap, thickness, and tip bypass height.

Prior to the investigation of flow and thermal details, it is first necessary to provide an idea of the global flow and thermal effects occurring inside a typical forced flow longitudinal fin heat sink with tip and lateral bypass. Figure 1.2 serves as a simple model to illustrate the various flow effects which may be encountered.

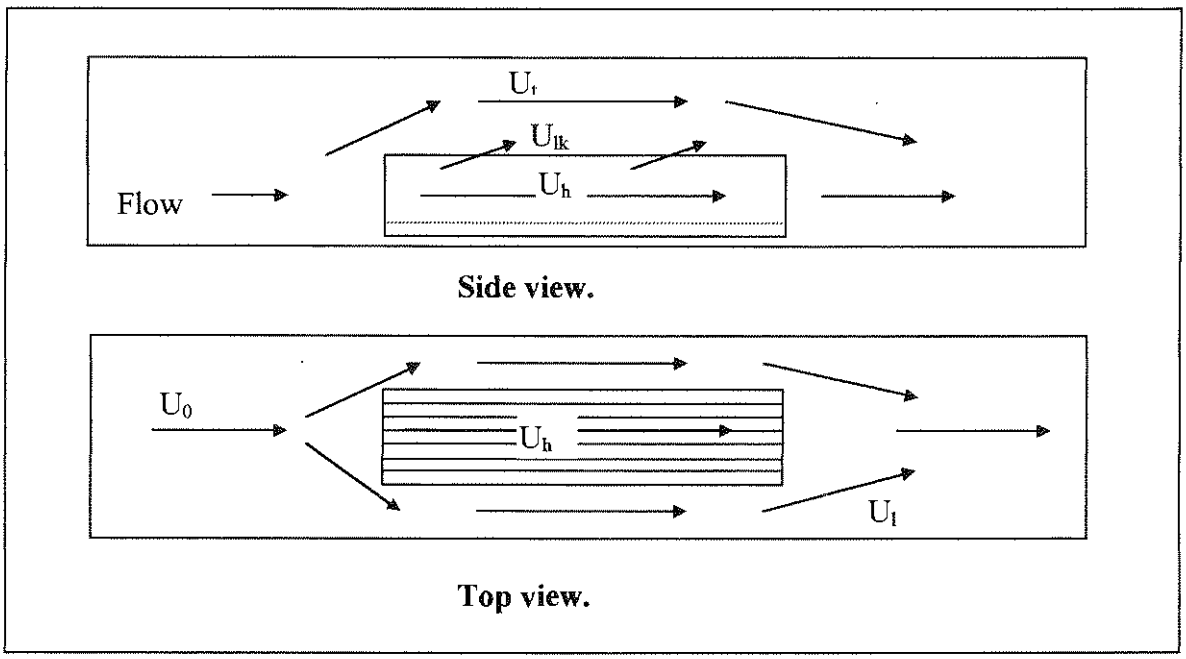

Figure 1.2 Flow characterisation.

The symbols are summarised as below:

- U_0 : Free stream approach velocity.
- U_t : Tip bypass velocity.
- U_h : Heat sink inter fin velocity.
- U_l : Lateral bypass velocity.
- U_{lk} : Leakage velocity.

It is clear that the flow pattern is fairly complex. The air approaches the heat sink with a certain freestream approach velocity *Uo*. When the heat sink is encountered, some of the flow enters the heat sink (U_h), while large amounts of flow tend to bypass the heat sink over the top (U_t) and sides (U_l). Along the length of the heat sink a certain amount of flow also leaks from the heat sink to join the bypassing flow at the tip [8], and is named the leakage velocity component U_{lk}. It is clear that lateral bypass is merely a simplified version of tip bypass, with the leakage velocity component not being present.

The heat sink Reynolds number is given by the following equation [8, 11]:

$$\mathrm{Re} = \frac{\rho U_o d_h}{\mu} \text{ , with } d_h = 2s \qquad [1.2]$$

The main effect of the flow bypass phenomenon is reduced heat transfer and pressure loss through the heat sink, which can cause failures due to overheating if not anticipated [14]. Therefore the accurate prediction of the velocity distribution and the effects of flow bypass on heat transfer is crucial for the design and optimisation of a heat sink assembly.

The heat transfer from the heat sink assembly to the surrounding atmosphere may be illustrated through the calculation of a series of thermal resistances, including conductive, radiative, and convective resistances [11]. The heat transfer scenario is depicted schematically in figure 1.3.

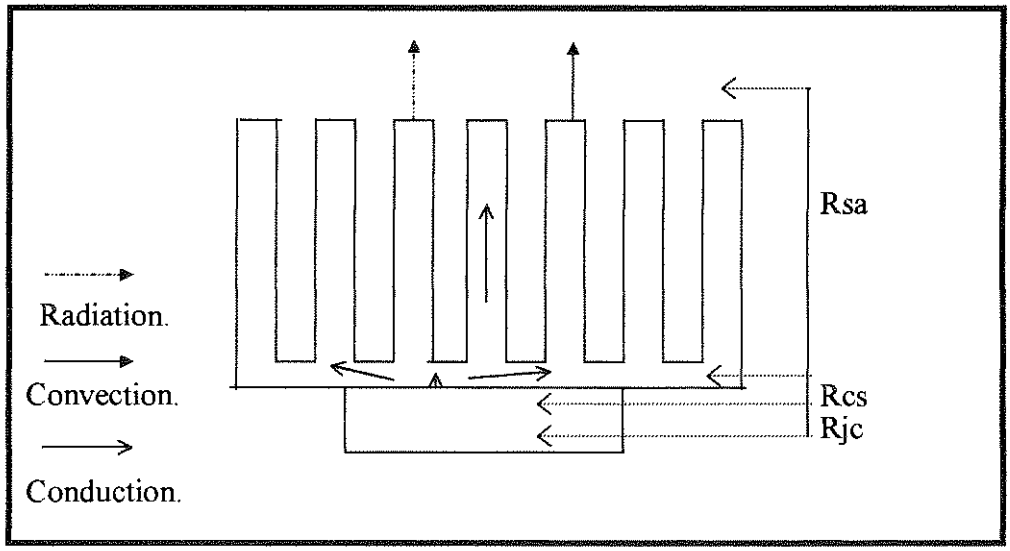

Figure 1.3 Thermal resistance circuit and modes of heat transfer.

The resistances are summarised as follows:

- Rjc: Junction to case resistance.
- Rcs: Case to sink resistance
- Rsa: Sink to ambient resistance, including the effects of conduction, convection, and radiation.

Rcs is a function of the bonding agents and methods used to join the heat sink and case, for which various methods exists [14]. The overall thermal performance can be measured by the total thermal resistance, which comprises of:

$$R_{total} = Rjc + Rcs + Rsa. \qquad [1.3]$$

The thermal resistance is defined by the temperature between two points and the rate of heat dissipation *(Q)*, such that:

$$R = \frac{\Delta T}{Q} \qquad [1.4]$$

The conductive resistance exists in three-dimensions, and is reasonably simple to calculate accurately once the convective boundary conditions to the conductive differential equations are known [15]. It is the prediction of the convective heat transfer boundary conditions, which are a function of the local velocity distribution, that is difficult to determine. The two main methods currently used to solve for the velocity and pressure distribution are CFD analysis and compact modelling.

CFD analysis consists of the solution of the three-dimensional Navier-Stokes equations for viscous fluid flow [16], which can be time consuming and hardware demanding to say the least. Results provide detailed flow and pressure characteristics information, where both local variations and global trends may be observed. The use of CFD analysis for heat sink modelling and design has proved to be the most complete method of prediction for this application to date [6,17]. The CFD analysis may also be extended to incorporate the thermal solution without undue effort through solution of the energy equation [15].

The flow and pressure characteristics may also be predicted using a suitable compact model [8], which uses analytical and empirical relations to predict pressure loss and velocity distributions. The empirical flow characterisation solutions are much easier and quicker to solve than the partial differential equations of CFD analysis, but do not provide the same degree of flow detail, and are not normally as accurate. Once the flow and pressure details are known, it may be used to calculate the convective heat transfer coefficients to be used in the thermal analysis of the heat sink in question. The complete compact model solver will therefore consist of an analytical flow solver, and a numerical conduction solver using the flow results to determine convective heat transfer resistances [11].

The role of the compact model is particularly important in the conceptual stages of the design process due to its inherent simplicity and quick modelling cycle. Parametric studies using compact modelling can quickly quantify design trade-offs, and help to demonstrate the feasibility of a particular design. CFD analysis becomes important once options are narrowed down or more complex designs evolve. Finally some prototype testing may be used to confirm final results [18]. The product development cycle and the role compact modelling plays in it may best be illustrated schematically in figure 1.4 [18].

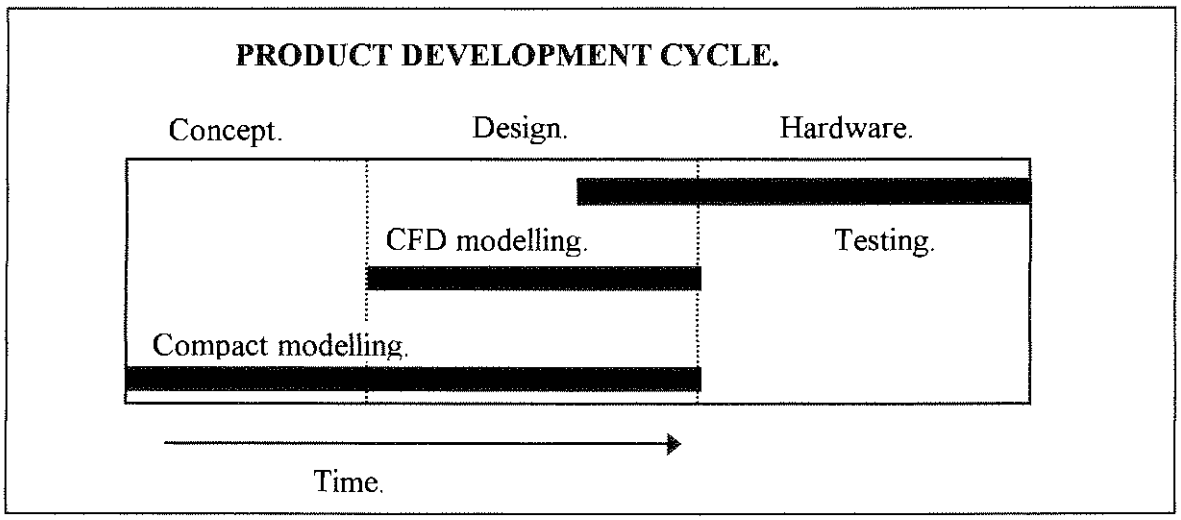

Figure 1.4 Compact modelling in the product development cycle.

Several compact models are already in existence in the industry today, with varying degrees of success. Current models unfortunately battle with constant accurate predictions over a wide range of heat sink geometries and Reynolds numbers.

The compact model used extensively in this study for comparative purposes is part of a program called QFIN, which includes a flow compact model created by the University of Pretoria [11], and based on the basic Butterbaugh and Kang flow compact model [8] with some improvements. The QFIN compact model however needs some improvement in specific regions, which is one of the objectives of this study.

1.3 LITERATURE REVIEW

Air cooling through the use of extended surfaces like heat sinks has always been an attractive technique for removing excess heat from electronic enclosures, mostly due to their inherent simplicity and cost effectiveness. An extensive literature survey has shown an ever increasing interest and application of this cooling strategy in practice [4], and as such the topic is currently researched extensively, both in South Africa and abroad. Where experimental work once used to dominate the field of electronics cooling [19], the viability and accuracy of both CFD and compact modelling of the heat sinks in question are now enjoying specific attention, with good results in most instances [4, 17].

As mentioned in section 1.2, there are two main different cooling methods in existence for heat sinks in electronic enclosures, namely natural and forced convection. Both vary in approach and effectiveness with its own advantages and disadvantages, with both having been investigated extensively in literature.

Several studies have investigated the phenomenon of natural convection in heat sinks. Natural convection is driven by buoyancy forces arising from density differences due to the heated fluid, much as in the case of natural draft cooling towers [11]. Visser and Gauche [11] have utilised the empirical correlations of Van de Pol and Tierny for vertical U-channel geometries in order to predict natural convection behaviour with good results, varying on average less than 6.2 % from experimental values. Morrison [20] has specifically focused on the optimisation of heat sink fin geometries for heat sinks in natural convection, utilising the methods used in conventional heat sink analysis [11]. His proposed algorithm hunts for the lowest temperature performance of a user specified range of fin geometries.

Forced convection in heat sinks has also enjoyed a lot of research attention, with studies focusing on actual heat sink geometries, selection, and optimisation, as well as the accurate modelling and characterisation of certain types of heat sinks utilising CFD or compact model methods.

The study of Gavali and Patankar [3], was one of the first to conduct numerical studies on heat sinks in electronic systems. The study was conducted using a CFD model to predict flow and heat transfer over a series of heat generating blocks with a thermally inactive heat sink on the wall of a rectangular duct. Specifically the effects of flow modification resulting from a heat sink present inside an electronic enclosure were determined. It was found that the heat transfer from components downstream of the heat sink may either increase or decrease depending on the flow conditions and geometry of the actual heat sink used.

Linton [21], shortly after Gavali and Patankar [3], applied CFD modelling on finned heat sinks. Results from a detail CFD model were compared to experimental results with good agreement, after which a coarse CFD model was developed for use in system level analysis. The coarse CFD model provided less flow and thermal detail, but resulted in less calculation time, which made it very useful for systems analysis. Agreement of results was reasonably good all round. The study was later extended to include the simulation of electronic enclosures [22], thus extending the CFD modelling capabilities. The flow and temperature within a typical desktop computer were also modelled to show the application of the model to a real life problem.

Obinelo [2], used CFD models to characterise the thermal and hydraulic performance of heat sinks for system level analysis. Specific attention was paid to the phenomenon of flow bypass. He used a finite difference thermal solver for solid conduction in conjunction with a finite volume control volume based flow solver to analyse the coupled conductive/convective problem. The flow solver uses near wall momentum wall functions and the thermal log law wall function [16] to approximate near wall flow and heat transfer. He also derived a fairly complicated reduced-parameter model using simplified CFD relations. The model was derived from detailed component level analysis of several heat sinks installed with different tip and lateral clearances, and delivers reasonable results

when compared to practice. The model however still requires some CFD modelling, but speeds up the iterative process through using simplified combined parameters.

Gopalakrishna [6] investigated the flow bypass phenomenon of forced flow convection in longitudinal fin heat sinks both experimentally and numerically, and used experimental results in order to verify the numerical simulations. He simulated both laminar and turbulent flows. Gopalakrishna uses the finite difference solver FLOTHERM as the numerical simulation package. FLOTHERM employs a simple algebraic mixing length model to simulate turbulent flow [16]. The code also assumes universal logarithmic velocity and temperature profiles near the wall. An input characteristic length and velocity is required for the turbulent model. Gopalakrishna suggests that the following values may be used with good results.

$$\bar{u} = Uo$$
$$\bar{d} = D_h = 2s. \qquad [1.5]$$

where

$\bar{u}$ = Turbulent velocity scale in m/s

and

$\bar{d}$ = Turbulent length scale in meters.

His results show that grid independent solutions are achieved even with relatively coarse grids, which make the simulations much faster than could be expected from normal CFD analysis. His results also show exceptionally good agreement between predicted and measured data for both laminar and turbulent flows, and serve to verify the use of FLOTHERM as a CFD package for the accurate prediction of heat sink performance in practice.

Biber [17] did extensive work on the use of CFD analysis for heat sink design and selection. All design steps are outlined from start to finish, with positive comments regarding the accuracy of CFD predictions in practice. It is also stressed that although CFD analysis provides very useful tools for heat sink modelling, the final prototype heat sink still has to be tested experimentally in order to finally verify CFD results. Differences between the CFD model and practice are to be expected, due to errors both inherent in experimental measurement and modelling. The importance of modelling the surrounding system accurately if good CFD results are to be obtained is also mentioned. According to Biber the representation of model trends using CFD results should also assist in reducing the total design cycle time.

Lee [10] was one of the first to investigate the effect of flow bypass during forced flow in longitudinal fin heat sinks, using a very simple compact model approach. He first covers a general discussion on various types and designs of heat sinks, including relative costing of the different heat sinks. Part two of his work derives an analytical flow prediction model to include the effects of tip and lateral bypass on the flow behaviour in longitudinal fin heat sinks. He formulated basic equations using the average interfin velocity to balance mass

and momentum equations over the heat sink control volumes. Heat sink entrance and exit losses are estimated using the results of Kays [23]. He uses the following equation to solve iteratively for the average heat sink interfin velocity:

$$(2a_f - 1)U_h^2 - 2a_f U_h + 1 = (1 - a_f)^2 \frac{\Delta P_f}{\rho U_d^2 / 2} = 0 \qquad [1.6]$$

where

$$a_f = (w.h) / (W.H) \qquad [1.7]$$

U_f = Normalised fin velocity

and

ΔP_f = Friction pressure losses.

ΔP_f is obtained through interpolation from available friction charts for parallel plate flows. His results compared reasonably good to measured values, and his approach to bypass modelling formed the basis for future trends.

Biber and Belady [18] investigated different empirical relations for laminar flow in forced flow heat sinks in order to find the best analytical relation. CFD simulations using FLOTHERM were also done in order to obtain a better understanding of the flow characteristics. An experimental set-up was used for testing the empirical model. Only laminar flows were investigated, and the effects of flow bypass were eliminated by allowing virtually no gaps between the heat sink and the channel. The effect of using developing and semi-developed flow empirical relations as compared to fully developed flow empirical relations was also investigated for a range of heat sinks. The results indicated that the fully developed flow correlations tended to provide the best results, while the semi-developed and developing flow models tended to overpredict the pressure loss. The results of the CFD model, as well as the fully developed flow correlation empirical model, showed good correlation with measured experimental values.

Wirtz et al [13] experimentally studied the effect of flow bypass on longitudinal fin heat sinks in a regular array of packages. These results showed that flow bypass significantly reduces the heat transfer from the heat sink. Wirtz found that up to 60 % of the flow in the test set-up tended to bypass the heat sink, with a 50 % reduction in heat sink thermal performance. Wirtz also provides a correlation between the flow bypass ratio, and the approach velocity as a function of the free stream Reynolds number, based on the fin density which is defined as the fin frontal area divided by the total duct area.

$$Df = \frac{Nt}{W} \qquad [1.8]$$

A series of studies conducted separately from the heat sink design application were also used in a number of the compact models to be discussed later in this review. Only two of the most important are mentioned here. Kays [23] experimentally investigated mainly compact heat exchangers, but in the process developed a series of relations for loss coefficients due to abrupt changes in flow cross section. Lessman [26] calculated pressure loss coefficients due to flow over a blunt body. Both the relations of Kays [23] and Lessman [26] are used extensively today for the analytical prediction of pressure losses in heat sinks.

Johnson [24], has focused on the modelling of thermal and hydraulic performance of plate fin, strip fin, and pin fin heat sink geometries. The effects of flow bypass on heat sink performance was investigated in detail using empirical correlations based on the Butterbaugh and Kang resistance network principle [8] with reasonable results.

Similarly, Chu and Belady [25] conducted a survey of various high performance, high aspect ratio, air cooled heat sinks. Specifically the performance of commercially available heat sink technologies was investigated, and provided an overview of the advantages and disadvantages inherent to individual heat sink geometries.

Butterbaugh and Kang [8] investigated the flow bypass phenomenon in high blockage ratio heat sinks both experimentally and using a compact model. To date this is probably one of the most significant studies conducted on compact modelling in longitudinal fin heat sinks with tip and lateral bypass. Only laminar flows were however investigated, with the turbulent flow extension left for future studies. A realistic model for the analytical flow solution was created, where a set of resistances in series and parallel are used to represent the pressure loss through the ducted section with the heat sink under tip and lateral bypass as depicted in figure 1.5.

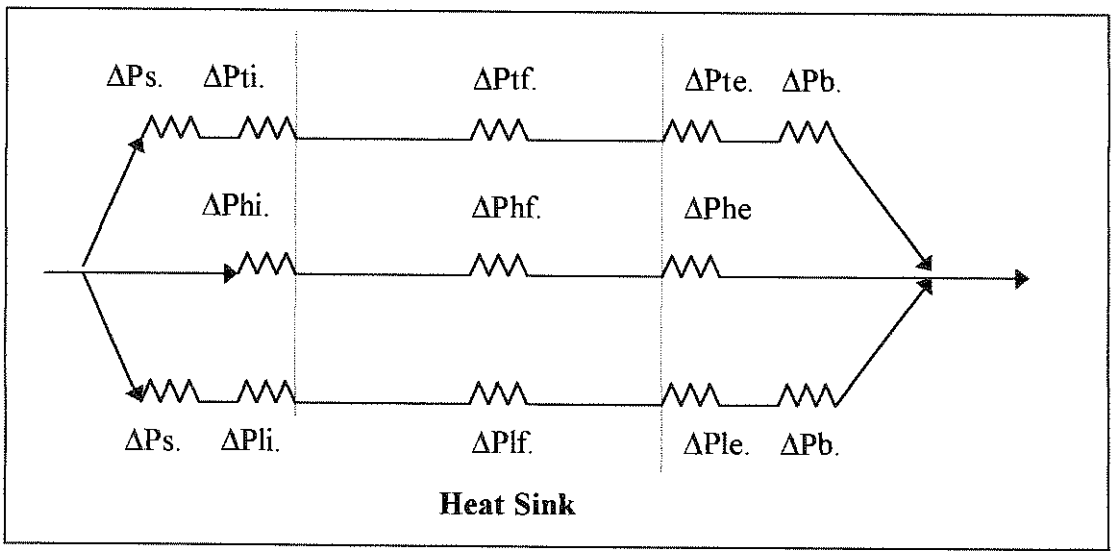

Figure 1.5 Parallel resistance network approach.

The heat sink is divided into three main flow paths, namely the heat sink path, the tip bypass path, and the lateral bypass path. The pressure loss through each of these paths is given by the following series of equations. (The subscripts note the various different locations and type of loss in the heat sink and are further described in the nomenclature):

$$\begin{aligned}\Delta P_{hs} &= \Delta P_{hi} + \Delta P_{hf} + \Delta P_{he} \\ \Delta P_t &= \Delta P_s + \Delta P_{ti} + \Delta P_{tf} + \Delta P_{te} + \Delta P_b \\ \Delta P_l &= \Delta P_s + \Delta P_{li} + \Delta P_{lf} + \Delta P_{le} + \Delta P_b\end{aligned} \quad [1.9]$$

where

$$\Delta P_i = (0.8 + 0.04\sigma - 0.44\sigma^2).\frac{1}{2}\rho U^2 \quad [1.10]$$

and

$$\Delta P_e = (1 - 1.84\sigma + 0.44\sigma^2).\frac{1}{2}\rho U^2, \text{ according to the relations of Kays [23]} \quad [1.11]$$

The contraction ratio's are calculated as below:

$$\sigma_l = \frac{U_0}{U_l}, \qquad \sigma_t = \frac{U_0}{U_t}, \qquad \sigma_h = \frac{s}{s+t} \quad [1.12]$$

The frictional pressure loss is calculated as follows:

$$\Delta P_f = (f.\frac{L}{d_h}) * \frac{1}{2}\rho U^2 \quad [1.13]$$

where the friction factor for developing flow is:

$$f = \frac{1}{\mathrm{Re}}\left(3.44x_p^{-0.5} + \frac{24 + 0.674x_p^{-1} - 3.44x_p^{-0.5}}{1 + 0.00029x_p^{-2}}\right) \quad [1.14]$$

where

$$x_p = \frac{L}{\mathrm{Re}\,d_h} \quad [1.15]$$

and

$$\mathrm{Re} = \frac{\rho U d_h}{\mu} \quad [1.16]$$

The parallel plate flow hydraulic diameter relation was used throughout for the heat sink and bypass regions [27] (see equation 1.2).

The additional pressure loss terms in the bypass sections were determined using the following equations deducted from Lessman [26], and independent CFD modelling of fluid flow over blunt bodies [8].

$$\Delta P_s = 0.8\frac{\rho}{2}\left(U^2 - U_{hs}{}^2\right) \qquad [1.17]$$

$$\Delta P_b = C_d\frac{\rho}{2}\left(U^2 - U_{hs}{}^2\right) \qquad [1.18]$$

with

$C_d = 0.2$ for tip or lateral bypass, and 0.1 for combined bypass.

The above equations are then solved iteratively for the heat sink fin, tip, and lateral bypass velocities using the following equations for closure:

Pressure balance:

$$\Delta P_h = \Delta P_t = \Delta P_l \qquad [1.19].$$

and continuity:

$$Q_h + Q_t + Q_l = Q_{total} \qquad [1.20].$$

This solution provides the heat sink total pressure loss, average interfin, and bypass flow velocities. Once the flow solution has been obtained the convective heat transfer coefficients may be determined, and the conductive heat transfer problem solved numerically as discussed earlier.

It was also confirmed during the course of the study [8], that the thermal resistance correlates directly with the pressure loss, regardless of the amount of bypass, as could indeed be expected. The predicted results using the compact model showed very good agreement with measured experimental values. In general the Butterbaugh and Kang compact is viewed as one of the leading compact models in the field today [11].

The Butterbaugh and Kang model unfortunately has several shortcomings and inherent inaccuracies in the modelling approach:

- It does not model turbulent flow.
- The model is highly inaccurate where low blockage ratio heat sinks are concerned.
- The model uses average regional velocities to calculate inlet and exit pressure losses, instead of local values. This leads to inherent inaccuracies where large bypass ratio heat sinks are considered.
- The model uses parallel plate frictional relationships when it is not strictly correct to do so.

Visser and Gauche [11], as well as Gauche and Coetzer [1] proposed a compact model similar in approach to Butterbaugh and Kang [8], but using some improved empirical relations for entrance and exit pressure losses, also adapted from Kays [23]. The model was also extended to include turbulent flow.

The laminar and turbulent entrance and exit losses are given by the following equations:

$$\Delta P_i = K_i \cdot \frac{1}{2} \rho U^2 \qquad [1.21]$$

$$\Delta P_e = K_{ei} \cdot \frac{1}{2} \rho U^2 \qquad [1.22]$$

The entrance and exit loss coefficients are adapted from Kays [23] for laminar and turbulent flows and are given by the following equations:

Laminar flow:

$$K_i = -0.41\sigma^2 + 0.02\sigma + 0.4 \qquad [1.23]$$

$$K_e = 1.0\sigma^2 - 2\sigma + 1.0 \qquad [1.24]$$

Turbulent flow:

$$K_i = -0.41\sigma^2 + 0.02\sigma + 0.8 \qquad [1.25]$$

$$K_e = 1.0\sigma^2 - 2.4\sigma + 1.0 \qquad [1.26]$$

with σ as per equation [1.12], and with transition from laminar to turbulent flow taken at $Re = 2300$.

Predictions from the Visser and Gauche [11] model were compared to the experimental measurements from Butterbaugh and Kang, as well as to predictions from the Butterbaugh and Kang compact model [8]. Results indicated some improvement compared to the Butterbaugh and Kang model, but with the same limitations as stated above, except for the inclusion of turbulent flow in the model. The model has subsequently been incorporated into a combined flow and thermal solver with the name of QFIN, and is used extensively in practice. Results from this study will also be compared to flow results from QFIN for comparative purposes.

Gauche and Coetzer [1] made a number of important observations regarding the detail flow behaviour in longitudinal fin heat sinks with tip bypass using both CFD and compact modelling. The most important of these are:

- Good collapsibility of normalised velocity data.
- Details of longitudinal, tip, and leakage velocity profiles using CFD modelling.
- Accuracy of the QFIN compact model in high blockage ratio heat sinks.
- Accuracy and quality of information of CFD modelling for longitudinal fin heat sinks with tip bypass.

Although not particularly applicable to this study, a number of studies have been conducted on various heat sink geometries and optimisation. Chapman [9] for instance, has done extensive work on the thermal performance of elliptical pin fin heat sinks. Lee [10; 28], has defined a selection process in order to select the optimal type of heat sink geometry for a specific application, varying the range from simple stampings to complex ducted extrusions and pin fin arrangements. Knight and Gooding have conducted both analytical [29], and experimental studies [5], in order to optimise the thermal design of air cooled forced flow heat sinks. Analytical results have proved to be reasonably accurate when compared to experimental values.

1.4 NEED FOR THIS STUDY

As is evident from the literature review, the field of electronics cooling is truly an international research topic. Much work has already been done in terms of experimental investigations [5], CFD analysis [6, 17], and compact modelling of heat sinks [8, 11]. The literature study has similarly indicated that while the thermal behaviour of heat sinks is reasonably straightforward to determine once the flow details are known, it is in the understanding and prediction of the flow behaviour using the compact modelling approach that current discrepancies in practice exists.

It is therefore clear that there remains much to be done in order to fully comprehend and accurately predict forced flow behaviour in longitudinal fin heat sinks, using both CFD analysis and the compact model approach. Current compact models all have certain modelling constraints and limitations in accuracy, while detailed flow behaviour and characterisation using CFD analysis have also not been fully investigated and documented as yet.

This thesis will therefore aim to contribute towards the understanding and prediction of forced flow behaviour in longitudinal fin heat sinks with tip bypass using both CFD analysis and compact modelling.

The proposed contribution will therefore be on the following main fronts:

- To provide an understanding of laminar and turbulent flow behaviour in ducted forced flow longitudinal fin heat sinks with tip bypass using CFD analysis. Both local variations and global trends will be observed.

- To determine the influence of geometric parameter variations on the flow behaviour in ducted forced flow longitudinal fin heat sinks with tip bypass using CFD modelling.

- The development of an improved compact flow model for both laminar and turbulent flows in ducted forced flow longitudinal fin heat sinks with tip bypass. This model should address the discrepancies in current leading models as discussed in section 1.3, and should be able to accurately predict the flow behaviour over a wide selection of heat sink geometries and Reynolds numbers.

The effects of lateral and combined bypass on forced flow behaviour, the study of heat transfer, and the instance of natural convection will be left for future research.

1.5 OUTLINE AND STRATEGY OF THIS STUDY

It will be the strategy of this dissertation to use CFD simulations of typical ducted forced flow longitudinal fin heat sinks with tip bypass to gain an in depth understanding of the flow characteristics and behaviour in such heat sinks. The CFD results will be verified by means of published experimental data and available literature, and will be used extensively in the development of an improved compact flow model for the analytical prediction of flow behaviour in such heat sinks. Results of the new compact model will be compared to both CFD results and results from other leading compact models in the industry in order to gauge performance. In specific the compact model of QFIN, outlined in section 1.3, will be utilised extensively for this purpose.

The thesis will follow the following outline:

In chapter two, relevant theory regarding the CFD analysis of longitudinal fin heat sinks will be provided. Modelling strategy, grid considerations, and any assumptions will also be discussed in detail. The computer package FLOTHERM from FLOMERICS will be used throughout for the CFD simulations.

Chapter three will entail a thorough discussion of the CFD results over a wide range of heat sink geometries. The influence of geometric parameter variations will also be included. Where possible the CFD results will also be compared to experimental results obtained from literature.

Chapter four will entail the derivation and implementation of a new compact model, where all assumptions and empirical correlations necessary will be discussed in more detail. Chapter four will also evaluate the accuracy of both the QFIN compact flow model and the proposed new compact model by comparing results to verified CFD results from FLOTHERM.

Chapter five will contain a synopsis, together with the main conclusions reached during the course of this study. Recommendations for future investigations of this nature are also provided.

Chapter 2

CFD MODELLING OF LONGITUDINAL FIN HEAT SINKS

2.1 PREAMBLE

Three-dimensional numerical simulations or CFD modelling as used during the course of this study is based on the simultaneous solution of the momentum equations, the continuity equation, and in the case where heat transfer is applicable, the energy equation [34,35].

From the literature review pertaining this study, it was determined that FLOTHERM by FLOMERICS can be considered one of the leading CFD computer packages in the field of modern electronics cooling [18]. As a result, FLOTHERM is also used extensively throughout this study for CFD analysis of forced flow in longitudinal fin heat sinks with tip bypass.

FLOTHERM employs a control-volume-based finite difference model in order to solve the Navier-Stokes equations for flow and the energy equation for heat transfer [32]. For turbulent flow, a simple algebraic mixing length model is used [16], while wall functions [16, 33] are used throughout in order to predict near wall flow behaviour without having excessively fine grids.

In this chapter, the relevant theory and assumptions used by FLOTHERM, as well as the modelling strategy, grid details, and data reduction process will be discussed. The test matrix range of heat sinks to be modelled will also be mentioned as part of the modelling strategy.

Analysis and discussion of CFD results will be presented in chapter 3.

2.2 RELEVANT THEORY

2.2.1 Governing equations

In the numerical simulation of flow and heat transfer, FLOTHERM makes use of the following partial differential equations that must be solved simultaneously [15]:

- The continuity equation.
- Momentum equations in each of the three directions (x, y, z).
- Turbulence equations, if turbulent flow is present.
- Energy equation.

In this study, only the first three of the above mentioned series of equations are being used for the solution of the flow details, and therefore only these three equations will be discussed. The energy equation is only a simple extension of the flow equations, and is discussed in more detail in a number of references [30; 31].

The continuity equation can be written in general form as:

$$\frac{\partial \rho}{\partial t} + \overline{\nabla}.\left(\rho \bar{v}\right) = 0 \qquad [2.1]$$

The momentum equations for laminar flow are known as the Navier-Stokes equations and can be written in general form as:

$$\frac{\partial}{\partial t}\left(\rho \bar{v}\right) + \left(\overline{\nabla}.\rho \overline{vv}\right) = -\overline{\nabla}P + \left(\overline{\nabla}.\tau\right) \qquad [2.2]$$

The shear force term on the right hand side may also be represented by a constant viscosity μ, multiplied with the velocity gradient for Newtonian flow with constant viscosity [16].

The flow is however not necessarily laminar, but may also be turbulent in nature. This makes it necessary to adapt the classical Navier-Stokes equations in order to simulate the flow accurately. The adapted equations may be written as follows:

$$\frac{\partial}{\partial t}\left(\rho \bar{v}\right) + \left(\overline{\nabla}.\rho \overline{vv}\right) = -\overline{\nabla}P + \left(\overline{\nabla}.\tau\right) + \left(\overline{\nabla}.\tau_t\right) \qquad [2.3]$$

The additional shear force term on the right hand side is modelled as a turbulent viscosity (μ_t) multiplied with the velocity gradient. This is an additional variable which has to be calculated, with the result that there are more variables than equations, and an extra equation has to be found. This extra equation is commonly known as a turbulence closure model [15]. FLOTHERM uses a simple algebraic algorithm known as the mixing length theory as this added equation. More complex and accurate turbulence closure models like the κ-ε model [33] are also available, but is unnecessarily complicated for this particular application. The mixing length theory uses the following equation to calculate the turbulent viscosity:

$$\mu_t = 0.01\rho \overline{vd} \qquad [2.4]$$

The code also assumes universal logarithmic velocity and temperature profiles near the walls. This reduces the need for very fine grids near walls, and therefore significantly decreases computational time [32].

Gopalakrishna [6] suggests that the following values for $\bar{v}$ and $\bar{d}$ may be used with good results:

$$\bar{u} = Uo$$
$$\bar{d} = D_h = 2s.$$

FLOTHERM also makes use of the energy equation to calculate temperatures and rate of heat transfer. A detailed discussion of the energy equation falls beyond the scope of this study, but can be found in a number of references [30, 31].

2.2.2 Boundary conditions

The momentum boundary conditions relate to the solution of the governing equations at the various boundaries. The correct numerical solution of a flow field is to a large extent dependent on the specification of the correct boundary conditions at the various walls.

Solid walls:

For the momentum equations, the so-called no-slip boundary condition is used at the various solid walls [32].

Symmetry planes:

On symmetry planes, a zero gradient boundary condition is used. This implies that no flow enters or leaves the flow field normal to the symmetry plane [32].

Inlet:

A block profile with a constant average velocity is used to specify the inlet conditions. In accordance with the Butterbaugh and Kang experimental investigations [8], an inlet length of at least $L = 5D_h$ is created prior to the heat sink itself in order to allow the flow to develop a boundary layer and proper velocity profile prior to entering the test section.

This may not be an entirely satisfactory solution to the problem, and can be overcome by assigning a velocity profile at the entrance. In this instance however, it was not considered necessary.

Exit:

The zero gradient, no flow split condition is applied at the exit. Physically this implies that diffusion is neglected at the exit.

2.3 MODELLING STRATEGY

2.3.1 *Heat sink configurations and detail*

The heat sink modelling strategy consisted of using a certain configuration of heat sink as a basis for simulation. This basic heat sink geometry was in accordance with the heat sinks tested by Butterbaugh and Kang [8], and was modelled for two laminar and two turbulent velocities (although Butterbaugh and Kang tested only the laminar situation). The Butterbaugh and Kang basic heat sink [8] had the following geometric parameters:

- Fin thickness : t = 1.27 mm.
- Fin gap : s = 2.4 mm.
- Fin height : h_f = 53 mm.
- Tip bypass height : H_b 0 - 38 mm.

The freestream velocities over the range of heat sinks modelled were as follows:

Uo = 1 m/s : Laminar flow.
Uo = 4 m/s : Laminar flow.
Uo = 8 m/s : Turbulent flow.
Uo = 12 m/s : Turbulent flow

Transition to turbulence was taken at Re = 2500 [27], where the Reynolds number was defined in accordance with Gopalakrishna [6] as:

$$\mathrm{Re} = \frac{\rho U_o D_h}{\mu} \quad \text{, where } D_h = 2s, \text{ and } U_o \text{ as the entrance velocity.} \qquad [2.5]$$

A variety of geometric parameters were then changed in the basic heat sink configuration discussed above in order to determine the effects of geometric parameter variation on the flow behaviour. A total number of six geometrically different heat sinks were modelled at various lengths and Reynolds numbers, with the freestream velocities as discussed previously. Wherever possible, the results were compared to the experimental test results of Butterbaugh and Kang for verification purposes [8]. Geometric parameter variations included:

- Heat sink length.
- Heat sink blockage ratio, which is a function of the following as per equation 1.1:
  - Fin height.
  - Fin thickness.
  - Fin gap.
  - Tip bypass height.

It was also decided to model all heat sinks at a length of 150 mm (except for length variation modelling) instead of the 46 mm as per Butterbaugh and Kang [8], as this allows all the flow bypass and leakage effects to become more apparent. A 46 mm. heat sink was however also modelled for comparison purposes with the Butterbaugh and Kang experimental results [8] (see appendix A table 8).

The modelling matrix may be represented schematically by the six heat very different sinks as depicted in figure 2.1, with exact geometric dimensions and modelled velocities to be found in appendix A.

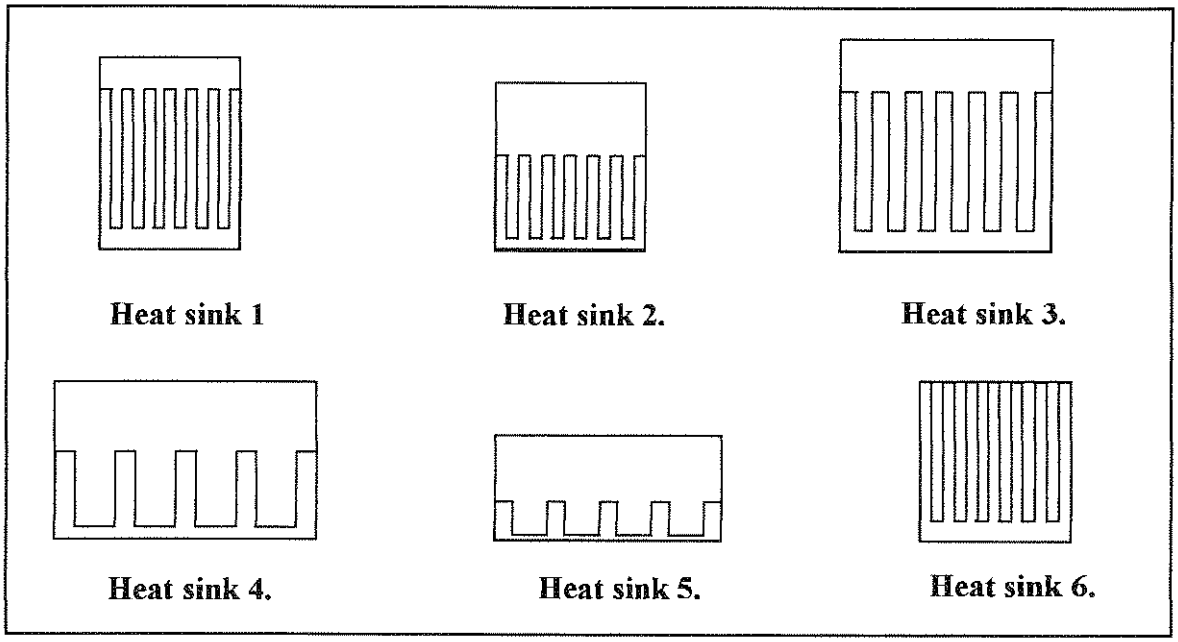

Figure 2.1 Schematical representation of CFD modelling matrix.

As is evident from figure 2.1, a wide variety of heat sinks was modelled comprising of all the basic geometric ranges and ratios often encountered in practice [18].

The heat sinks 1 - 3 in figure 2.1 are essentially high blockage ratio heat sinks (see equation 1.1) with varying fin height (2) and gap (3). Heat sink 1 represents the basic Butterbaugh and Kang [8] heat sink discussed earlier in this section.

Heat sinks 4 and 5 are essentially low blockage ratio heat sinks with varying fin height and constant tip bypass. Fin height, thickness, gap, as well as tip bypass height differ significantly from the basic heat sink 1 configuration.

Heat sink 6 is a standard heat sink with the exact same dimensions as heat sink 1, but with no tip bypass. Modelling of this heat sink serves to illustrate typical flow contraction and expansion behaviour.

As mentioned earlier it was not deemed necessary to simulate lateral bypass, as lateral bypass is essentially similar to tip bypass with no leakage velocity component present, and will not be investigated as part of this study.

2.3.2 The CFD modelling strategy

The CFD modelling strategy addresses the problem of modelling the range of above mentioned heat sinks in the most accurate and efficient manner possible, with the minimum time and computational requirements. The CFD modelling strategy largely makes use of symmetry planes in order to accomplish this.

This is possible owing to the fact that a longitudinal fin heat sink lends itself to symmetry simulations without any inherent inaccuracies [6]. The model used to represent any longitudinal fin heat sink with tip bypass, regardless of actual width and number of fins can schematically be depicted as in figure 2.2.

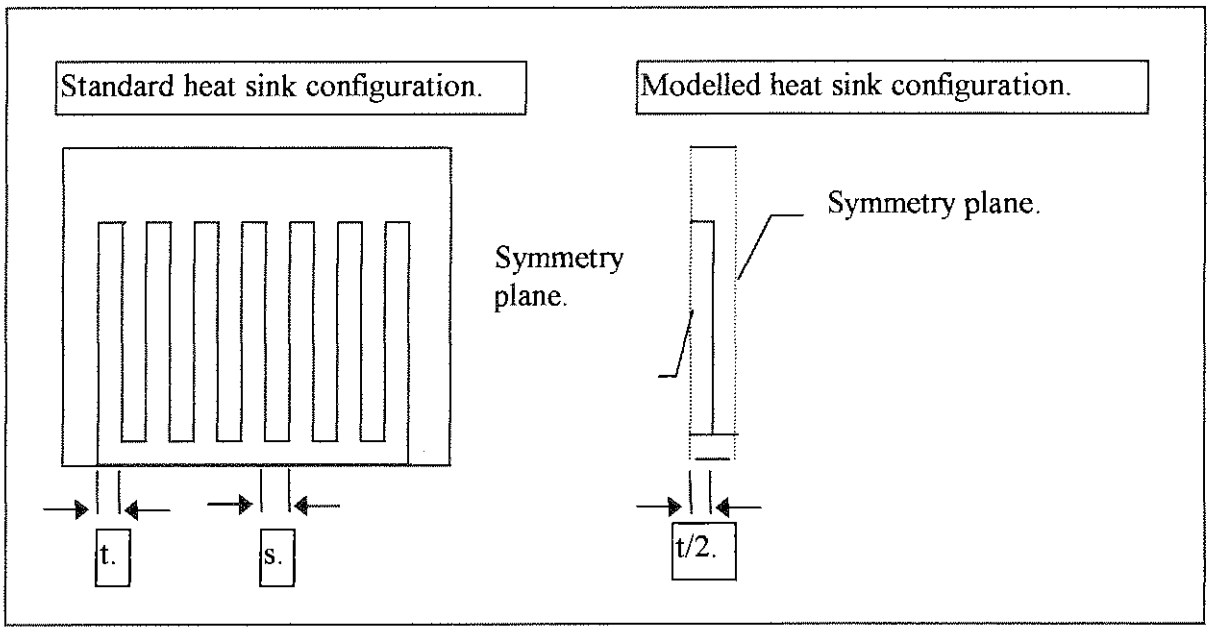

Figure 2.2 **Modelling strategy showing symmetry plains for longitudinal fin heat sinks with tip bypass.**

2.4 GRID CONSIDERATIONS

The grid being used in this study is in accordance with grids used in other studies of a similar nature [6]. Due to the reasonably simple geometry a plain orthogonal grid was used throughout. The actual grid size depended on the amount of flow detail desired. The final grid resolution resulted from a combination of computational time limits and final flow detail desired. Additional flow detail was obtained without additional grid cells by refining the grid in the focus areas where complex flow phenomena are expected. These areas are summarised below and can be seen clearly in figure 2.4.

- Heat sink bottom wall.
- Channel top wall.
- Heat sink fin top.
- Heat sink entry.
- Heat sink exit.
- Over the width of the simulated model as depicted in figure 2.2, a fine uniformly spaced grid was used throughout due to the fin boundary which runs along the entire length of the model.

The final solution was in each instance completely grid independent.
The cell distribution for figure 2.2 heat sink 1 (see appendix A for detail) is depicted below in figure 2.3 by way of example. The other grid resolutions are proportionally very much the same.

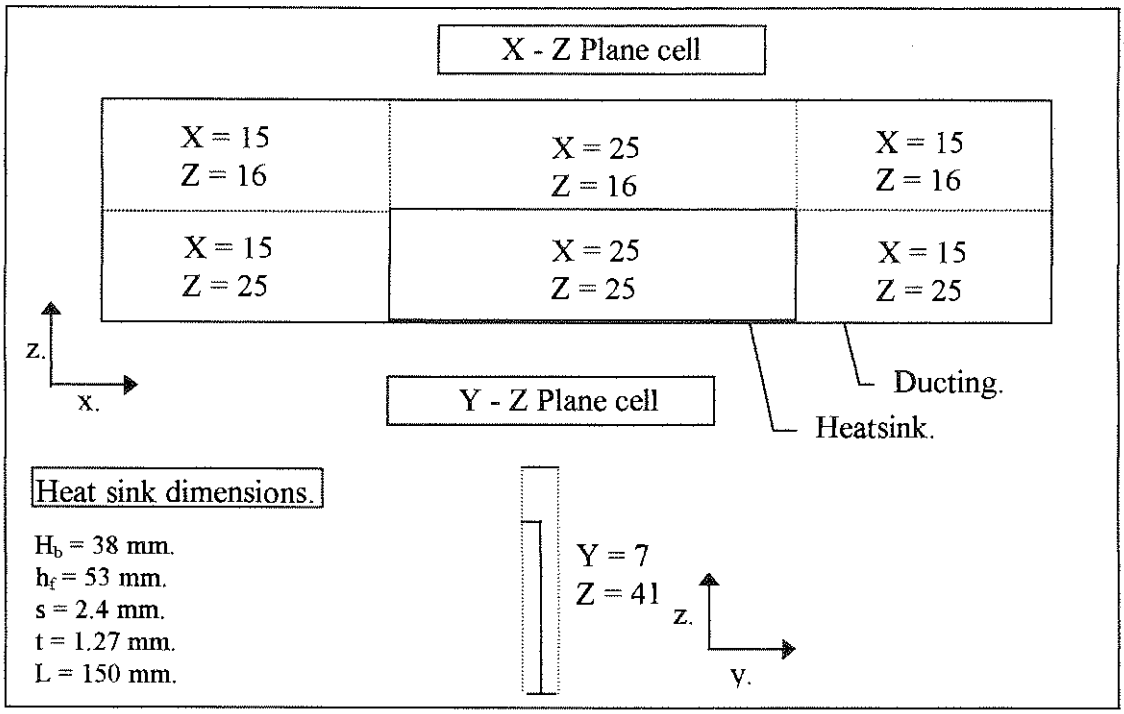

Figure 2.3 Schematical representation of grid resolution for heat sink 1.

An example of the actual grid in the X-Z plane for the same heat sink model as depicted in figure 2.3 may be viewed below in figure 2.4. Figure 2.4 clearly demonstrates the grid resolution and refinement areas of the grid in question.

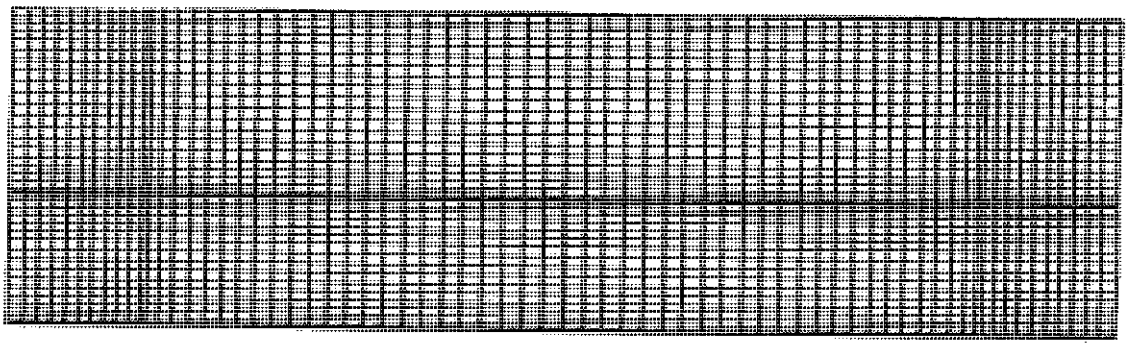

Figure 2.4 Actual grid example depicting grid resolution and refinement areas.

2.5 DATA REDUCTION AND PRESENTATION

Relevant data to be presented in order to characterise the behaviour of forced flow in longitudinal fin heat sinks with tip bypass are as follows:

- Distance progression (x).
- Pressure loss (ΔP).
- Velocity distribution in 3 dimensions (Vx, Vy, Vz).

The pressure and velocity data will be presented in the form of vector and contour plots directly from the CFD analysis, and also in reduced format in order to illustrate and highlight certain principles and behaviour. The data reduction formulas and presentation is discussed below:

- Distance progression will be non-dimensionolised according to fluid dynamics practice [27], and presented as x/D_h, with D_h defined as per equation 1.2

- Pressure loss data will be presented in the form of the dimensionless Fanning friction factor given by the following equation [34]:

$$f = \frac{\Delta P D_h}{2x\rho V^2}, \text{ where } D_h = 2s \qquad [2.6]$$

- Velocity will be non-dimensionolised and presented throughout by dividing the actual local velocity with the free stream velocity Uo, therefore:

$$V_x = \frac{V_{actual}}{Uo} \qquad [2.7]$$

2.6 CONCLUSION

In chapter two the CFD analysis of forced flow behaviour in longitudinal fin heat sinks with tip bypass using FLOTHERM from FLOMERICS has been discussed in detail. Relevant theory, governing equations, and all assumptions have been clearly mentioned and discussed.

The modelling strategy and approach, which employs the use of a variety of geometrically different longitudinal fin heat sinks and the extensive use of symmetry planes in simulation have also been substantiated. Grid considerations as well as data presentation and reduction have also enjoyed attention.

The CFD results and verification are discussed in chapter 3.

Chapter 3

CFD MODELLING RESULTS AND DISCUSSION

3.1 PREAMBLE

In chapter 3 the CFD results from the simulations in chapter 2 will be analysed and discussed in detail. Prior to discussing the simulation results, the CFD modelling strategy as presented in chapter 2 will be verified through comparison of results to existing experimental data from literature [8].

The second part of this chapter deals with the pressure and flow characteristics of a forced flow longitudinal fin heat sink with no tip bypass. This serves to illustrate some of the basic flow principles in contracting and expanding flows. Following that, the flow and pressure characteristics of a typical representative longitudinal fin heat sink with tip bypass will be investigated in order to determine general flow behaviour. All flow details and relevant deductions will be clearly noted.

The influence of geometric parameter variation on flow behaviour in longitudinal fin heat sinks will also be thoroughly investigated. The most important parameter changes to be discussed are as described in section 2.3.1 and briefly mentioned below, with details on exact geometry to be found in appendix A.

- Heat sink length variation.
- Heat sink blockage ratio variation, which is a function of the following geometric parameters:
    - Fin height.
    - Fin thickness.
    - Fin gap.
    - Tip bypass height.

Due to the nature and quantity of the data obtained from the parametric study, only the most important and relevant conclusions will be discussed in this chapter. More details and additional data may be found in appendix B.

The chapter will conclude with a summary of the most important aspects determined through the course of the CFD simulations.

3.2 VERIFICATION OF CFD RESULTS

Prior to the confident presentation and analysis of CFD results over the range of heat sinks as described in chapter 2, it was necessary to verify the complete numerical modelling strategy and approach as described in sections 2.3 and 2.4. The verification problem was approached by modelling the heat sink as in table 7 appendix A, for which Butterbaugh and Kang [8] did experimental testing over a range of laminar flow velocities. The numerical and experimental results could then be compared.

Unfortunately it was not possible to find any experimental results in literature of turbulent flow velocities for the range of heat sinks used in this study. Gopalakrishna [6] however did extensive CFD modelling and experimental work on longitudinal fin heat sinks over *Re = 1200 - 15000*, thus well into the turbulent range using FLOTHERM. Excellent agreement of results was obtained throughout for both turbulent and laminar flow velocities (refer to section 1.3). The industry has also at this stage accepted the accuracy of CFD modelling in this application as sufficient for practical intents and purposes [17].

As a result of the literature review and in specific the study conducted by Gopalakrishna [6], it was considered sufficient to verify the modelling strategy used in this study by only comparing CFD results for laminar flow with experimental results obtained from Butterbaugh and Kang [8]. The conclusions of Gopalakrishna [6] will be taken as sufficient for the turbulent flow scenario.

Results for laminar flow in the heat sink as described by table 7 appendix A are as follows when compared to experimental results from Butterbaugh and Kang [8].

Table 3.1: Comparison of CFD and experimental results for laminar flow:

Freestream Velocity [m/s].	ΔPhs - CFD [Pa].	ΔPhs - Experimental [Pa].	Variance %
Uo = 1 m/s.	2.24	2.06	8.74
Uo = 4 m/s.	15.7	17.6	10.80

It is evident from table 3.1 that experimental and CFD results for laminar flow in longitudinal fin heat sinks with tip bypass compare reasonably well with one another. For *Uo = 1 m/s* the pressure loss is overpredicted by 8.74 %. For *Uo = 4 m/s* the pressure loss is underpredicted by 10.8 %. The difference in results arise from inherent modelling inaccuracies, and practical experimental errors [17], which can be significant. In terms of CFD analysis, the above results show good agreement and serves as suitable verification of the modelling strategy as discussed in chapter 2.

3.3 CFD MODELLING OF A LONGITUDINAL FIN HEAT SINK WITH NO TIP BYPASS

Prior to the modelling of more complex heat sink geometries it was decided to first model a basic ducted heat sink with no tip bypass in order to examine pure flow contraction and expansion behaviour.

The heat sink in question was modelled with the geometry as per table 6 appendix A, with a fin height h_f = *53 mm.*, while all other geometric parameters were as per Butterbaugh and Kang [8], with s = *2.4 mm*, t = *1.27 mm and* L = *150 mm.* The heat sink is schematically represented by Heat sink 6 in figure 2.1. Two laminar and two turbulent velocities were modelled in each instance for comparative purposes:

- Uo = 1, 4 m/s : Laminar flow.
- Uo = 8, 12 m/s : Turbulent flow.

For the purpose of this document the flow details of only one turbulent and one laminar velocity will be discussed, as the other simulations at different Reynolds numbers exhibit similar flow characteristics and will be compared through the course of the study.

3.3.1 Laminar flow and pressure details

As mentioned previously, two laminar velocities were modelled, but only the instance of *Uo = 1 m/s.* will be discussed as the flow behaviour is representative of typical laminar flow in a longitudinal fin heat sink with no tip bypass. A vector plot of the flow details and a contour plot for pressure loss are presented in figure 3.1. The plots of figure 3.1 are in each instance made on the X-Z plane, (see figure 2.3) on the symmetry plane, in the centre of the interfin region.

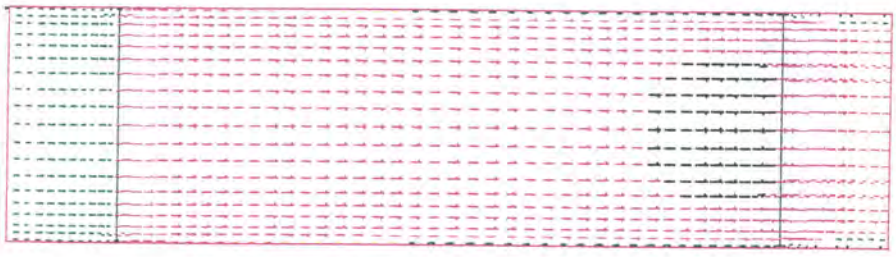

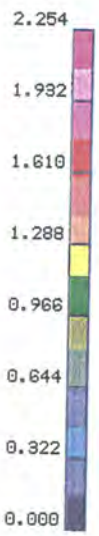

Figure 3.1 **Vector plot of velocity and contour plot of pressure for a laminar flow heat sink with no tip bypass.**

As is evident from figure 3.1 the laminar flow accelerates from 1m/s. to a maximum of 2.2 m/s. in the interfin region as the flow contracts. The Reynolds number increases from 302 to 664 in the interfin region, but still remains well within the laminar region. As may be seen the flow develops along the length of the heat sink as a definite boundary layer starts to form at $x/D_h = 17$ into the heat sink. This developing flow behaviour can also be seen prominently in the friction factor plot of figure 3.4, but is less noticeable at higher Reynolds numbers in the laminar range. As the flow exits the heat sink it decelerates again but is still higher than the entry velocity of 1 m/s due to the recirculation zone occurring directly after the heat sink fin. The size of this recirculation zone extends with increasing Reynolds numbers.

The pressure contours stay reasonably constant over the height of the heat sink as may be expected. Upon entry to the heat sink the highest pressure gradient occurs, after which the pressure then drops in gradual linear increments towards the exit of the heat sink.

3.3.2 Turbulent flow and pressure details

The turbulent flow situation is slightly different from the laminar flow scenario discussed earlier. Note that only the $Uo = 8$ *m/s.* heat sink flow details will be discussed, as it is representative of other turbulent flow behaviour as well. The vector plots for velocity and the pressure contour plots are presented below in figure 3.2. Both the vector plot of velocity and pressure contour plot are plotted on the symmetry plane, in the centre of the interfin region on the X-Z plane, as for the laminar flow instance.

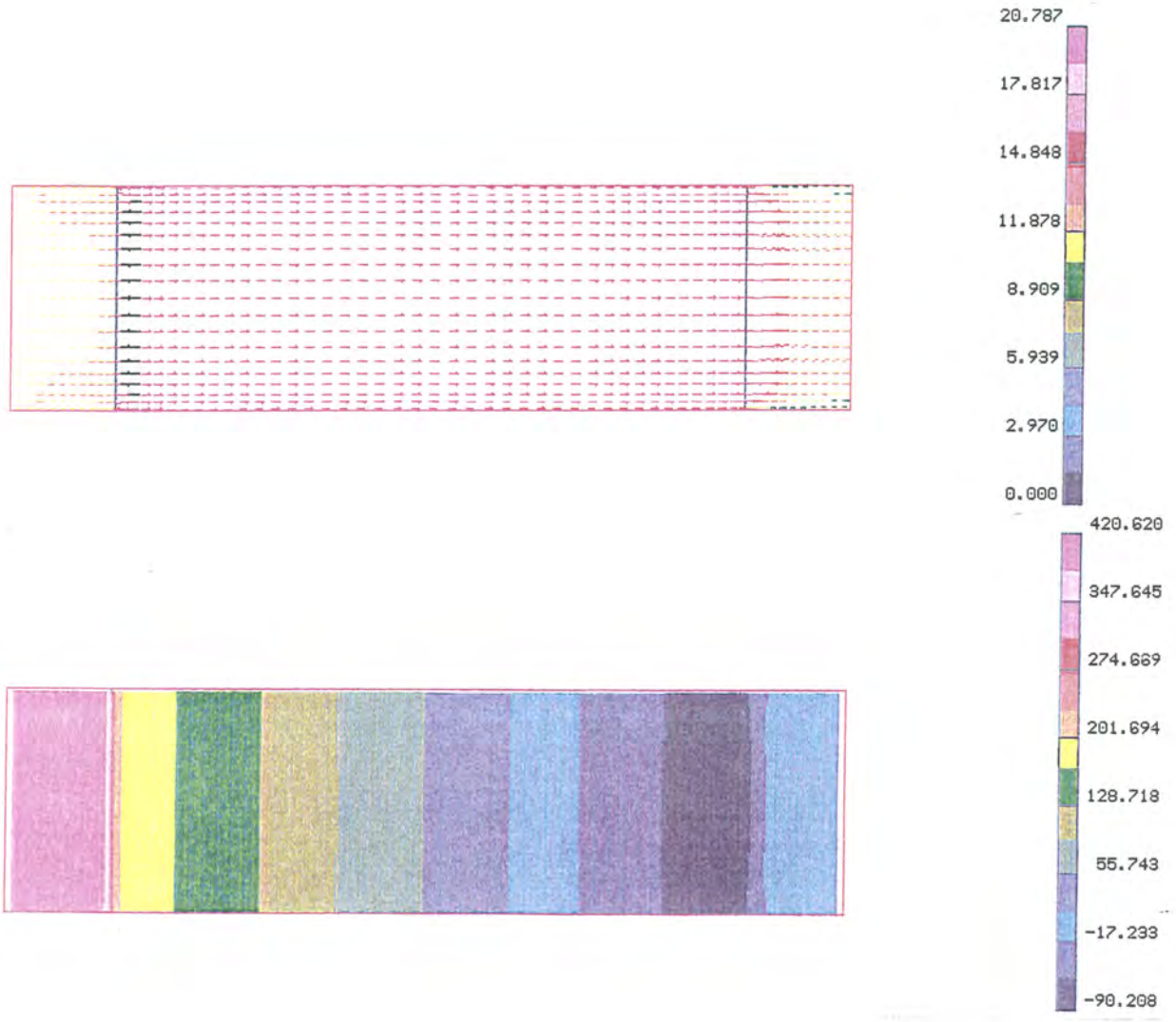

Figure 3.2 **Vector plot of velocity and contour plot of pressure for a turbulent flow heat sink with no tip bypass.**

The turbulent flow exhibits some very interesting behaviour. The flow starts to accelerate approximately 20 mm ($x/D_h = 4$) prior to the heat sink entrance due to the huge flow recirculation zone present in this area. This recirculation zone even extends to the centre of the interfin region upon entry. The velocity remains virtually constant throughout the length of the heat sink with no visibly boundary layer developing as was evident as for the laminar instance. A large recirculation zone is also present upon exit of the heat sink. Simulation has indicated that the size of both recirculation zones extend with increasing Reynolds numbers.

The pressure plot exhibits similar characteristics as the laminar instance, except that the pressure gradient upon heat sink entry is much steeper. In the heat sink itself the pressure drops once again in an almost linear fashion with gradual increments due to internal friction losses.

3.3.3 *Laminar and turbulent flow pressure characteristics and data reduction*

The flow details may be reasonably straightforward, but the pressure characteristics of the heat sink in question deserve some further attention. The average pressure loss over the length of the entire heat sink model can be graphically presented as in figure 3.3 for all simulated velocities.

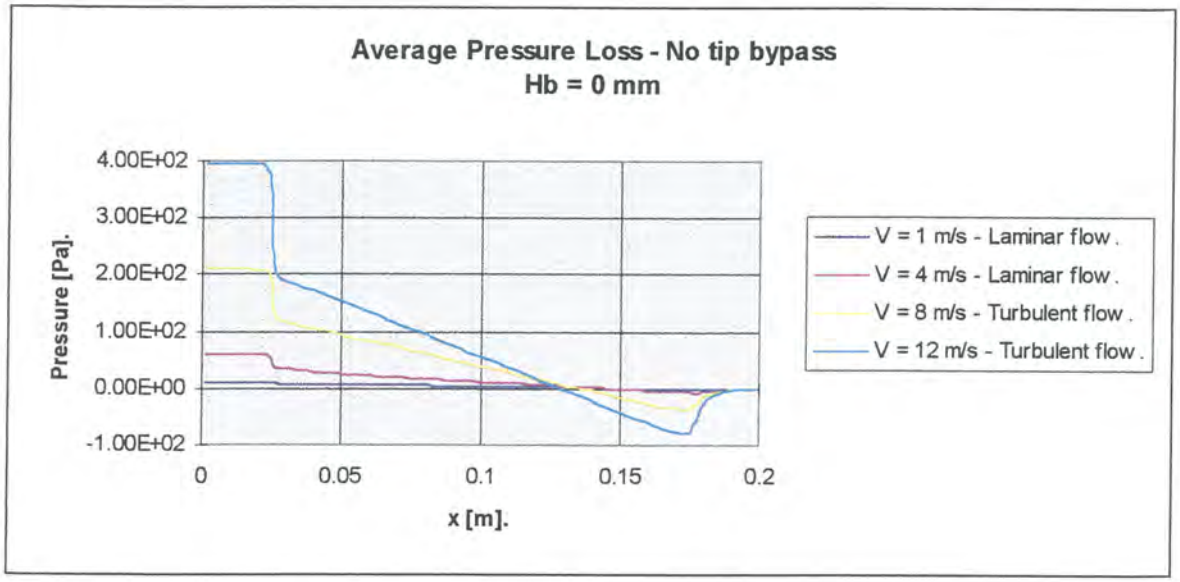

Figure 3.3 Pressure loss vs. Distance - No tip bypass.

As is evident from figure 3.3 the average pressure drops sharply upon entrance to the heat sink, whereafter it stabilises and decreases in a linear fashion due to internal channel friction losses, and regains some pressure in the expansion zone of the heat sink.

As mentioned in section 2.5 the average pressure loss may also be expressed in terms of a dimensionless friction factor which provides more insight into the flow behaviour, and plotted versus a dimensionless x/D_h.

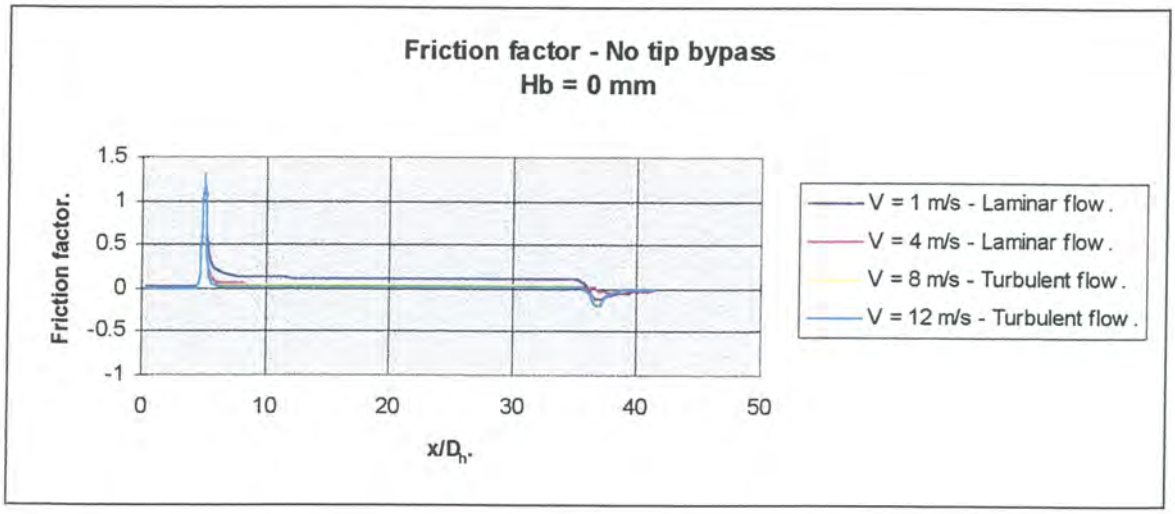

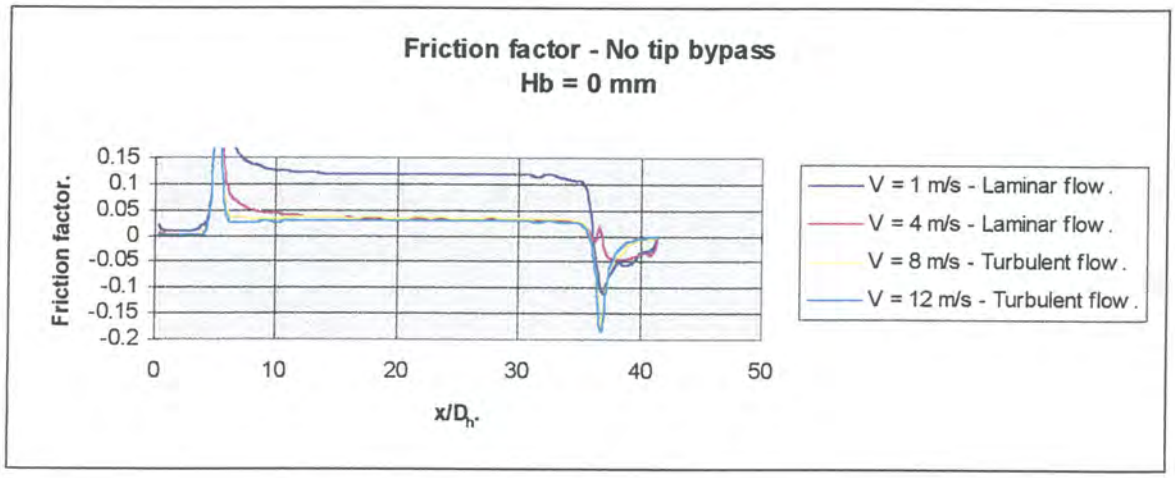

Figure 3.4 Friction factor vs. X/D_h - No tip bypass.

The friction factor plots of figure 3.4 indicates the same trends as the pressure plots of figure 3.3, but does highlight some interesting aspects.

Regardless of freestream entrance velocity *Uo*, the maximum friction factor upon entry to the heat sink equals approximately 1.3. This agrees to a large extent with the results from Kays [23], which suggests that contraction losses are only dependant on the Reynolds number to a very small extent, and much more on actual contraction ratio and geometry.

The friction factor stabilises quickly upon entry to the heat sink for the turbulent flows ($x/D_h = 6$), while the laminar flows exhibit a short developing flow region prior to stabilisation ($x/D_h = 10$). The laminar friction factor ($Uo = 1$ & 4 *m/s*) in the interfin region varies considerably as a function of the Reynolds number, while the turbulent friction factor ($Uo = 8$ & 12 *m/s*) remains more or less the same independent of the actual Reynolds number. The well known Moody chart illustrates the principle noted here very well [16]

The pressure recovery on flow expansion is once again evident, and is in agreement with the results from Kays [6], in that both the laminar and turbulent expansion friction factor stays very much the same independent of the actual Reynolds number. A significant difference however exists between laminar and turbulent flow friction factor expansion values.

3.3.4 Summary

In conclusion the following flow and pressure characteristics for forced flow in a longitudinal fin heat sink with no tip bypass need to be highlighted:

- The existence of significant flow recirculation zones on heat sink exit, as well as on heat sink entry for turbulent flows.
- The developing nature of laminar flows along the length of the heat sink, which is much less evident for turbulent flows.
- Contraction and expansion loss behaviour are in agreement with the trends presented by Kays [23].
- Interfin friction factor is a function of the Reynolds number for laminar flows, but stays more or less constant independent of the Reynolds number for turbulent flows.

The same characteristics could also be expected to be present in a forced flow longitudinal fin heat sink with tip bypass as discussed in the following section.

3.4 CFD MODELLING OF A LONGITUDINAL FIN HEAT SINK WITH TIP BYPASS

CFD modelling of a number of longitudinal fin heat sinks with tip bypass was conducted in accordance with the strategy discussed previously in chapter 2, modelling two laminar and two turbulent velocities for each geometric parameter variation as depicted in section 2.3. The freestream velocities were as follows for every heat sink modelled:

Uo = 1, 4 m/s. : Laminar flow.
Uo = 8, 12 m/s : Turbulent flow.

The geometric parameters varied are as follows:

- Heat sink length.
- Heat sink blockage ratio.

The blockage ratio is of course a function of the following geometric parameters as calculated using equation 1.1

- Fin thickness.
- Fin height.
- Fin gap.
- Tip bypass height.

In this section only the flow and pressure details for one representative heat sink with tip bypass will be discussed, as similar flow behaviour is exhibited to a greater or lesser extent by all the heat sinks in question. The influence of the Reynolds number on flow behaviour will also be clearly illustrated.

The representative heat sink to be discussed have the following geometric parameters in accordance with the study conducted by Butterbaugh and Kang [8] (See appendix A table 1, and section 2.3.1).

- H_f = 53 mm.
- L = 150 mm.
- H_b = 38 mm.
- S = 2.4 mm.

3.4.1 *Laminar flow characteristics*

As discussed above the heat sink was modelled for 2 laminar velocities, but only the instance of *Uo = 1 m/s.* will be further discussed as it is representative of the general laminar flow behaviour. Figure 3.5a. provides a velocity vector plot for the centre of the interfin region, on the symmetry plane. Figure 3.5b. is plotted on the centreline of the fin itself.

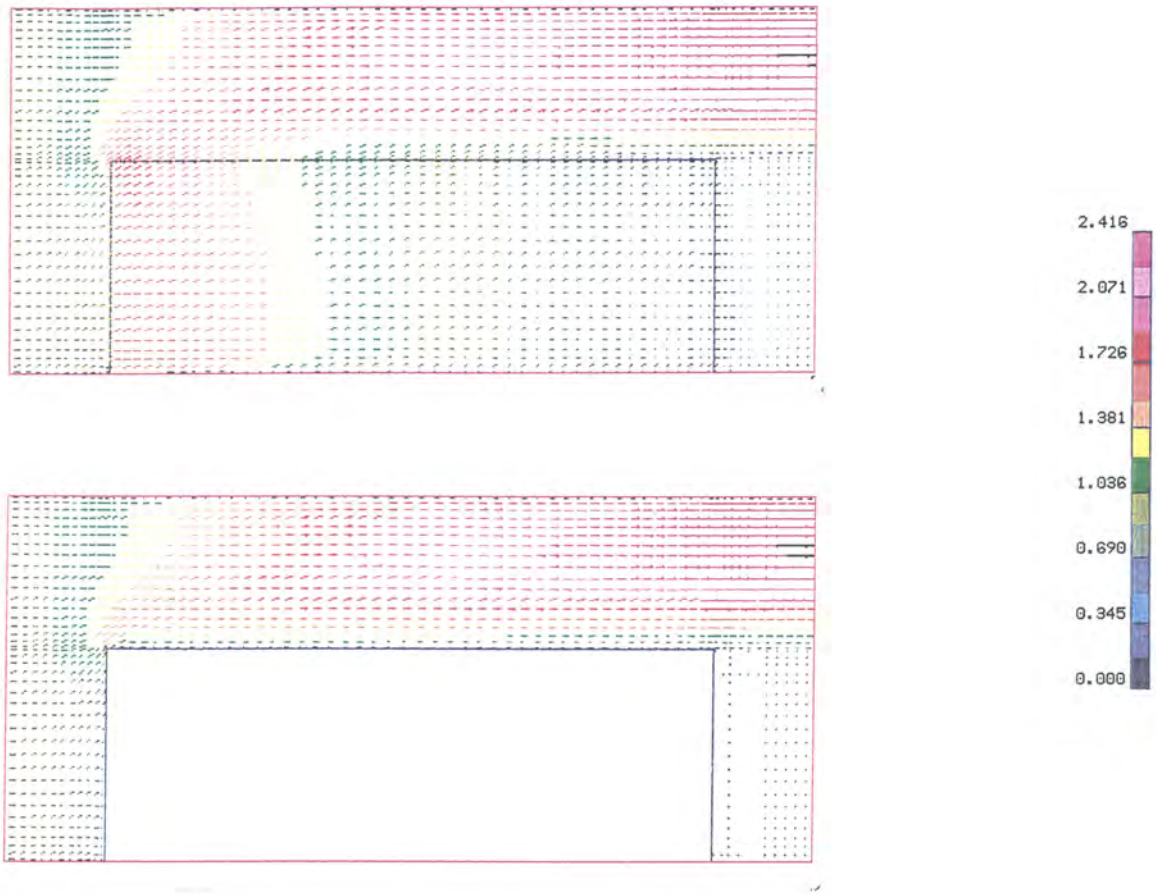

Figure 3.5 Vector plots of velocity for Uo = 1 m/s - Laminar.

As is evident from the velocity vector plots of figure 3.5 for a heat sink with an entrance velocity *Uo = 1 m/s*, a significant amount of flow bypass occurs. By far the largest amount of tip bypass occurs at the entrance to the heat sink, as this is where the single largest pressure gradient exists. The tip bypass velocity reaches a maximum of up to 2.5 times the entrance velocity. Figure 3.5b also indicates the presence of a large flow recirculation zone at the exit to the heat sink behind the fins. The longitudinal length of this recirculation zone is approximately $3D_h$.

Figure 3.6 provides the average velocity in normalised format for both the horizontal and vertical directions along the length of the heat sink. The average interfin, tip bypass, and leakage velocity is depicted.

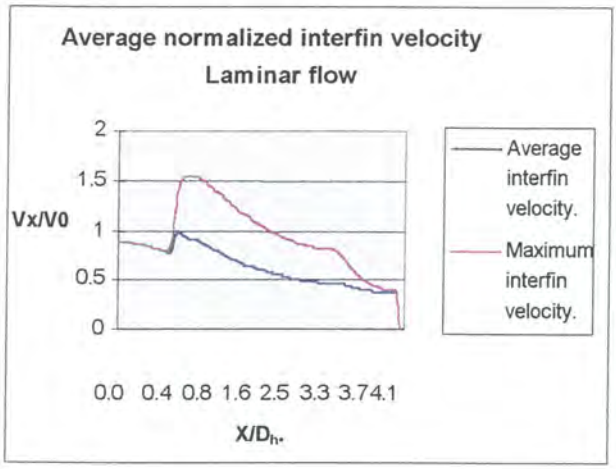

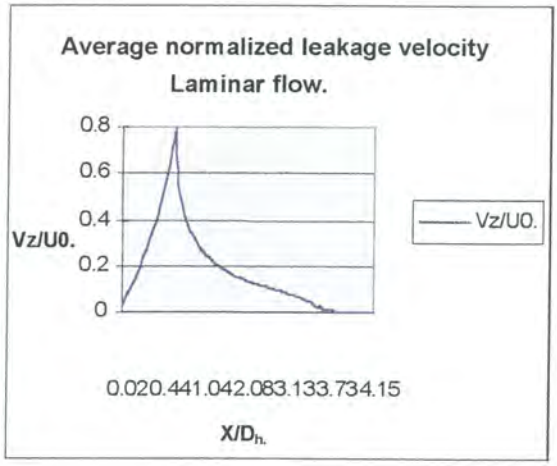

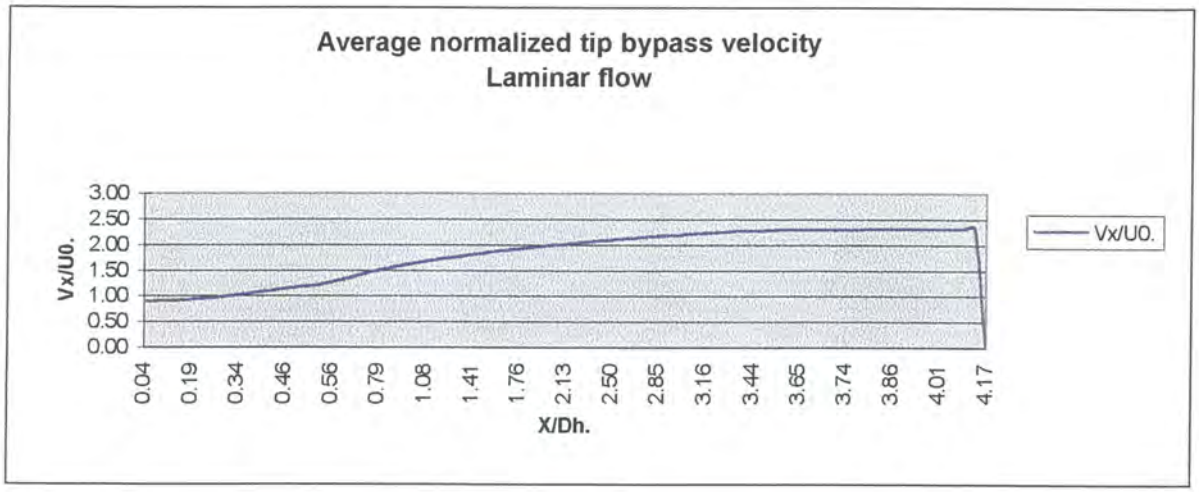

Figure 3.6 Average interfin velocity, Average leakage velocity, Average tip bypass velocity.

Figure 3.6 confirm what the vector plots of figure 3.5 indicate. As the flow enters the heat sink the leakage velocity reaches its maximum value, as high as *0.8Uo*. The leakage velocity then falls in an almost exponential fashion towards the end of the heat sink, which means that the tip bypass velocity stabilises at *2.4Uo* as is evident from fig. 3.6. The average interfin velocity reaches its peak at the heat sink entrance as may be expected. As the effects of flow bypass decreases the interfin velocity decreases in an exponential fashion, much as the tip velocity stabilises in a similar manner.

The difference between the average and maximum interfin velocity indicates that a significant velocity profile does exist within the channel. Both the horizontal and vertical velocity profiles are depicted at various places along the length of the heat sink in figure 3.7. The horizontal velocity profile is plotted at ½ H_f, while the vertical velocity profile is depicted in the centre of the interfin region on the symmetry plane.

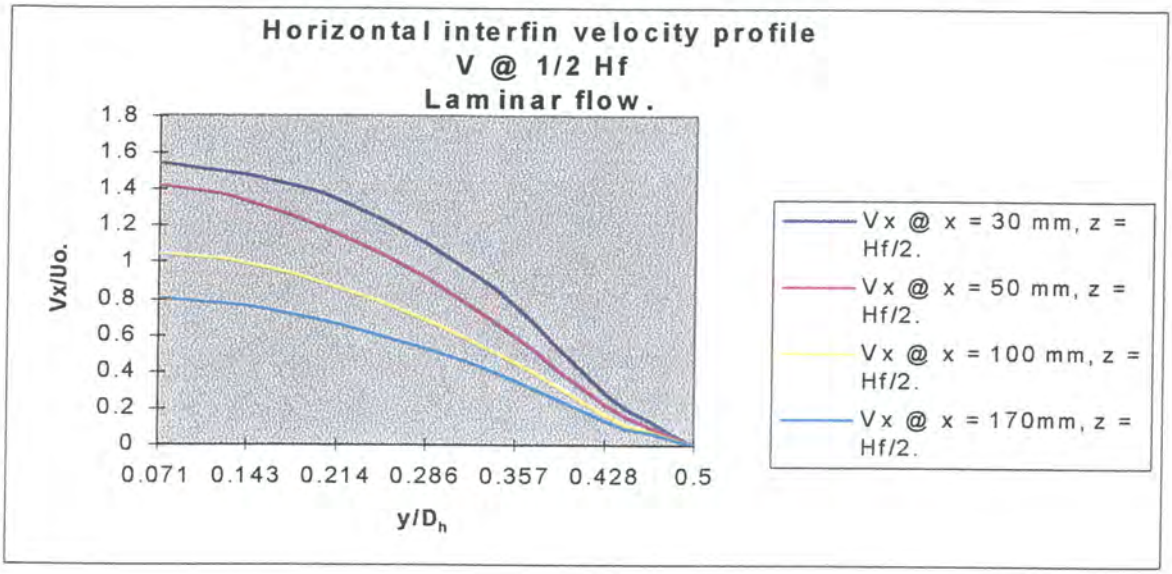

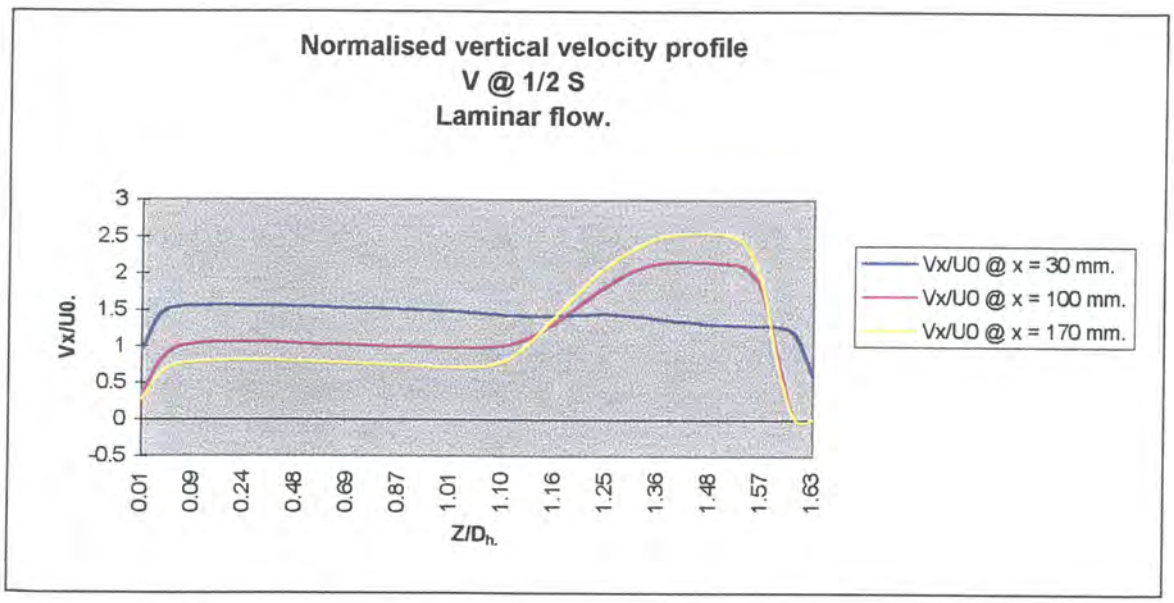

Figure 3.7 **Normalised horizontal and vertical laminar interfin velocity profiles depicted at various positions along the length of the heat sink.**

As is evident from figure 3.7 a significant horizontal velocity profile does develop within the fin region very quickly after entry, while the vertical velocity profile does take some time to stabilise due to the flow bypass effects. The horizontal velocity profile actual value decreases with progression in the heat sink due to the effects of flow bypass. Eventually a proper vertical laminar velocity profile also develops in the tip bypass region, but the vertical velocity profile within the interfin region stays flat and almost turbulent in nature, which is surprising. The horizontal velocity profile in the interfin region does however exhibit all the characteristics of classical laminar flow behaviour.

The development of the vertical flow profile along the entire length of the heat sink also serves to illustrate the developing nature of the flow, and the continual influence of the flow bypass effect.

3.4.2 *Turbulent flow characteristics*

The same heat sink as above was also modelled at two turbulent velocities, namely *Uo = 8 m/s*, and *Uo = 12 m/s*. Only the 8 m/s instance flow details will be discussed, as they are representative of most turbulent flows in heat sinks with tip bypass. As for fig. 3.5, figure 3.8 shows velocity vector plots on two planes of the heat sink, namely on centre of the fin plane and also on the centreline of the interfin region on the symmetry plane.

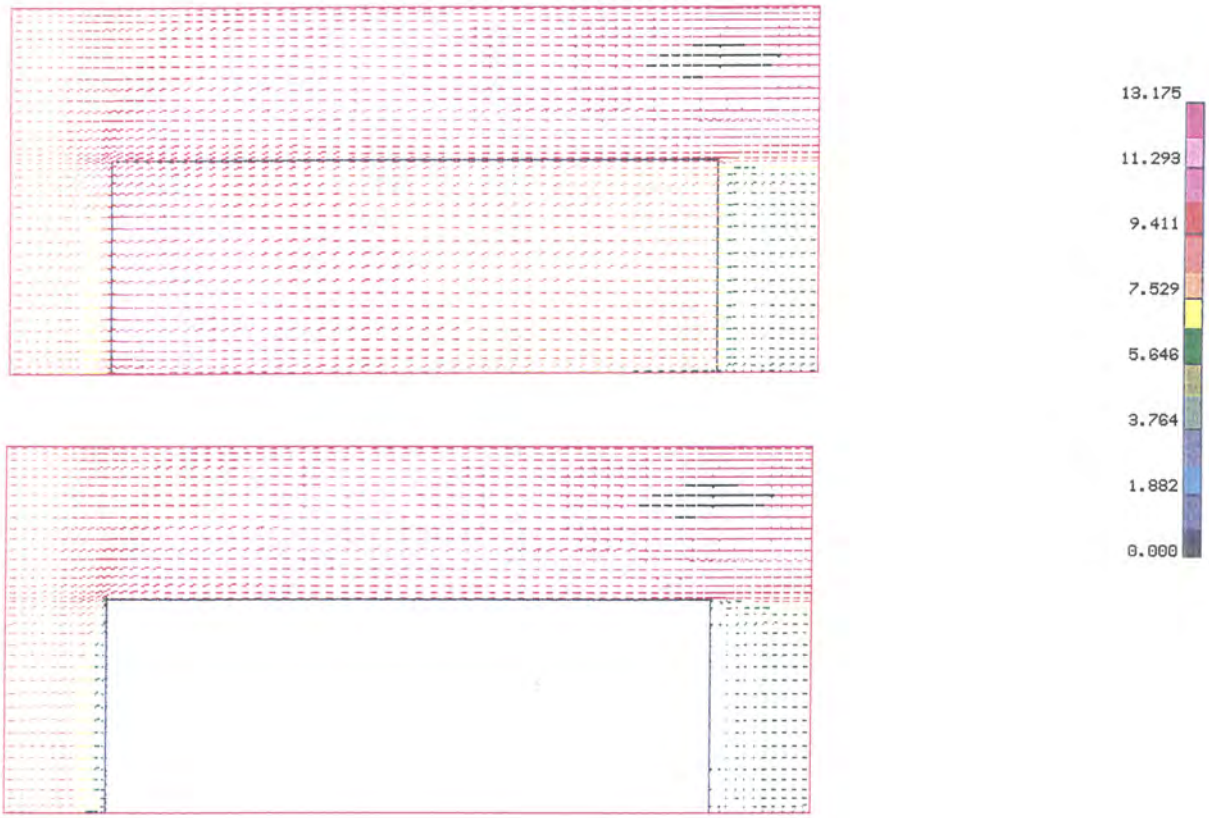

Figure 3.8 Vector plots of velocity for Uo = 8 m/s - Turbulent flow.

The turbulent vector plots exhibit the same characteristics as the laminar flow scenario. There are however two flow separation areas instead of just one as for the laminar instance. Together with flow separation at the heat sink exit, there is now also a small flow separation area prior to entry of flow into the heat sink. Figure 3.9 provides more information regarding the flow behaviour in normalised form.

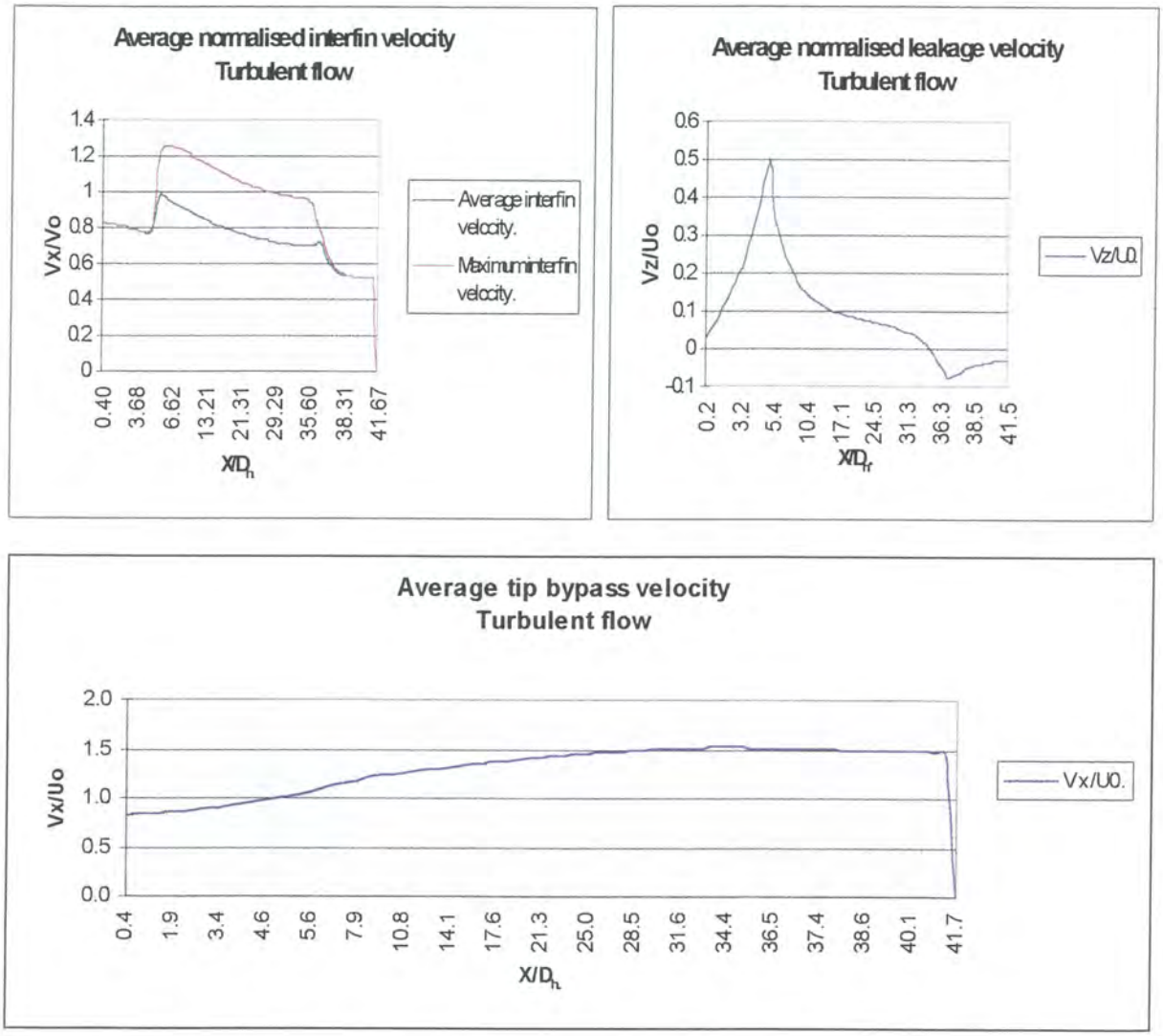

Figure 3.9 **Average interfin velocity, average leakage velocity, average tip bypass velocity.**

Due to the highly forced nature of the flow the tip bypass effects seem to be less pronounced than in the laminar case. Maximum leakage velocity only increases up to *0.5 Uo*, and the maximum tip bypass velocity only extends to *1.5Uo*. The longitudinal interfin velocity behaviour is also exponential in nature as for the laminar instance.

Once again the difference between the average and maximum interfin velocity shows that significant flow development and velocity profiles are present in the interfin region. Both the vertical and horizontal velocity profiles can be depicted as in figure 3.10. The horizontal interfin flow profile is once again depicted at a height of ½ H_f, at various positions within the heat sink length. The vertical velocity profile is presented on the centreline of the interfin region over the entire height of the heat sink fins and tip bypass area.

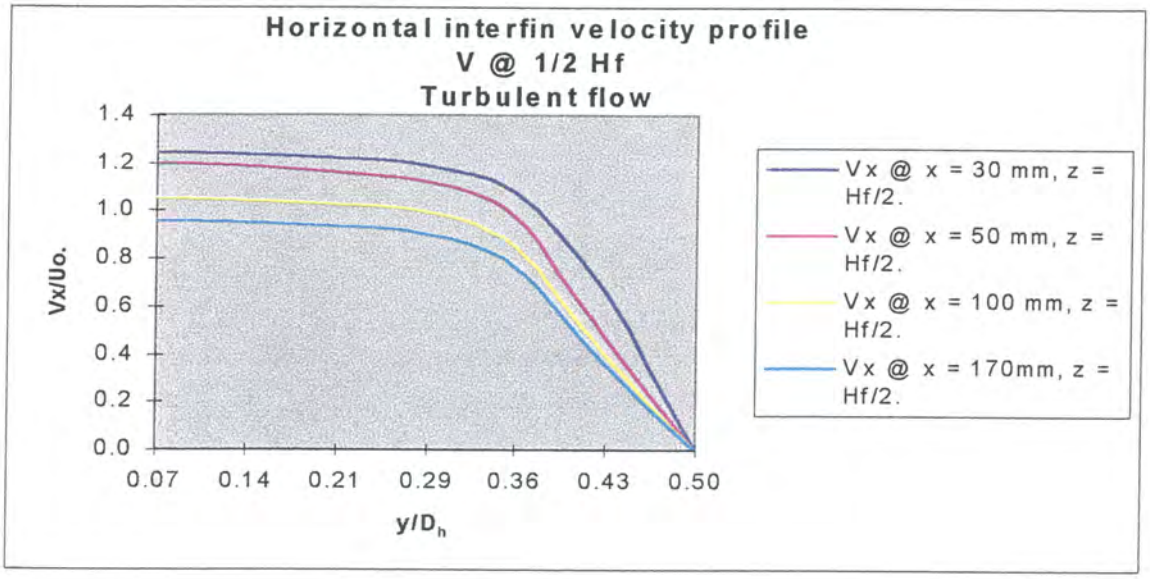

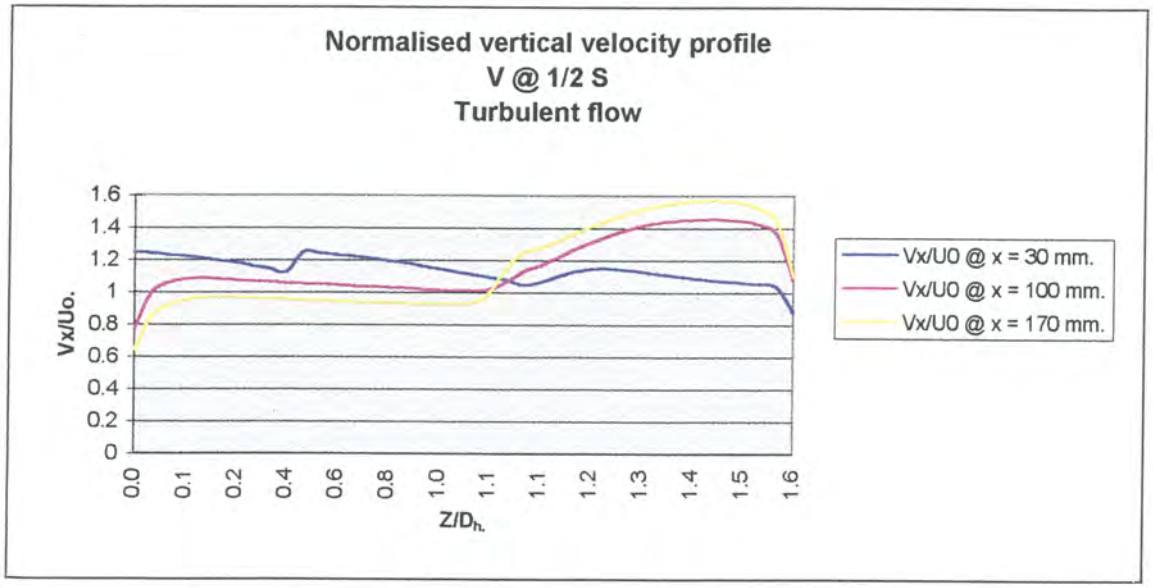

Figure 3.10 Horizontal and vertical turbulent velocity profiles.

The horizontal flow profile clearly shows classical turbulent flow characteristics, with a flatter, less pronounced profile than in the laminar instance. The smaller change in actual flow velocity value with progressive length of heat sink is also much less severe than for the laminar flow instance, and adds to the suggestion that the effects of flow bypass is much less severe than for the laminar scenario.

The vertical velocity profile plot exhibits much the same characteristics as the laminar flow instance. The interfin flow develops into a turbulent velocity profile, while the tip bypass region has an equally pronounced, turbulent velocity profile. Once again it can be detected from the above graph that the effects of flow bypass are less pronounced in this instance than for the laminar case.

3.4.3 Laminar and turbulent flow pressure characteristics and data reduction

The turbulent and laminar flow average pressure loss characteristics are presented comparatively for the heat sink as mentioned earlier in section 3.4 in terms of the dimensionless friction factor for two laminar and two turbulent velocities. This will serve to illustrate the pressure characteristics and the influence of Reynolds number variation on flow behaviour. Also provided are the pressure contour plots which provide graphic detail regarding the pressure distribution inside the channel.

Laminar flow pressure characteristics

A graphic representation in contour format of the heat sink pressure distribution can be viewed in figure 3.11, where pressure contours are plotted for *Uo = 1 m/s* in the centre of the interfin region. Only one laminar contour plot is provided as the other exhibits very similar behaviour.

Figure 3.11 Pressure contour plot on the centre of interfin region - Uo = 1 m/s - Laminar flow.

As may be expected there exists a major pressure gradient at the entrance to the heat sink, which causes the flow tip bypass effect. As is also evident throughout the remainder of the heat sink the pressure gradient driving flow tip bypass decreases with distance travelled. This causes the stabilisation of the flow bypass effect as the heat sink length progresses, and is in agreement with the flow results of figure 3.6.

Turbulent flow pressure characteristics.

The pressure characteristics for turbulent flow may be presented in a similar manner as for the laminar instance. In figure 3.12 the pressure contours for $Uo = 8\ m/s$ are once again presented in the centre of the interfin region on the symmetry plane as in the laminar case. The instance of $Uo = 12\ m/s$ exhibits similar characteristics and is not provided here.

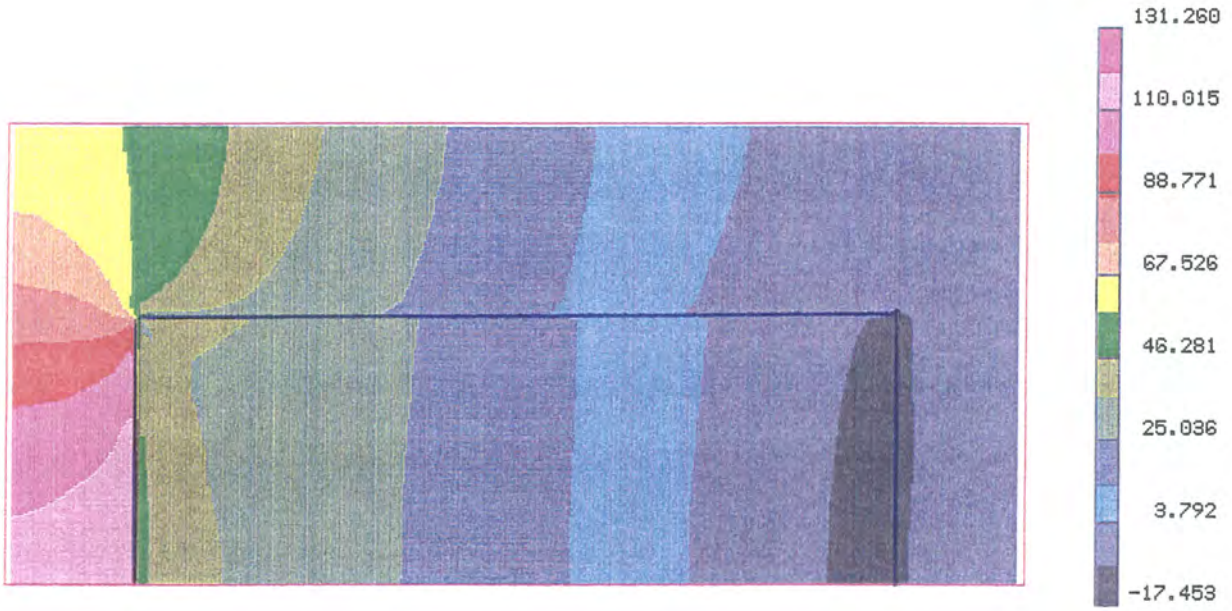

Figure 3.12 **Pressure contour plot on the centre of the interfin region - Uo = 8 m/s - Turbulent flow.**

From the turbulent pressure plot it is noticed that the pressure gradient driving flow bypass is much less pronounced than the laminar instance. This is confirmed when the flow results for the same instances are viewed as in figures 3.6 and 3.9. This confirms that the effects of flow bypass are much less pronounced in the case of highly forced turbulent flows.

Laminar and turbulent flow friction factor:

The laminar and turbulent flow pressure loss can also be presented in terms of the friction factor at the various Reynolds numbers as shown below in figure 3.13

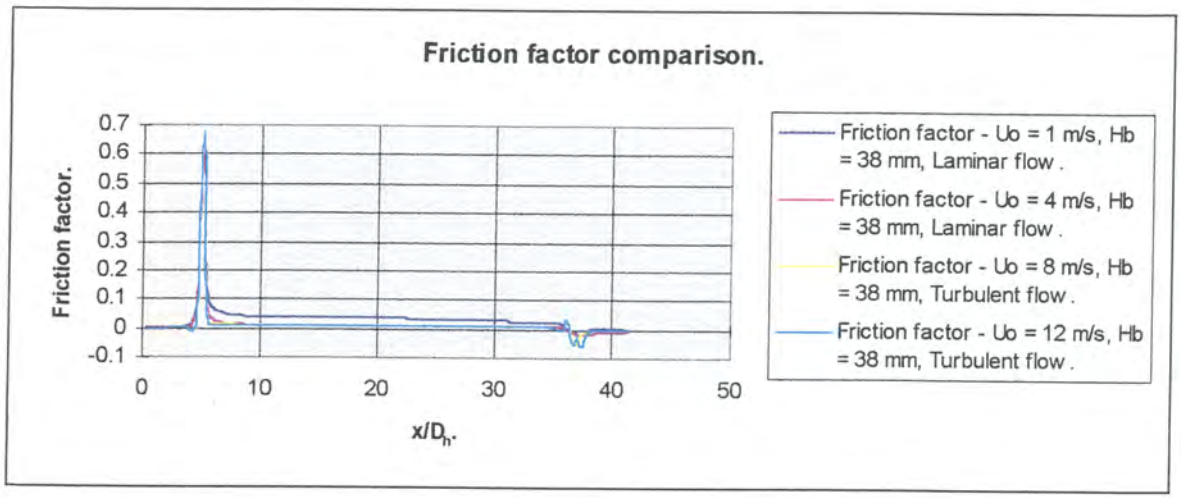

The graph scale can also be reduced as below in order to show more interfin friction factor detail:

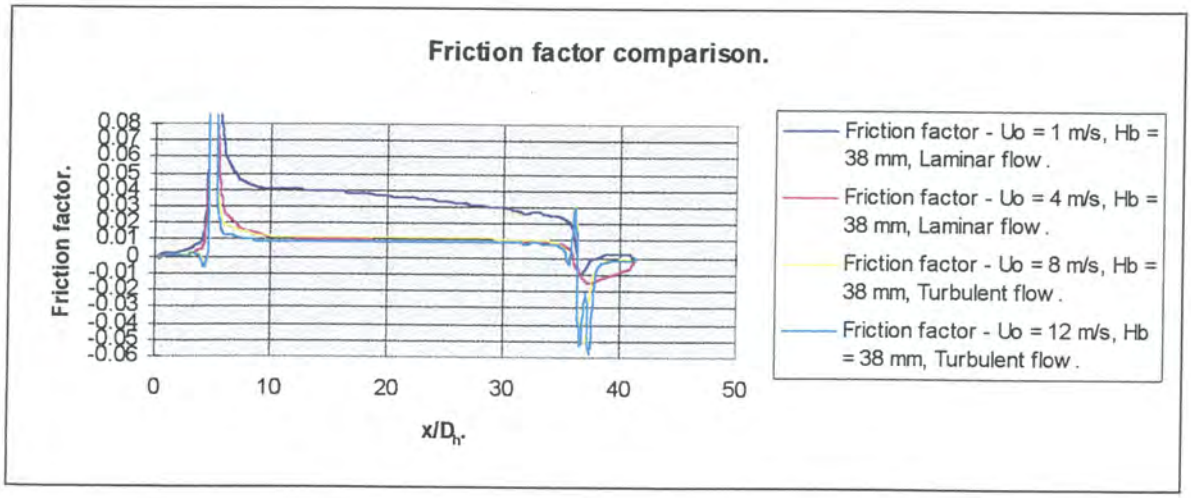

Figure 3.13 Laminar and turbulent friction factor comparison.

As is evident the laminar friction factor rises to a maximum of approximately *0.59* for both velocities at the entrance to the heat sink. The friction factor for the remainder of the heat sink stays reasonably constant but decreases slowly due to the flow bypass effect, only to significantly increase in the flow recirculation zone upon exit of the heat sink as may be expected before the actual pressure recovery upon expansion. Once again the influence of the Reynolds number on the laminar interfin friction factor plays a major role, as is exhibited by the two instances of $Uo = 1\ m/s$ and $Uo = 4\ m/s$. The interfin friction factor for $Uo = 1\ m/s$ is equal to *0.04 - 0.02*, while for $Uo = 4\ m/s$ the friction factor remains almost constant at *0.01*.

The turbulent friction factor displays similar characteristics to the laminar instance, except that the flow seems to stabilise slightly quicker and the effects of flow bypass seem less pronounced. The actual value of the friction factor is also lower. This behaviour was also displayed by the friction factor plot for a heat sink with no tip bypass in figure 3.4. The turbulent flow entrance friction factor rises to a maximum of *0.67* for both turbulent velocities modelled before stabilisation in the fin region take place. Upon exit of the heat sink the presence of a large flow recirculation zone is evident, which is reflected in the large friction factor increase. Upon exit there is once again a regaining of pressure resulting in the negative friction factor as expected. The influence of the actual Reynolds number on the turbulent friction factor once again seems much less pronounced than for the laminar instance.

The influence of geometric parameter variation on pressure and flow behaviour will be determined in the following section.

3.4.4 Summary

In conclusion the following very important characteristics of laminar and turbulent flow in a ducted forced flow longitudinal fin heat sink with tip bypass have been highlighted by section 3.4:

- The longitudinal interfin flow as well as the tip bypass flow behaviour exhibits exponential characteristics with length progression due to the effects of flow bypass.
- Definite flow profiles and flow development exists within the fin and tip bypass regions. These flow profiles are in accordance with classical laminar and turbulent flow profiles as mentioned in literature [27], and should be taken into account in heat transfer coefficient calculations.
- The effects of tip bypass is less pronounced for highly forced turbulent flows when compared to laminar flow behaviour.
- The contraction and expansion pressure losses seem to follow the behaviour described by Kays [23].
- The Reynolds number has a definite influence on the interfin friction factor for laminar flows, but much less so for highly turbulent flows.

3.5 THE INFLUENCE OF GEOMETRIC PARAMETER VARIATION ON FLOW BEHAVIOUR

There are a large number of geometric parameters which may be varied in a typical longitudinal fin heat sink, but it can be summarised as below:

- Heat sink length.
- Heat sink blockage ratio.

The blockage ratio is a function of the following geometric parameters as calculated using equation 1.1

- Fin thickness.
- Fin height.
- Fin gap.
- Tip bypass height.

The effect of heat sink length will be discussed first, whereafter the effects of heat sink blockage ratio variation will also be discussed briefly.

3.5.1 The effect of heat sink length on flow behaviour

The previous discussion in section 3.4 have clearly illustrated the finer flow details for both laminar and turbulent instances. The influence of actual heat sink length on flow characteristics is however still an important aspect that remains outstanding. It is of particular importance in chapter 4, where the compact flow model will be deduced.

Figure 3.14 has been modelled by way of example for a low blockage ratio heat sink with the following geometric parameters (see appendix A table 8):

Hf = 20 mm.
Hb = 25 mm.
s = 5 mm.
t = 5 mm.
L = 50, 150, 300 mm.

The results are presented in normalised format for one laminar ($Uo = 1\ m/s$) and one turbulent velocity ($Uo = 8\ m/s$).

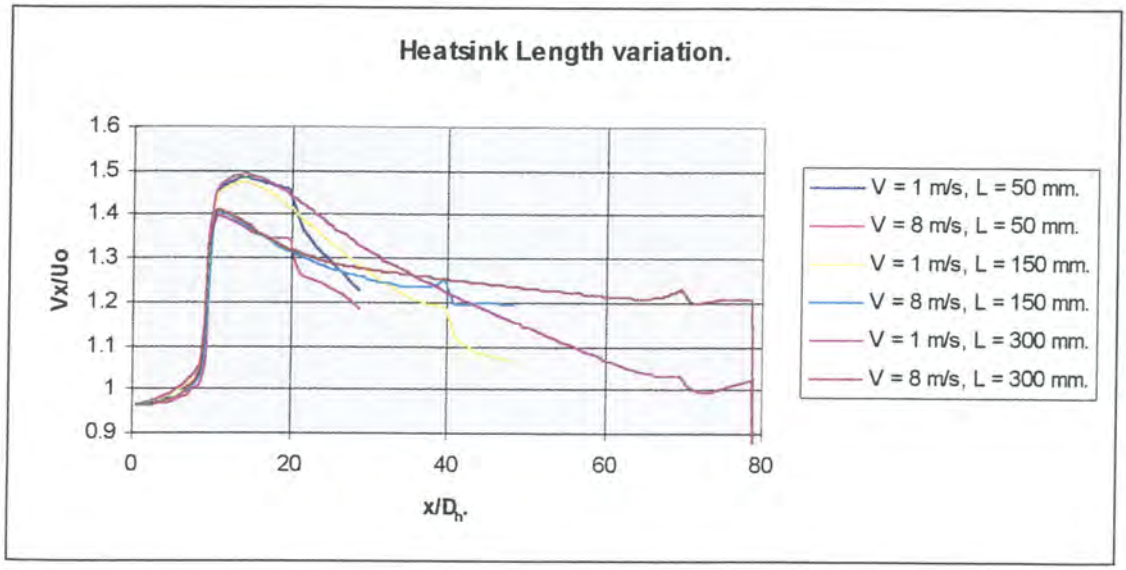

Figure 3.14 The effect of length on heat sink flow behaviour.

Figure 3.14 clearly illustrates that heat sinks of the same geometric configuration and blockage ratio exhibit very similar longitudinal flow behaviour, independent of actual heat sink length. It therefore suggests that it is possible to predict long heat sink flow characteristics if shorter heat sink detail is available, and vice versa. Other heat sink geometries modelled exhibit similar flow behaviour with heat sink length variation.

3.5.2 The effect of heat sink blockage ratio on flow behaviour

The effects of heat sink blockage ratio on flow behaviour is very extensive due the variety of geometric parameters which have an influence on the blockage ratio. Details of the geometric parameter variation are as per chapter 2 figure 2.1, with details on heat sink geometries to be found in appendix A tables 1-6.

Due to the nature and quantity of the data which exhibit very similar behaviour to the results of section 3.4, no details will be presented in this section. All results and simulations may be found in appendix B, with only the most important conclusions discussed in this section, which are as follows:

- The effects of flow bypass become more pronounced as the blockage ratio increases.
- The contraction and expansion losses exhibit significant change with blockage ratio variation, but much less with variation in Reynolds number. This is in agreement with trends presented by Kays [23].
- The interfin friction factor for low fins with wide fin gaps differ significantly from the friction factor for high fins with small gaps at similar Reynolds numbers. This suggests that the parallel plate friction factor approach used in many compact models [8, 11] is not valid for some heat sink configurations.
- Other flow behaviour is very much in line with what was discussed in section 3.4.

3.6 CONCLUSION

In this chapter, the results of FLOTHERM for CFD modelling of longitudinal fin heat sinks over both laminar and turbulent velocity ranges have been discussed in detail for a variety of heat sinks with and without tip bypass as mentioned in chapter 2.

The heat sink geometric parameters varied for the CFD study were as follows:

- Heat sink length.
- Heat sink blockage ratio, which is a function of the following parameters:
    - Fin height.
    - Fin gap.
    - Fin thickness.
    - Tip bypass height.

Only representative results were presented and discussed, while the remainder and comparison of results may be found in appendix B.

For verification purposes, the CFD results were first compared to the experimental results of Butterbaugh and Kang [8], with good agreement throughout for laminar flow. Unfortunately it was impossible to compare turbulent results with experimentally determined values, although excellent results was obtained by Gopalakrishna [6] for turbulent flows in longitudinal fin heat sinks, which was taken as sufficient for the purpose of this study.

Some important conclusions were determined through the course of the chapter through detailed examination of flow and pressure results. The most important of these are listed below:

- The flow and pressure details of the simulation combine well to create a detailed overall picture of the flow characteristics within the particular heat sink. Both local variations and global trends may be observed.

- The effects of flow bypass increase with an increase in heat sink blockage ratio.

- Flow contraction and expansion details for a variety of heat sinks agree well with the trends presented by Kays [23].

- For a heat sink with tip bypass the longitudinal interfin flow as well as the tip bypass flow exhibits predictable exponential behaviour with length progression due to the effects of leakage velocity. The similarity extends to geometrically similar heat sinks of different lengths, which suggests that the flow behaviour of a long heat sink may be predicted with confidence if the flow details of a geometrically similar heat sink of shorter length are known, and vice versa.

- Standard laminar and turbulent flow profiles may be found in the channel interfin region and tip bypass region, depending on the Reynolds number. This is very important when the heat transfer coefficients are calculated.

- The effects of flow bypass are much more pronounced for low velocity laminar flows than for highly turbulent flows. The Reynolds number also has a definite influence on the interfin friction factor for laminar flow, but this effect is much less pronounced for highly turbulent flows.

The results and conclusions determined during the course of chapter 3 may now be used in chapter 4 for the development of a compact model for the prediction of flow and pressure loss in longitudinal fin heat sinks with tip bypass.

CHAPTER 4

COMPACT MODELLING OF LONGITUDINAL FIN HEAT SINKS

4.1 PREAMBLE

Thus far in this study the flow characteristics of the longitudinal fin heat sink with and without tip bypass have been examined extensively utilising CFD methods for a variety of Reynolds numbers and geometric parameters, with good results. Details of both flow and pressure have been obtained and presented in chapter 3.

As discussed earlier CFD modelling is unfortunately both time consuming and computationally expensive, which is why the industry has identified the need for lumped parameter or compact models. These models should be easy and fast to use, and must provide accurate flow and pressure predictions over a wide range of heat sink geometries and Reynolds numbers.

Chapter 4 will focus on the development and evaluation of a new compact flow model for forced flow in longitudinal fin heat sinks. It should address the problems and inherent inaccuracies of other compact flow models in use today (see section 1.3), and be able to accurately predict flow behaviour over a wide range of heat sink geometries and Reynolds numbers. The mathematical computer program MATLAB for Windows will be used throughout for all programming purposes, due to its inherent simplicity and ease of use.

The first section of this chapter will focus on expanding the theory of the QFIN compact model [11] (briefly discussed in the literature review of section 1.3). QFIN utilizes one of the leading compact models in use in the industry today. Both inherent modelling inaccuracies and practical problems with the QFIN compact model will be addressed.

A new compact model will then be developed, using the CFD results and conclusions reached during the course of chapter 3, as well as a variety of other results obtained from literature.

The flow predictions of both the new compact flow model and the QFIN model will then be evaluated through comparison with the CFD results of chapter 3 over the range of heat sinks as represented in figure 2.1 and detailed in appendix A. All results and variances will be discussed.

The chapter will be concluded in a brief summary, after which chapter 5 will present the final conclusions and recommendations of the study.

4.2 RELEVANT THEORY

4.2.1 THE QFIN MODEL

As discussed in the literature review of section 1.3, the QFIN model is an improved version of the basic Butterbaugh and Kang model [8], and probably one of the leading compact flow models in use today. The QFIN modelling strategy for forced flow in longitudinal fin heat sinks with tip bypass is presented below.

Modelling strategy and limitations

For a given approach velocity Uo and known heat sink duct dimensions, the airflow rate Q is used to determine the flow velocity in the finned region by applying pressure balance and mass conservation conditions. The model takes into account the area ratio of the heat sink, contraction and expansion losses in all regions, stagnation effects and frictional pressure drops.

To determine the fin flow velocity, the flow rate in the heat sink needs to be determined. This is done by considering each flow path in the duct with the heat sink obstruction and then determining the associated pressure losses in the system using a simple flow network system. This network identifies the mass flow rate (Q) , velocities U, and pressure losses (ΔP) in each section of the flow path. Subscripts identify the flow path (h = heat sink, t = tip), and the pressure drop mechanism (i = inlet contraction, f = frictional, e = exit expansion). A stagnation region occurs at the entrance to the heat sink, as well as at the exit of the heat sink. These are denoted by the subscripts s and b respectively. These components are added to the bypass region as losses and not as gains in the heat sink flow path so that the pressure drop directly across the heat sink can be calculated. The individual flow paths for a heat sink with tip bypass only can be modelled in a resistive flow network as below in figure 4.1 [11].

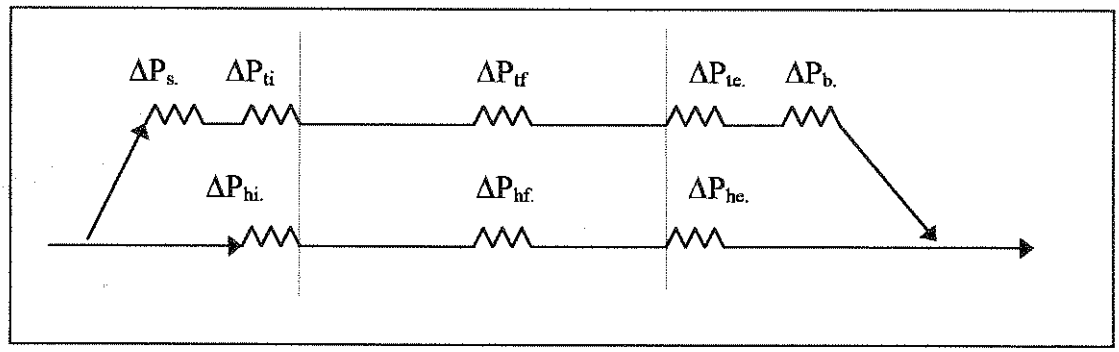

Figure 4.1 Flow resistance network.

Each individual flow path has to conform to a pressure drop balance and mass conservation laws so that

$$\Delta P_h = \Delta P_t \quad [4.1]$$

and

$$Q_h + Q_t = Q_{total} \quad [4.2]$$

This is achieved by estimating initial flowrates and then calculating the sum of each individual pressure drop mechanism in each flow path. The pressure drop in each flow path is then used to redefine the flow rates in each path and the process is repeated iteratively until both equations are satisfied. The results are presented as follows:

- Average interfin and tip velocity.
- Average pressure loss through the heat sink.

The inlet contraction losses and the exit expansion losses are adapted from Kays [23] and are represented as

$$\Delta P_i = K_i x \frac{1}{2} \rho U^2 \quad [4.3]$$

and

$$\Delta P_e = K_e x \frac{1}{2} \rho U^2 \quad [4.4]$$

where

$$K_i = -0.4152\alpha^2 + 0.0195\alpha + 0.3975 \quad [4.5]$$

and

$$K_e = 0.995\alpha^2 - 1.9913\alpha + 0.9989 \quad [4.6]$$

for turbulent flow and

$$K_i = -0.4152\alpha^2 + 0.0195\alpha + 0.7975 \quad [4.7]$$

and

$$K_e = 0.9911\alpha^2 - 2.3911\alpha + 1.0021 \quad [4.8]$$

for laminar flow.

U represents the average velocity for either the heat sink or the tip bypass region.

Transition from laminar to turbulent flow is assumed to take place at a Reynolds number of 2300. The contraction ratios for the two regions are assumed to be the following.

$$\alpha_t = \frac{U}{U_t}, \qquad \alpha_h = \frac{s}{s+t} \tag{4.9}$$

where $U = Uo$ is the average freestream duct velocity, s is the fin gap width, t is the fin thickness and the subscripts as defined above.

The frictional pressure drop in each region is calculated as

$$\Delta P_f = \frac{4Lf}{d_h} x \frac{1}{2} \rho U_f^2 \tag{4.10}$$

The Fanning friction factor (f) is as follows for hydrodynamically developing flow [5]:

$$f = \frac{1}{\mathrm{Re}} \left[\frac{3.44}{\left(x^+\right)^{\frac{1}{2}}} + \frac{24 + \frac{0.674}{\left(4x^+\right)} - \frac{3.44}{\left(x^+\right)^{1/2}}}{1 + 0.000029\left(x^+\right)^{-2}} \right] \tag{4.11}$$

And the hydrodynamic development length is equal to

$$x^+ = \frac{L}{\mathrm{Re}\left(d_h\right)} \tag{4.12}$$

The hydraulic diameter for the interfin region is assumed to be twice the fin gap as in the case for infinite parallel plates and is used as such for all calculations.

$$d_h = 2.s \tag{4.13}$$

The tip bypass region hydraulic diameter is similarly equal to

$$d_h = 2.H_b \tag{4.14}$$

The stagnation effects are treated as losses in the bypass region and are given as per Lessman [26] as

$$\Delta P_s = 0.8x \frac{1}{2} \rho \left(U^2 - U_{hs}^2\right) \tag{4.15}$$

$$\Delta P_b = C_d x \frac{1}{2} \rho \left(U^2 - U_{hs}^2\right), \quad \text{where } C_d = 0.2 \text{ for tip bypass.} \tag{4.16}$$

The QFIN model limitations

The QFIN model unfortunately has several shortcomings and inherent inaccuracies built into the solution procedure, which is briefly summarised below:

- The definition of the hydraulic diameter of the heat sink as $d_h = 2s$, as per parallel plate flow definition is not entirely satisfactory. It might be sufficient for high, narrow fins, but will be inadequate for short, wide type of fin arrangements. The hydraulic diameter used for the tip bypass region $d_h = 2\,H_b$ is similarly not correct for heat sinks with a large tip bypass height, where the parallel plate prediction will also be inaccurate.

- The solution obtains an average interfin and average tip velocity. It therefore uses the average velocity to determine the heat sink and tip contraction and expansion losses, which leads to inaccurate pressure loss predictions as it does not take the effects of leakage velocity into account.

- The equations used for the determination of the Kays [23] loss coeffisients can be improved upon.

- The solution only provides an average heat sink interfin and tip velocity with an average pressure loss. It therefore assumes uniform flow in the heat sink, which the results from chapter 3 has clearly shown to be exponential in nature due to the effects of flow leakage from the heat sink. This assumption may lead to inaccurate heat transfer coefficients being used to determine heat sink temperatures at a later stage in the thermal solver.

- The model uses velocity relations for determination of the α parameter in equation 4.9 for the tip bypass region, instead of actual geometric relations.

The above mentioned inaccuracies and shortcomings might have a small effect in some instances, but may cause large prediction inaccuracies in other heat sink configurations. It is therefore crucial that the new model address these issues if it is to be accurate over a range of different heat sink geometries and Reynolds numbers.

4.2.2 *The new model derived*

The new compact flow model to be derived in this section is based on the QFIN model, but uses some additional techniques and relations obtained through a variety of sources, including the CFD analysis of chapter 3, to address the discrepancies and inadequacies of the QFIN model discussed in section 4.2.1.

The exact flow resistance model approach of figure 4.1 is used, with some differences in the calculation methods of the various ΔP values.

Each individual flow path in figure 4.1 has to conform to a pressure drop balance and mass conservation laws so that

$$\Delta P_h = \Delta P_t \qquad [4.1]$$

and

$$Q_h + Q_t = Q_{total} \qquad [4.2]$$

In the new model this is achieved by calculating initial flowrates and then calculating the sum of each individual pressure drop mechanism in each flow path. The pressure drop in each flow path is then used to redefine the flow rates in each path and the process is repeated iteratively until both equations are satisfied. This is all very similar to the QFIN approach. The results are presented as follows:

- Average interfin and tip velocity.
- Average pressure loss through the heat sink.
- Interfin velocity distribution, which QFIN is unable to predict at this stage.

The inlet contraction and exit expansion losses are improved relations adapted from Kays [23] and Mills [34] and are represented as

$$\Delta P_i = \frac{1}{2}\rho U_i^{\,2}\left(1-\sigma^2\right)+\frac{1}{2}\rho U_i^{\,2}K_c \qquad [4.17]$$

and

$$\Delta P_e = -\left(\frac{1}{2}\rho U_e^{\,2}\left(1-\sigma^2\right)-\frac{1}{2}\rho U_e^{\,2}K_e\right) \qquad [4.18]$$

(Note the use of U_i and U_e instead of Uo as per QFIN).

where the coefficients are as follows:

Turbulent flow:

$$K_c = 0.0926\sigma^3 - 0.537\sigma^2 + 0.0435\sigma + 0.4009 + \zeta \quad [4.19]$$

where $\zeta = 0.003\left(\frac{\mathrm{Re}}{1e4}\right)^2 - 0.0411\frac{\mathrm{Re}}{1e4} + 0.0081$ for Re <= 100000 [4.20]

and $\zeta = 0$ for Re > 100 000. [4.21]

and

$$K_e = 0.0861\sigma^3 + 0.8235\sigma^2 - 1.9403\sigma + 0.9857. \quad [4.22]$$

Laminar flow:

$$K_c = -0.0856\sigma^3 - 0.2626\sigma^2 - 0.0582\sigma + 0.8088 \quad [4.23]$$

and

$$K_e = -0.0887\sigma^3 + 1.197\sigma^2 - 2.539\sigma + 1.0304 \quad [4.24]$$

Transition from laminar to turbulent flow is assumed to take place at Reynolds number *Re = 2500*. The above relations are similar in nature to the QFIN calculated contraction and expansion losses, but with some improved relations in the calculation of K_c and K_e. The problem lies in the calculation of the U_i and U_e velocities, which is to be used rather than the average velocities as per the QFIN model. This aspect will be discussed later during the course of this section.

The contraction ratios for the two regions are defined differently from the QFIN model and are calculated as follows from the definition of Kays [23]:

$$\sigma_t = \frac{H_b}{H_f + H_b}, \qquad \sigma_h = \frac{sH_f}{H_f(s+t)} \quad [4.25]$$

where H_f is the fin height, H_b the bypass height, s the fin gap width, and t the fin thickness.

The frictional pressure drop in each region is calculated in the same manner as per QFIN

$$\Delta P_f = \frac{4Lf}{d_h} x \frac{1}{2}\rho U_f^2 \quad [4.10]$$

The Fanning friction factor (f) is as follows for hydrodynamically developing flow:

$$f = \frac{1}{\mathrm{Re}}\left[\frac{3.44}{\left(x^{+}\right)^{\frac{1}{2}}} + \frac{24 + \frac{0.674}{\left(4x^{+}\right)} - \frac{3.44}{\left(x^{+}\right)^{1/2}}}{1 + 0.000029\left(x^{+}\right)^{-2}}\right] \qquad [4.11]$$

And the hydrodynamic development length is equal to

$$x^{+} = \frac{L}{\mathrm{Re}\left(d_h\right)} \qquad [4.12]$$

The hydraulic diameter for the interfin and tip bypass regions is calculated as per White [27].

$$d_h = \frac{4xArea}{Wetted\_perimeter} \qquad [4.26]$$

This gives the following equations for the tip and interfin regions:

Interfin region:

$$d_h = \frac{4sH_f}{\left(2H_f + s\right)} \qquad [4.27]$$

Tip bypass region:

$$d_h = \frac{4H_b\left(s+t\right)}{\left(2t + s + 2H_b\right)} \qquad [4.28]$$

The stagnation effects are once again treated as losses in the bypass region and are given as per Lessman [26] as

Laminar flow:

$$\Delta P_s = 0.8x\frac{1}{2}\rho\left(U^2 - U_t^2\right) \qquad [4.29]$$

$$\Delta P_b = C_d x\frac{1}{2}\rho\left(U^2 - U_t^2\right), \text{ where } C_d = 0.2 \text{ for tip bypass.} \qquad [4.30]$$

Turbulent flow:

$$\Delta P_s = 0.4x\frac{1}{2}\rho\left(U^2 - U_t^2\right) \quad [4.31]$$

$$\Delta P_b = C_d x\frac{1}{2}\rho\left(U^2 - U_t^2\right), \text{ where } C_d = 0.1 \text{ for tip bypass.} \quad [4.32]$$

Transition to turbulent flow is once again taken at $Re = 2500$. The above equations differ from the QFIN relations in two main aspects. As the above equations represent the flow losses over a blunt body for the tip bypass region [26], the velocity U_t should be used in equations 4.28 and 4.29 rather than the velocity U_h as per QFIN (Eq.4.15 & 4.16). Extensive testing over the range of heat sinks modelled in this study has also shown the coefficients for the turbulent stagnation pressure loss to be approximately ½ the losses for the laminar instance.

The only aspect which remains to be determined is the calculation of U_i and U_e to be used in equations 4.31 & 4.32 for calculation of contraction and expansion pressure losses. This will address one of the major discrepancies of the QFIN model.

Calculating U_i and U_e.

Calculation of U_i and U_e consists of modelling three geometrically similar heat sinks of different lengths using the new model instead of just one heat sink, using the equations as discussed in section 4.2.2. The three heat sinks modelled are as follows:

- Infinitely short heat sink.
- Infinitely long heat sink.
- Intermediate length heat sink.

This approach allows the elimination of certain errors from which the relation between maximum inlet, minimum exit, and average regional velocity may be determined. The approach therefore artificially takes the effects of leakage velocity into account. The results of chapter 3 section 3.5 then allows the incorporation of these relations in the final solution.

The infinitely short heat sink approach.

Firstly, an infinitely short heat sink of exactly similar geometry as the desired heat sink in question is modelled. This heat sink can safely ignore the effects of flow leakage due to the short length, and provide an accurate estimate of the flow contraction behaviour according to the relations of Kays [23]. An average tip and fin velocity is obtained from the simulation, which eliminates the inherent fault of ignoring flow leakage effects in the determination of local contraction and expansion velocities.

The infinitely long heat sink approach

In the second calculation an infinitely long heat sink of similar geometry is modelled. In this heat sink the effects of flow contraction on entrance to the heat sink and flow expansion on exit from the heat sink can be assumed negligible compared to the interfin friction losses. This eliminates the error of using average velocities for the calculation of ΔP_i and ΔP_e as the effect of contraction and expansion losses are negligible. Once again an average tip and fin velocity is obtained as a result.

The intermediate length heat sink

An intermediate length heat sink is also modelled using average fin and tip velocities in order to provide a third reference value of fin and tip average velocity values. Although these values include all the inherent faults evident in the normal compact models, it serves as a third point of reference for the curve fit.

Due to the predictable nature of the interfin flow behaviour in a heat sink with tip bypass as is evident from the results of chapter 3, and the effects of heat sink length as discussed in section 3.5 it is now possible to fit a hyperbolic curve through the average fin velocities obtained in the long, short, and intermediate heat sink simulations [37]. The curve equation is of the form

$$y = \frac{1}{Ax + B} \qquad [4.33]$$

This provides a relationship curve between the interfin velocity and the heat sink length. Due to the inherently predictable behaviour of the flow as a function of heat sink length as determined from chapter 3 section 3.5 it is now possible to estimate the fin entrance and exit velocities of the actual heat sink to be modelled. Through integration of the interfin velocity curve the average interfin velocity of the actual heat sink may also be estimated. The tip entrance, exit, and average velocities may in each case be obtained from continuity relations. This entire process may be presented schematically as in figure 4.2.

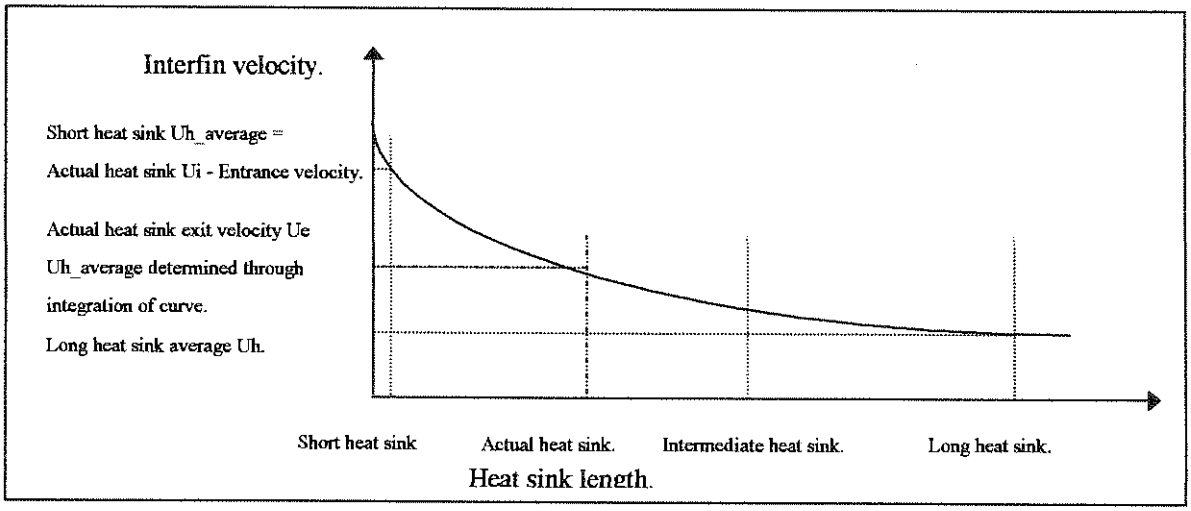

Figure 4.2 Schematical representation of long and short heat sink approach

As mentioned the average interfin heat sink velocity U_h can be estimated for the actual heat sink through integration of equation 4.33 over the length of the actual heat sink. It may then be used to estimate the relationship between heat sink entrance, exit, and average velocity for the actual heat sink. From continuity the same relationship can be determined for the tip bypass region.

Therefore for the heat sink: $$\alpha_{Hf\_in} = \frac{U_{hi}}{U_h},\ \alpha_{Hf\_out} = \frac{U_{he}}{U_h} \quad [4.34]$$

and for the tip region: $$\alpha_{Hb\_in} = \frac{U_{ti}}{U_t},\ \alpha_{Hb\_out} = \frac{U_{te}}{U_t} \quad [4.35]$$

The above relations can then be used in the iterative procedure for the actual heat sink flow modelling to determine U_i and U_e in equation 4.17 and 4.18.

Through testing it was found that the estimated average interfin velocity using integration and the long/short heat sink approach is within 5 % of the final predicted average interfin velocity. This highlights once again the highly predictable nature of the flow behaviour once certain detail becomes available, and makes further iteration to determine the absolute exact relationships in equations 4.34 and 4.35 unnecessary.

4.3 RESULTS AND DISCUSSION

In section 4.2 the relevant theory of both QFIN and the new compact model has been discussed in detail. What remains is the testing of both models over a variety of heat sink geometries and Reynolds numbers in order to compare performance. Both models will be evaluated against the heat sinks depicted in section 2.1, and detailed in appendix A, and will be compared to the CFD results of chapter 3. The results will be presented in graph format in this section, while the tabled results of actual values may be found in appendix C.

As mentioned the two compact models provide results in terms of the following:

- Average interfin and tip velocity.
- Average pressure loss.
- The new model also provides a predicted interfin velocity distribution.

The following section will evaluate the predicted pressure loss results as it is indicative of the flow prediction accuracy, while section 4.3.2 will focus on the prediction of interfin flow velocity distribution by the new compact model.

4.3.1 *Compact model predicted pressure loss results and variance discussion*

As mentioned the compact model results will be evaluated for the range of heat sinks (no. 1 - 6) discussed in chapter 2 and detailed in appendix A. Two graphs will be presented for each heat sink modelled, namely:

- Actual pressure loss prediction in [Pa] vs. Freestream velocity *Uo* for:
  - CFD model.
  - QFIN.
  - New model.
- Prediction variance vs. Freestream velocity when results of QFIN and the New model is compared to the CFD results of FLOTHERM.

The results of each heat sink will be followed by a short discussion.

Heat sink 1

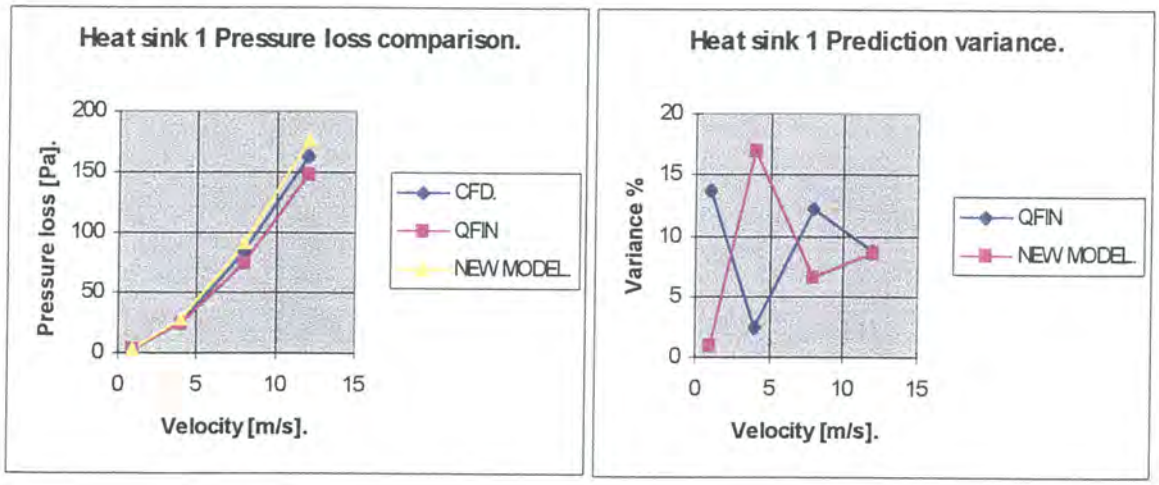

Fgure 4.3 Heat sink 1 results and variance graph.

The results for heat sink one which is essentially a high blockage ratio heat sink with high narrow fins are quite good for both models, with QFIN having an average variance of 9.3 % and the new model a variance of 8.2 %.

Heat sink 2

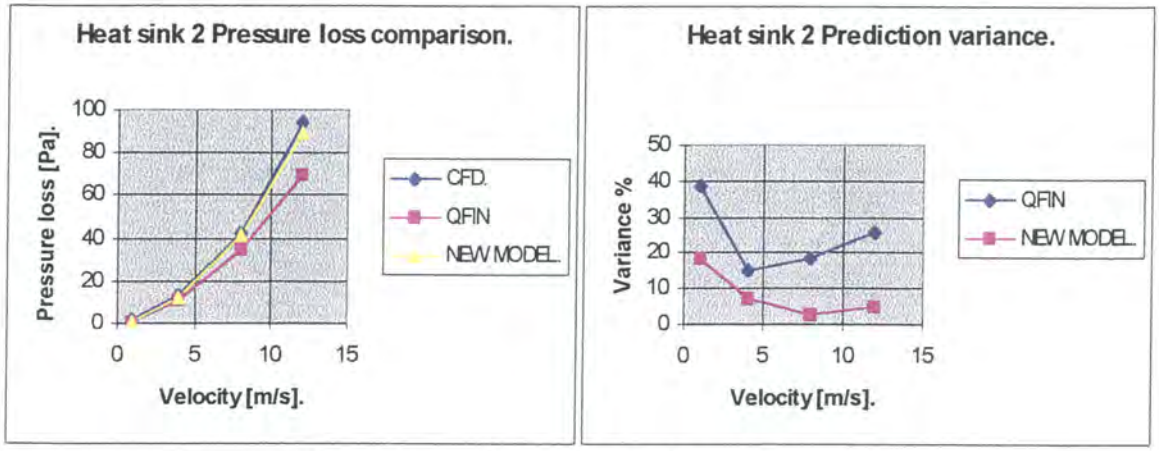

Figure 4.4 Heat sink 2 results and variance graph.

The predicted results for heat sink 2 which is essentially a small fin gap, short fin heat sink with a high bypass height is also reasonably good for the new model, with an average variance of 8.3 % and a highest variance of 18.3 %. The QFIN results are not quite so accurate with an average variance of 24.5 % and a highest variance of 38. 8 % for a velocity of 1 m/s.

Heat sink 3

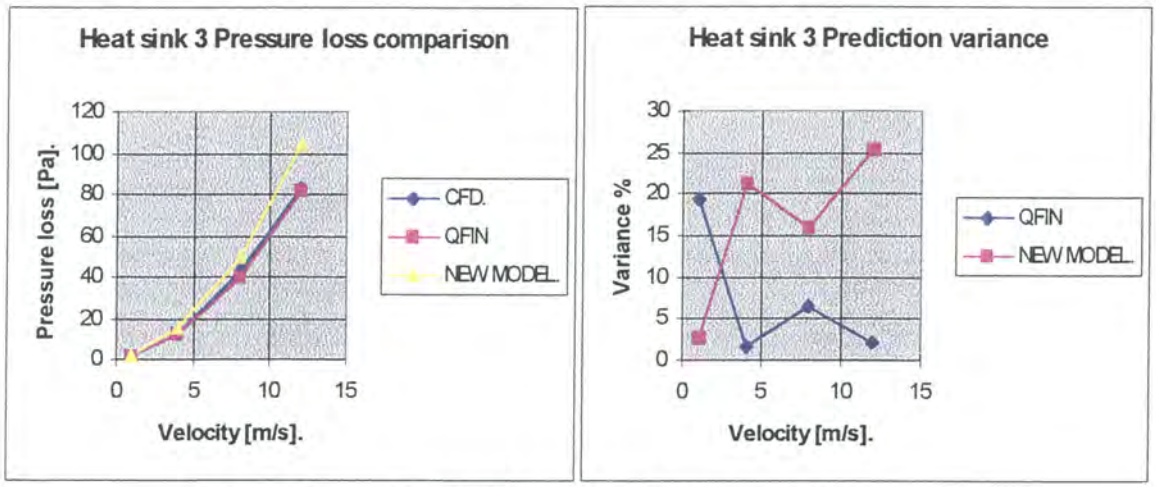

Figure 4.5 Heat sink 3 results and variance graph.

Heat sink 3 is essentially a high fin heat sink with an increased fin gap compared to heat sink 1, and the same bypass height. The QFIN results are very good in this particular instance with the new model tending to over predict the pressure loss. Average variance for QFIN is 7.4 %, while the new model has an average variance of 16.2 %.

Heat sink 4.

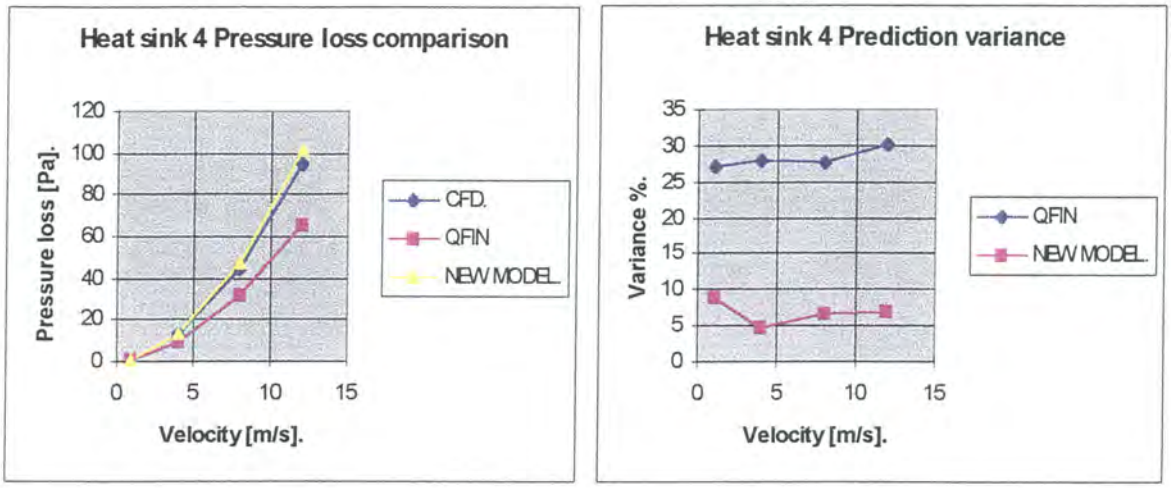

Figure 4.6 Heat sink 4 results and variance graph.

Heat sink 4 is a low, thick finned heat sink with a large interfin gap, and an intermediate tip bypass height. In this instance the new model tends to under predict the pressure loss with an average variance of 6.8 %, while the QFIN results completely underpredict the pressure loss with a value of 28.3%. The QFIN model is therefore utterly unsuitable for this particular application.

Heat sink 5

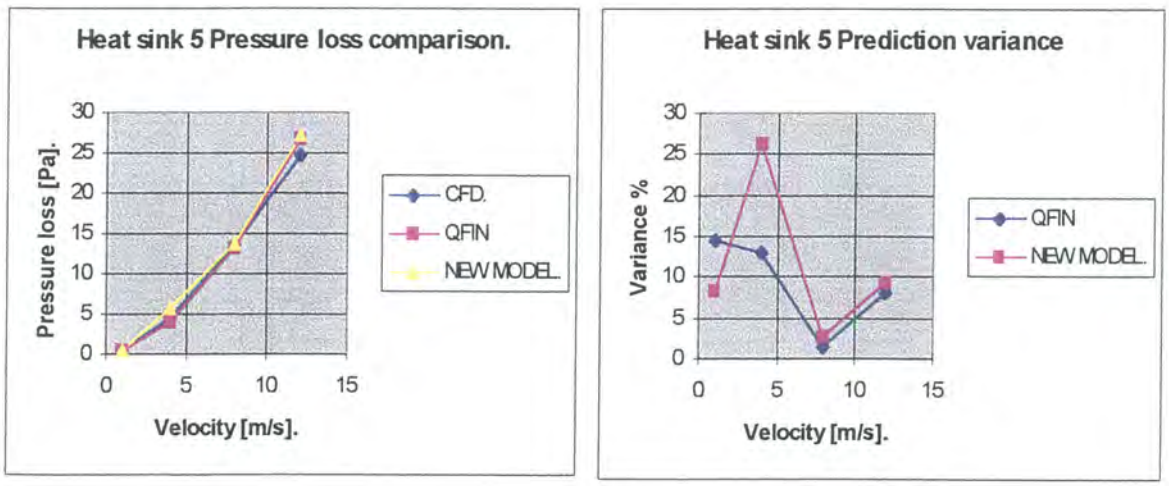

Figure 4.7 Heat sink 5 results and variance graph.

Heat sink 5 is a heat sink with the same dimensions and tip bypass height as heat sink 4, but with a fin height of only ¼ that of heat sink 4 *(Hf = 5 mm)*. For this application both QFIN and the new model proves to be quite accurate, with an average variance of 9.3 % for QFIN and 11.7 % for the new model.

Heat sink 6.

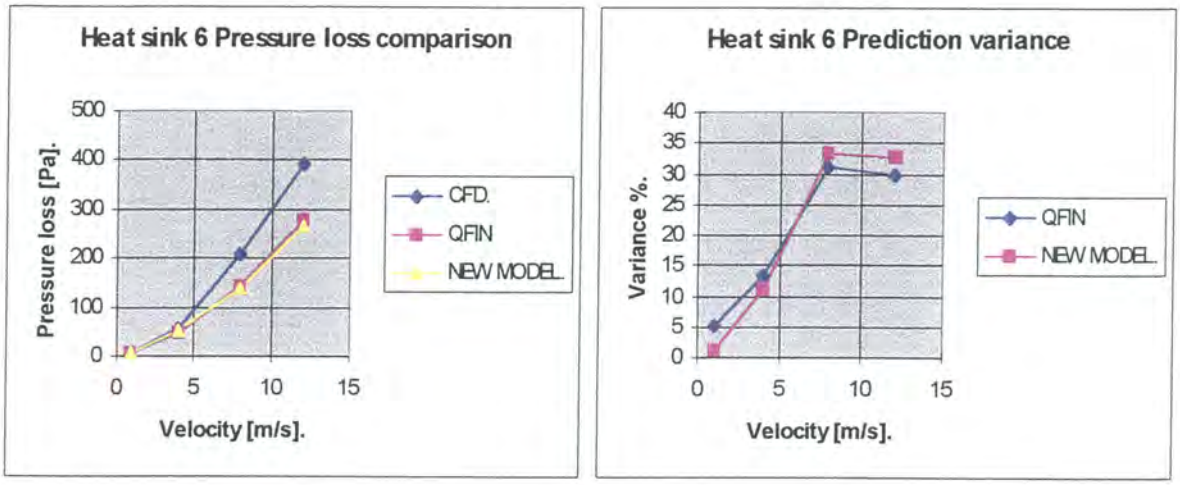

Figure 4.8 Heat sink 6 results and variance graph.

Heat sink 6 is a high, narrow finned heat sink with no tip bypass. Both QFIN and the new model predicts the lower laminar velocity range pressure loss very well, but fail in the prediction of pressure loss at higher turbulent velocities. The occurrence of such flows for this particular type of heat sink in practice is however very limited. Average variance for both QFIN and the new model is approximately 19.7 %.

Average variance as a function of geometry and velocity

While the previous graphs provide much detail on the various compact model predictions over a range of heat sink geometries, a summary of variances is still necessary to fully characterise the behaviour and accuracy of the two compact models in question. In this section two graphs will be presented, which will compare the compact models' accuracy with CFD results over all heat sink geometries tested as a function of freestream velocity, as well as a graph summarising the variance for both models over all velocity ranges for a particular heat sink.

Figure 4.9 plots average variance in percentage over all heat sink geometries discussed in section 4.3.1 as a function of freestream velocity.

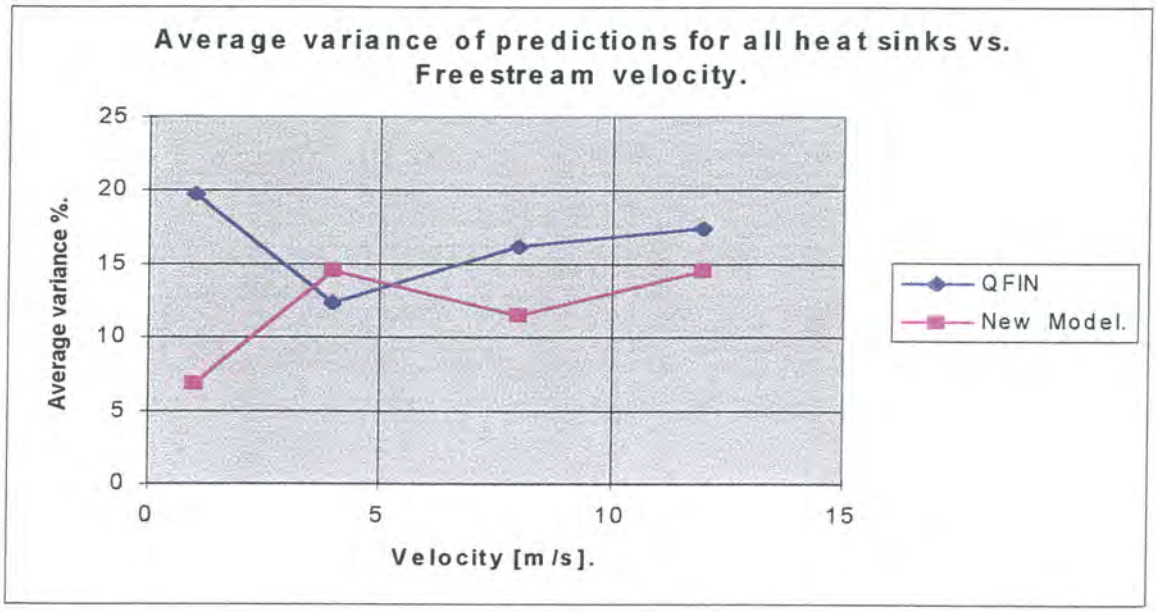

Figure 4.9 **Average predicted variance for all heat sinks vs. Freestream velocity.**

As is evident from figure 4.9 the QFIN model predicts the average pressure loss over the lower laminar velocity ranges for all heat sink geometries modelled with a variance of 19.8 %, which decreases to 17.5 % at the highly turbulent flow range. The poor prediction of QFIN in the lower laminar velocity ranges is especially a cause for concern.

The new model predicts the pressure loss over the lower laminar velocity ranges extremely accurately over the entire variety of heat sink geometries, with an average variance of less than 7 %. It then predicts progressively worse with the increase in Reynolds number until a final average variance of 14.6% is attained.

In almost all instances the new model average variance is much less than the average variance of the QFIN model.

Figure 4.10 plots the average variance in percentage over the entire velocity range modelled versus each individual heat sink configuration. It illustrates the accuracy of the two compact models over a range of heat sink geometries.

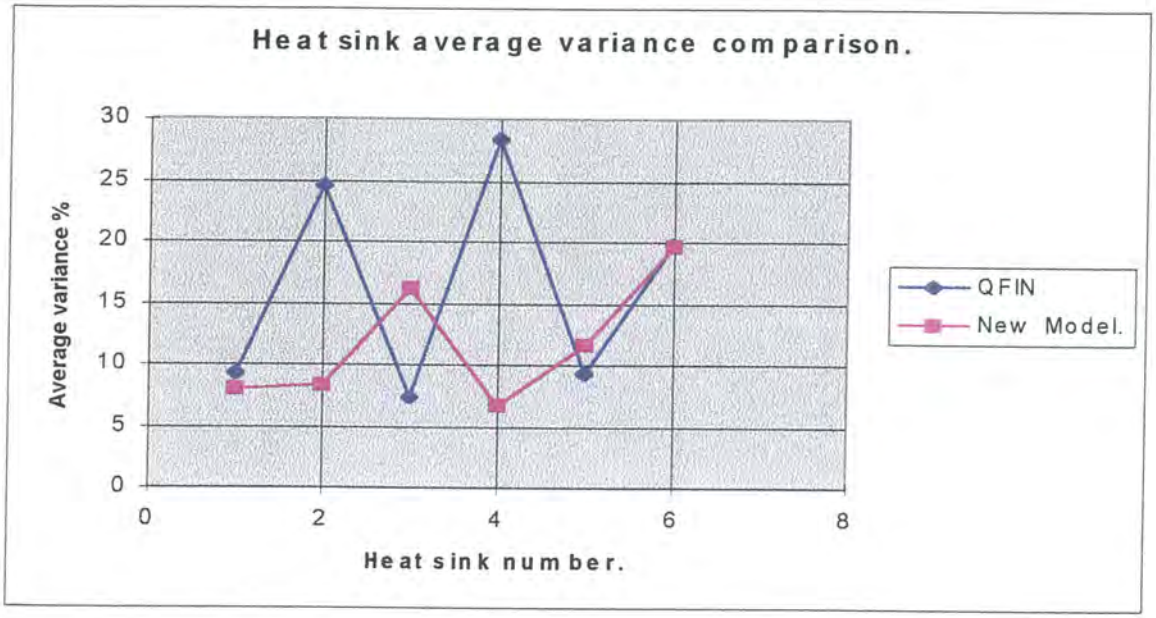

Figure 4.10 Average predicted variance vs. Heat sink geometry.

As mentioned figure 4.10 illustrates the accuracy of both QFIN and the new model for each individual heat sink configuration over the entire range of velocities modelled.

As is evident the accuracy of the results from QFIN vary considerably as a function of the heat sink geometry. QFIN provides particularly poor predictions for short fin, low blockage ratio heat sinks, where the average variance is in the region of 24 % for heat sink 2 and 28 % for heat sink 4. The QFIN average variance over all heat sink geometries and velocities tested is 16. 5 %, but the highest individual variance is 28 %. The model therefore has some problems with consistent accuracy in predicting the pressure loss independent of the heat sink geometry.

The new model proves to be very consistent in the prediction of pressure loss over most of the heat sinks and velocities modelled. With the exception of heat sink 6, the average variance never exceeds 17 %, independent of heat sink geometry. Heat sink 6 is an application which is very seldomly used in practice, where the average new model variance is in the order of 19.7%, and still compares favourably to the average variance of 19.8% from QFIN.

The average new model variance over the entire range of heat sinks and velocities modelled is 11.8 %, and compares very well with the 16.5 % achieved by the QFIN model. The new model therefore represents a 4.6 % improvement of predicted results compared to one of the leading compact models in the industry today.

4.3.2 *Prediction of interfin velocity distribution*

As discussed earlier the new model also has the capability to determine the interfin velocity distribution. This is particularly important in the calculation of heat transfer coefficients. In this section the velocity distribution predicted by the new compact model will be illustrated by comparison to the velocity distribution predicted by CFD analysis as in chapter 3. The heat sink to be evaluated is as per the detail of heat sink 1 as discussed in chapter 2 and detailed in appendix A. One laminar and one turbulent velocity will be modelled, with the freestream velocities as follows:

Uo = 1 m/s : Laminar flow.
Uo = 8 m/s : Turbulent flow.

The results are presented in figure 4.11.

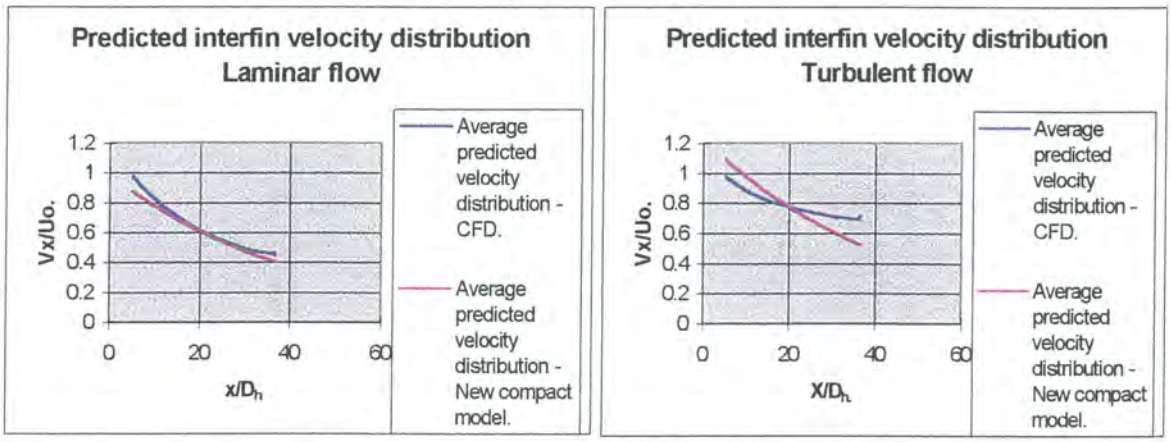

Figure 4.11 Predicted interfin velocity distribution.

As is evident from figure 4.11 the interfin velocity distribution for laminar flow is predicted very well by the new compact model, while the distribution for turbulent flow shows more variance compared to the CFD results. For both instances the distribution is however predicted more than accurate enough for heat transfer coefficient calculation purposes.

4.4 CONCLUSION

In this chapter a new compact flow model for the prediction of forced flow behaviour in longitudinal fin heat sinks with and without tip bypass was derived using the results and conclusions from chapter 3 and other data available from literature.

Results from the new model were compared to the CFD results from chapter 3 and QFIN, a compact flow model developed by Visser and Gauche [11] at the University of Pretoria. Results were compared using standard variance graphs over a range of heat sinks and Reynolds numbers, with data on the heat sink geometries to be found in appendix A and detailed result tables in appendix C.

Results from the new model compared favourably to results from QFIN over the range of Reynolds numbers and heat sink geometries examined. The new model proved to be consistently more accurate, with an average variance of 11.8 % compared to available CFD results. QFIN proved to be accurate in some instances, but highly inaccurate for certain heat sink geometries with an average variance of 16.5 % compared to the same CFD results. The new model therefore represents a 4.6 % improvement when compared to the results from QFIN. The new model also allows the prediction of an interfin velocity distribution, which is essential in the calculation of the heat transfer coefficients. The predicted velocity distribution compares well to available CFD results.

The new compact flow model may now with very little effort be extended to incorporate lateral and combined bypass, before inclusion into an overall compact solver for the temperature distribution in longitudinal fin heat sinks.

CHAPTER 5

CONCLUSIONS AND RECOMMENDATIONS

5.1 SYNOPSIS

The field of electronic systems design is rapidly advancing, and with it the ever increasing need for effective cooling of electronic enclosures using heat sinks. The modern trend of decreasing electronic component size, together with increased heat generation capacity makes it essential that optimal heat sink design is achieved for a given application. The two methods currently used extensively to that effect are CFD analysis, and compact modelling. CFD analysis is accurate, and provides a good understanding of flow behaviour, but is time consuming and computationally demanding. Compact modelling is in general faster and easier to use, but with much reduced accuracy compared to CFD results.

The study first provided some background on the field of electronics cooling, as well as an extensive literature survey on the subject. The study subsequently identified the need in the industry for better understanding and prediction of forced flow behaviour in longitudinal fin heat sinks with tip bypass, utilising both CFD and compact modelling to that effect.

The aim of the study was therefore to gain a better understanding of the flow behaviour using CFD modelling, and the eventual development of an improved compact model for the prediction of flow behaviour in longitudinal fin heat sinks with tip bypass. This effort will assist in the global drive for the use of compact modelling in the field of electronic enclosure design.

The commercially available CFD package FLOTHERM from FLOMERICS was used exclusively in the analysis of flow behaviour, after verification of the modelling strategy using available data from literature. Relevant laminar and turbulent flow behaviour, as well as the influence of the Reynolds number and geometric parameter variations on flow behaviour were investigated. A number of important deductions and conclusions were derived for later use in the development of a new compact model.

The mathematical computer program MATLAB was used as a programming device for the development of the new compact model. The new compact model was derived from available literature and the CFD results and conclusions derived earlier during the course of the study. Predicted results from both the new compact model and QFIN, a leading compact model in the field today, were compared to the CFD results from FLOTHERM for a variety of heat sink configurations and Reynolds numbers in order to gauge model performance.

Results from the new compact model represent on average a 4.6 % improvement over the predicted results from QFIN. It also proved to be consistently more accurate over the entire range of heat sinks and Reynolds numbers under consideration in this study. The new compact model also allows for the prediction of a heat sink interfin velocity distribution, which other existing compact models have been unable to achieve thus far. This aspect is essential in the accurate calculation of heat transfer coefficients for the thermal solution of the heat sink temperature distribution.

The study therefore contributed significantly towards the general understanding of flow behaviour in forced flow longitudinal fin heat sinks with tip bypass. The influence of geometric parameter variations on said heat sinks have also been documented extensively for future reference. The study also contributed significantly towards the improvement of the compact flow modelling approach for above mentioned heat sink configurations. The new compact model may finally be extended and incorporated in a complete compact model package for the accurate and fast solution of heat sink and electronic component temperature distributions.

5.2 CONCLUSIONS

Several important conclusions were determined through the course of the study. The most important of these are as follows:

- The use of CFD analysis for the simulation of forced flow in longitudinal fin heat sinks with tip bypass provides an excellent overall picture of the flow behaviour and characteristics. Both local variations and global trends may be observed. The most notable flow behaviour characteristics evident from the CFD analysis and parametric study are as follows:
    - The heat sink contraction and expansion losses agree with the trends described by Kays [23].
    - There is definite evidence of flow development in the heat sink. This development is more evident for laminar than turbulent flows.
    - The interfin friction factor varies considerably as a function of the Reynolds number. This behaviour is especially evident for laminar flows, but to a much lesser extent for turbulent flows.
    - Definite velocity profiles exist within the heat sink, in agreement with classical laminar and turbulent flow behaviour.
    - The tip bypass effect is more pronounced for laminar flows than highly turbulent flows.
    - The heat sink interfin flow is exponential in nature, and very predictable if information from a geometrically similar heat sink is available.

- The use of CFD analysis for the above mentioned application, although accurate and informative is rather time consuming and financially restrictive to the average individual.

- Compact modelling of heat sinks provide a very real alternative to CFD analysis in the prediction of heat sink flow behaviour. It is quick, less costly than CFD, and easy to operate, but accuracy in existing compact models is not always guaranteed. Current models also do not provide all the necessary flow information for the accurate calculation of heat transfer coefficients.

- Accurate compact modelling of forced flow in longitudinal fin heat sinks with tip bypass is indeed possible, and such a compact model has been derived during the course of this study. In addition this compact model also provides more flow information than existing models, and allows for the accurate calculation of heat transfer coefficients in the solution of the heat sink temperature distribution.

- Through extension of the newly developed compact flow model to include other effects like lateral and combined bypass it will indeed be possible to use the compact modelling approach with accuracy and confidence in modern electronic enclosure design.

5.3 RECOMMENDATIONS

Although much work has already been done in this and other similar studies in the field of electronics cooling, there are still much work remaining for future studies. This study recommends that future studies concentrate on the following main areas of concern:

- Improvement on the new compact model results in areas of poor performance as discussed in chapter 4.
- Extension of the new compact flow model developed in this study to include lateral and combined bypass effects in analysis.
- The extension of the new compact flow model to other heat sink geometries, for instance pin fins and stacked fin arrangements.
- Incorporation of the compact flow model and the velocity profile results of chapter 3 in a total compact model for the solution of temperature distribution in a typical heat sink.
- Extension of the complete compact model (flow and heat solver) in one package able to perform complete electronics systems design on a macroscopic level.

Once the above mentioned areas have been addressed it will truly allow compact modelling of heat sinks to become a cost effective and realistic alternative to CFD modelling in the design and development of electronic systems.

5.4 FINAL REMARKS

The field of electronics cooling has seen a lot of development and progress in recent times, due to the modern trend of smaller and more powerful electronic equipment. Even so, there is much that remains to be done in certain areas.

This study has identified some of the areas where major shortcomings exist, and addressed some of the discrepancies that were found. The study provided more understanding of flow behaviour in heat sink assemblies, and made a positive contribution towards the development of an accurate compact model approach to heat sink design and selection.

There is however still much remaining work to be done in the field of compact modelling of heat sinks prior to it fulfilling its full potential in the field of heat sink selection, design, and optimisation. The compact modelling of heat sinks therefore currently remains, and will continue to do so for a long time to come, a truly international research topic.

REFERENCES

[1]. Gauche, P., Coetzer, C. B., *" Characteristics of heat sink flow bypass for thermal modelling "*, Proc 5th International Conference for Advanced Computational Methods in Heat Transfer, Poland, pp 307 – 316, 1998.

[2]. Obinelo, I. F., *" Characterization of thermal and hydraulic performance of longitudinal fin heat sinks for system level modelling using CFD methods"*, ASME, 1997.

[3]. Gavali, S., Patankar, S., *" Effect of heat sink on forced convection cooling of electronic components: A numerical study "*, Advances in Electronic packaging, EEP-Vol. 4-2, ASME, 1993

[4]. Bar-Cohen, A., *" Air-Cooled heat sinks - Trends and future directions "*, Advances in electronics packaging, EEP-Vol. 19-2, ASME, 1997.

[5]. Knight, W., Goodling, J., *"Optimal thermal design of air cooled forced convection finned heat sinks - Experimental verification "*, IEEE Transactions on Components, Hybrids, and manufacturing Technology, Vol. 15, No. 5, October 1992.

[6]. Gopalakrishna, S., *" Numerical and experimental study of forced convection over power supply heat sinks"*, ASME Winter annual meeting, pp 1-6, December 1991.

[7]. Addison, S., *"Emerging trends in thermal modelling"*, Electronic packaging and Production, pp36 – 42, April 1999.

[8]. Butterbaugh, M. A., Kang, S. S., *"Effect of airflow bypass on the performance of heat sinks in electronic cooling "*, Advances in Electronic Packaging, EEP-Vol. 10-2, ASME, 1995.

[9]. Chapman, C., Schmidt, B., *" Thermal performance of an elliptical pin fin heat sink "*, Tenth IEEE semi-Therm, pp 24-31, 1994.

[10]. Lee, S., *" Optimum design and selection of heat sinks "*, Eleventh IEEE SEMI-THREM Symposium, 1995.

[11]. Visser, J.A., Gauche,P., *"Simulation of heat transfer in heat sinks"*, Proc. 4th International Conference for Advanced Computational Methods in Heat Transfer, Udine, pp 105 – 114, 1996

[12]. Chapman. C., Johnston, C., *" Cooling hot printed circuit assemblies "*, Electronic Packaging and Production pp 32 – 36, May 1999.

[13] Wirtz, R. A., Chen, W., *" Effect of* Flow *Bypass on the Performance of Longitudinal Fin Heat Sinks "*, Transactions of the ASME, Vol. 116, September 1994.

[14]. Ritchie, B., Serenson, J., *"Keeping your components cool"*, Electronic packaging and production pp 37 – 41, December, 1999

[15]. Patankar, S.V., *" Numerical heat transfer and fluid flow "*, McGraw-Hill, 1980.

[16]. White, F.M, *"Viscous Fluid Flow"*, second edition, McGraw Hill, New York, 1991.

[17]. Biber, C. R., *" Applying computational fluid dynamics to heat sink design and selection "*, Electronics cooling, Vol. 2, Jan 1996.

[18]. Biber, C. R., *" Pressure drop prediction for heat sinks: What is the best method ? "*, ASME, Vol 2, 1997.

[19]. Kim, S. J., Lee, S., *" On Heat sink measurement and characterization "*, INTERPACK'97, Hawaii, pp.1903 - 1909, 1997.

[20]. Morrison, A.T, *" Optimization of Heat sink fin Geometries for heat sinks in natural convection "*, InterSociety conference on thermal phenomena, 1992.

[21]. Linton, L. R., *" Coarse and detailed CFD modelling of a finned heat sink "*, InterSociety conference on Thermal phenomena, pp 156 - 161, 1994.

[22]. Linton, R, *" CFD modelling of electronic enclosures "*, Heat transfer in electronic equipment, ASME, 1991.

[23]. Kays, W.M, *" Loss coefficients for abrupt changes in flow cross section with low Reynolds number flow in single and multiple tube systems"*, Transactions of the ASME, pp 1067 - 1074, November 1950.

[24]. Jonsson, H., Moshfegh, B., *" Modelling of the thermal and hydraulic performance of plate fin, strip fin, and pin fin heat sinks – Influence of flow bypass "*, 2000 Inter Society Conference on Thermal Phenomena pp 185 – 192

[25]. Chu, H., Belady, C., *" A survey of high performance, high aspect ratio, air cooled heat sinks "*, ISPS'99 Proceedings pp71 – 76.

[26]. Sam, R.G, Lessman, R. C, *" An experimental study of flow over a rectangular body"*, Journal of Fluids engineering, Vol. 101, pp 443 - 448, December, 1979.

[27]. White, F.M, *" Fluid Mechanics"*, second edition, McGraw Hill, New York, 1988.

[28]. Lee, S., *" How to select a heat sink "*, Electronics cooling, Vol. 1, no. 1, June 1995.

[29]. Knight, R.W, Goodling, J.S., *" Optimal thermal design of forced convection heat sinks - Analytical "*, Journal of electronic packaging, Vol. 113, pp 313 - 321, September 1991.

[30]. Sparrow, E. M., Schneider, G. E., *" Handbook of numerical heat transfer "*, Wiley-Interscience publication, New York, 1988.

[31]. Anderson, D. A., Tannehill, J. C., *" Computational fluid mechanics and Heat Transfer "*, Hemisphere publishing corporation, USA, 1984.

[32]. *" FLOTERM REFERENCE MANUAL version1.4 "* , Flomerics Limited, England, 1995.

[33]. *"STAR-CD version 2.1 Methodology "*, Computational dynamics limited, 1991.

[34]. Mills,A.F,*"Basic heat and mass transfer"*, Donnoly and Sons company,USA,1995.

[35]. Beckwith, Marangoni, *" Mechanical measurements "*, Fifth edition, Addison-Wesley, USA, 1993.

[36]. Mathews, J.H, *" Numerical methods"*, second edition, Prentice Hall, USA, 1992.

[37]. O' Neil, P., *" Advanced Engineering Mathematics "*, third edition, PWS publishing company, Boston, 1993.

APPENDICES

APPENDIX A

CFD MODELLING STRATEGY SIMULATION MATRIX

HEAT SINK SIMULATION MATRIX AS PER FIGURE 2.1

Table 1.

Heat sink 1 - Basic heat sink model.

Uo - [m/s]	L - [mm]	Hb - [mm]	Fin thickness - [mm]	s - [mm]	Hf - [mm]	Turbulent/laminar
1	150	25	1.27	2.4	53	Laminar.
4	150	25	1.27	2.4	53	Laminar.
8	150	25	1.27	2.4	53	Turbulent.
12	150	25	1.27	2.4	53	Turbulent.

Table 2.

Heat sink 2 - Reduced fin height model.

Uo - [m/s]	L - [mm]	Hb - [mm]	Fin thickness - [mm]	s - [mm]	Hf - [mm]	Turbulent/laminar
1	150	38	1.27	2.4	26	Laminar.
4	150	38	1.27	2.4	26	Laminar.
8	150	38	1.27	2.4	26	Turbulent.
12	150	38	1.27	2.4	26	Turbulent.

Table 3.

Heat sink 3 - Increased fin gap model.

Uo - [m/s]	L - [mm]	Hb - [mm]	Fin thickness - [mm]	s - [mm]	Hf - [mm]	Turbulent/laminar
1	150	38	1.27	3.6	53	Laminar.
4	150	38	1.27	3.6	53	Laminar.
8	150	38	1.27	3.6	53	Turbulent.
12	150	38	1.27	3.6	53	Turbulent.

Table 4.

Heat sink 4 - Reduced fin height, increased fin gap and thickness.

Uo - [m/s]	L - [mm]	Hb - [mm]	Fin thickness - [mm]	s - [mm]	Hf - [mm]	Turbulent/laminar
1	150	27	5	5	20	Laminar.
4	150	27	5	5	20	Laminar.
8	150	27	5	5	20	Turbulent.
12	150	27	5	5	20	Turbulent.

Table 5.

Heat sink 5 - Extremely reduced fin height, else same as heat sink 4.

Uo - [m/s]	L - [mm]	Hb - [mm]	Fin thickness - [mm]	s - [mm]	Hf - [mm]	Turbulent/laminar
1	150	27	5	5	5	Laminar.
4	150	27	5	5	5	Laminar.
8	150	27	5	5	5	Turbulent.
12	150	27	5	5	5	Turbulent.

Table 6.

Heat sink 6 - No tip bypass heat sink.

Uo - [m/s]	L - [mm]	Hb - [mm]	Fin thickness - [mm]	s - [mm]	Hf - [mm]	Turbulent/laminar
1	150	0	1.27	2.4	53	Laminar.
4	150	0	1.27	2.4	53	Laminar.
8	150	0	1.27	2.4	53	Turbulent.
12	150	0	1.27	2.4	53	Turbulent.

Table 7.

Butterbaugh and Kang verification heat sink as per section 3.2

Uo - [m/s]	L - [mm]	Hb - [mm]	Fin thickness - [mm]	s - [mm]	Hf - [mm]	Turbulent/laminar
1	46	38	1.27	2.4	53	Laminar.
4	46	38	1.27	2.4	53	Laminar.

Table 8.

The influence of heat sink length on flow behaviour

Uo - [m/s]	L - [mm]	Hb - [mm]	Fin thickness - [mm]	s - [mm]	Hf - [mm]	Turbulent/laminar
1	50, 150, 300	25	5	5	20	Laminar.
8	50, 150, 300	25	5	5	20	Laminar.

APPENDIX B

THE INFLUENCE OF GEOMETRIC PARAMETER VARIATION ON FLOW BEHAVIOUR IN LONGITUDINAL FIN HEAT SINKS

HEAT SINK TIP BYPASS HEIGHT VARIATION.

Geometric parameters:

Hf = 53 mm
t = 1.27 mm.
s = 2.4 mm.
Hb = 25 & 38 mm.
Uo = 1 & 4 m/s - Laminar flow.
Uo = 8 & 12 m/s - Turbulent flow.

Laminar flow comparison.

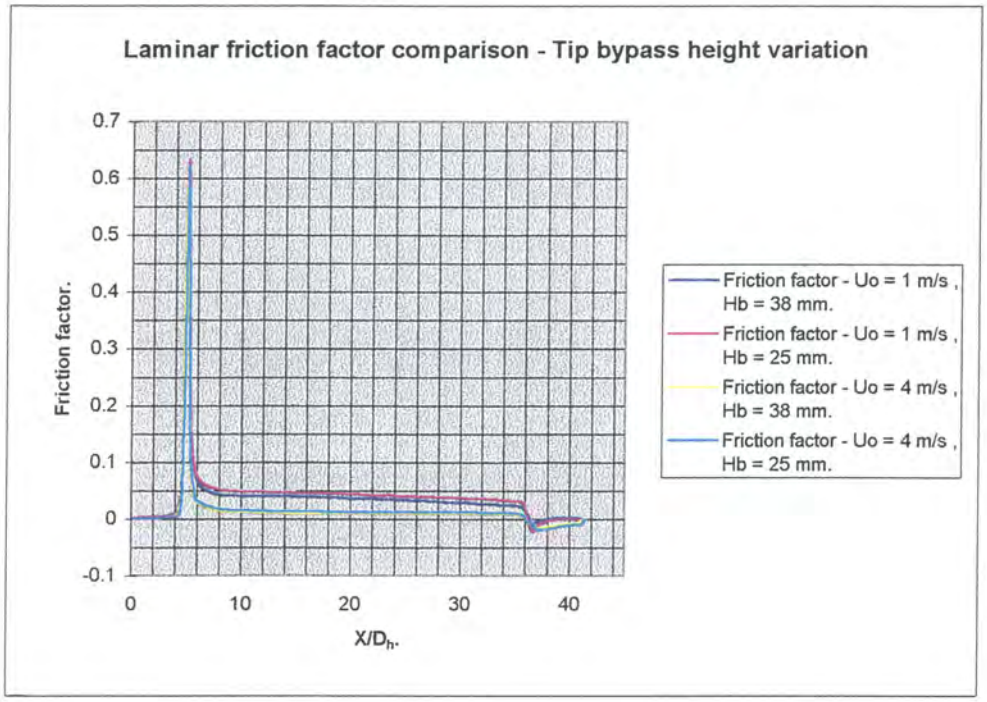

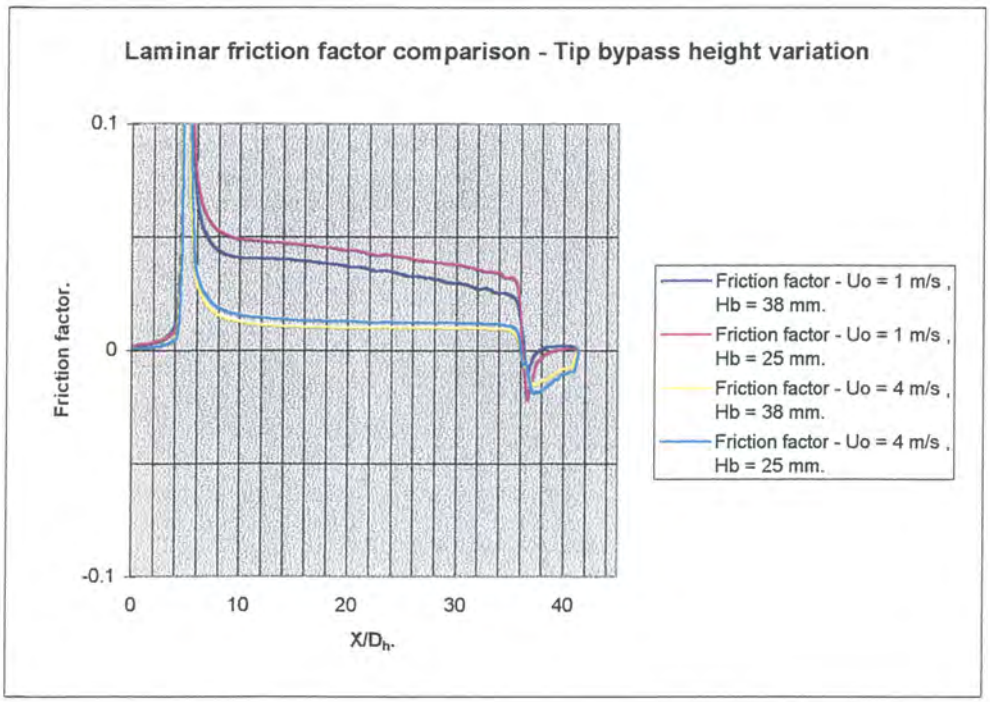

Turbulent flow comparison.

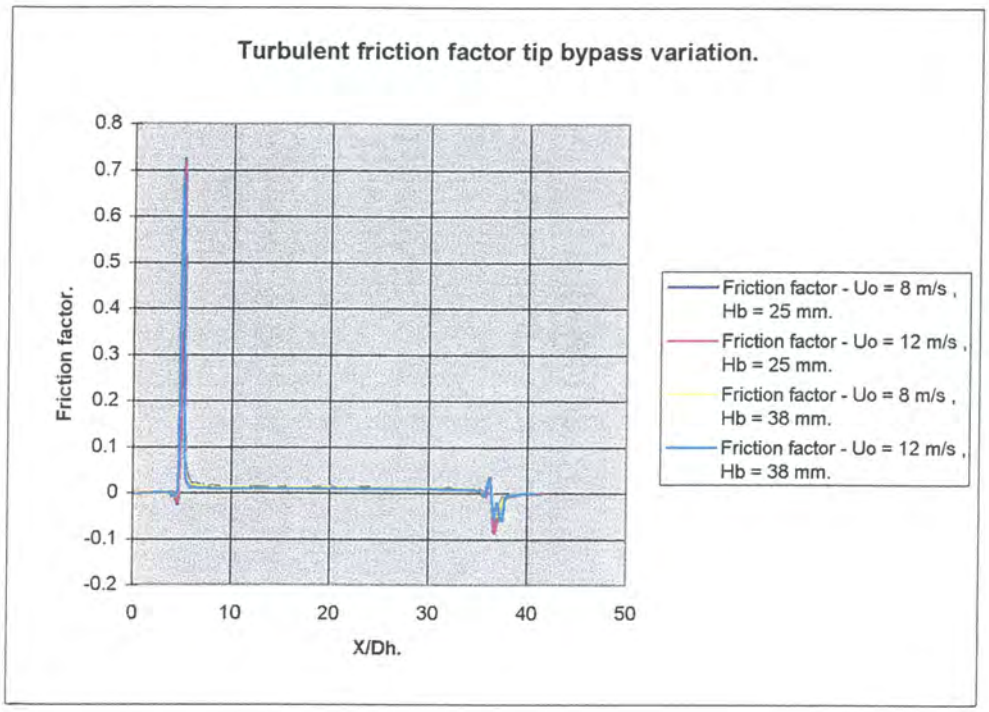

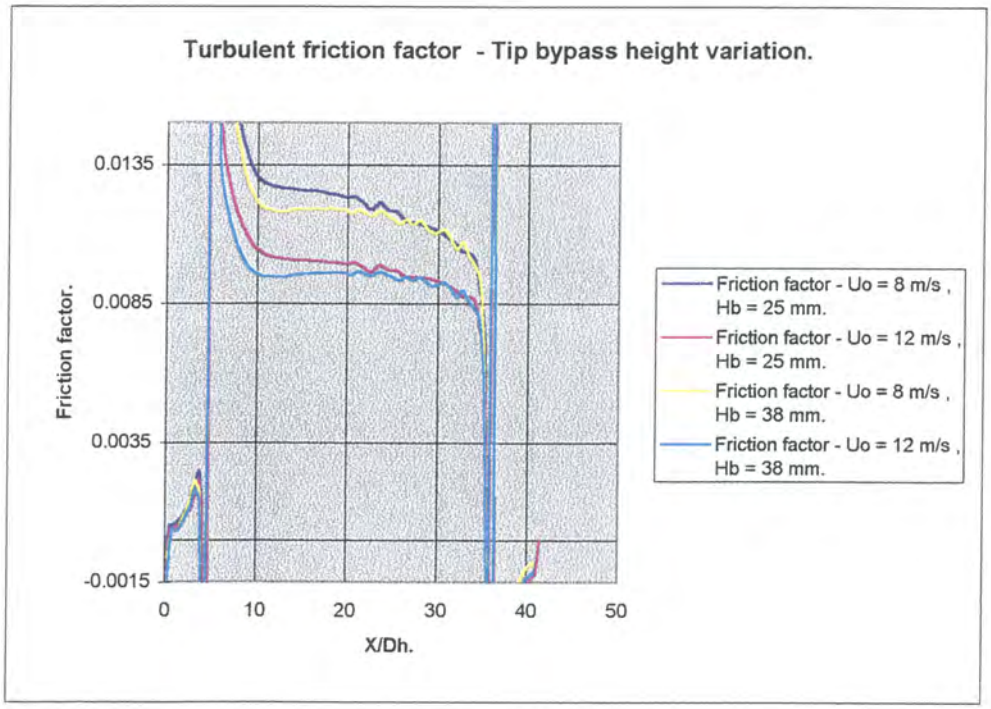

HEAT SINK FIN HEIGHT VARIATION.

Geometric parameters:

Hf = 53 & 26 mm
t = 1.27 mm.
s = 2.4 mm.
Hb = 38 mm.
Uo = 1 & 4 m/s - Laminar flow.
Uo = 8 & 12 m/s - Turbulent flow.

Laminar flow comparison.

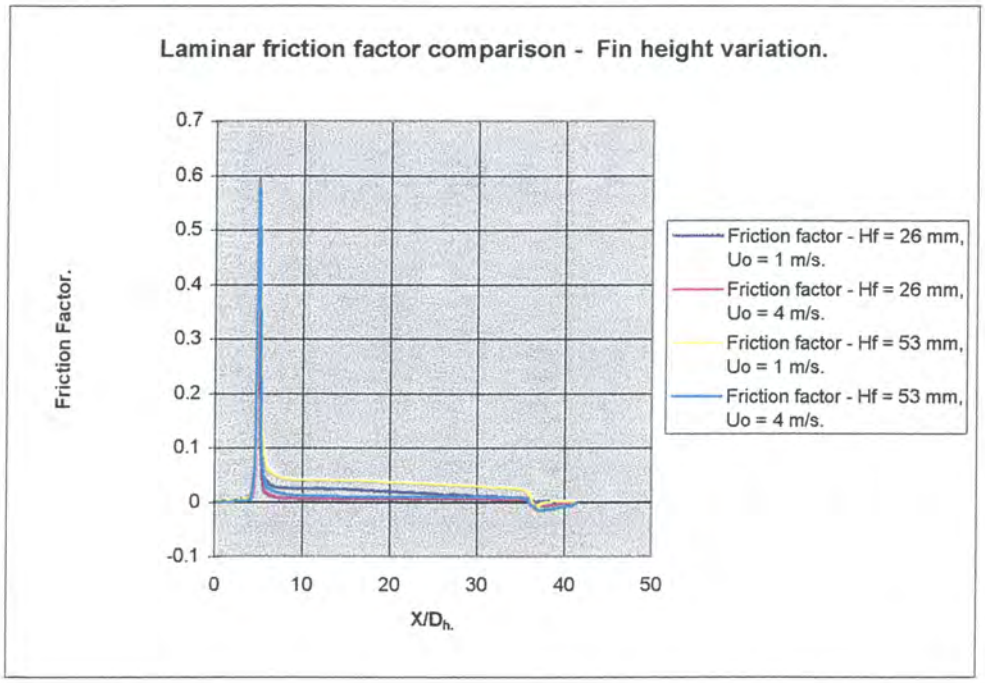

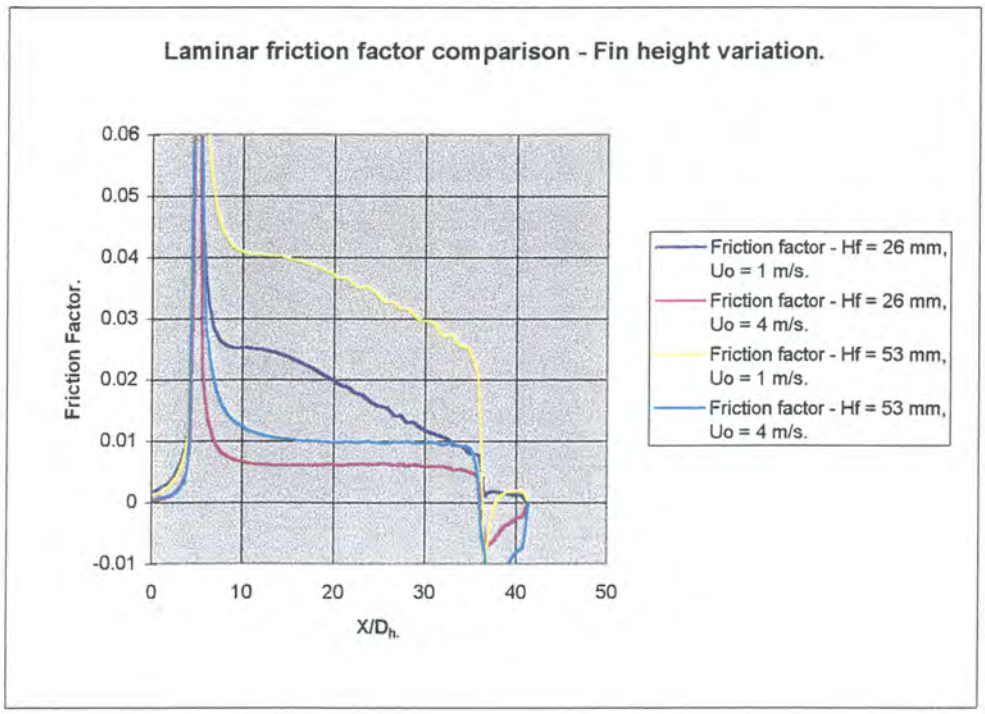

Turbulent flow comparison.

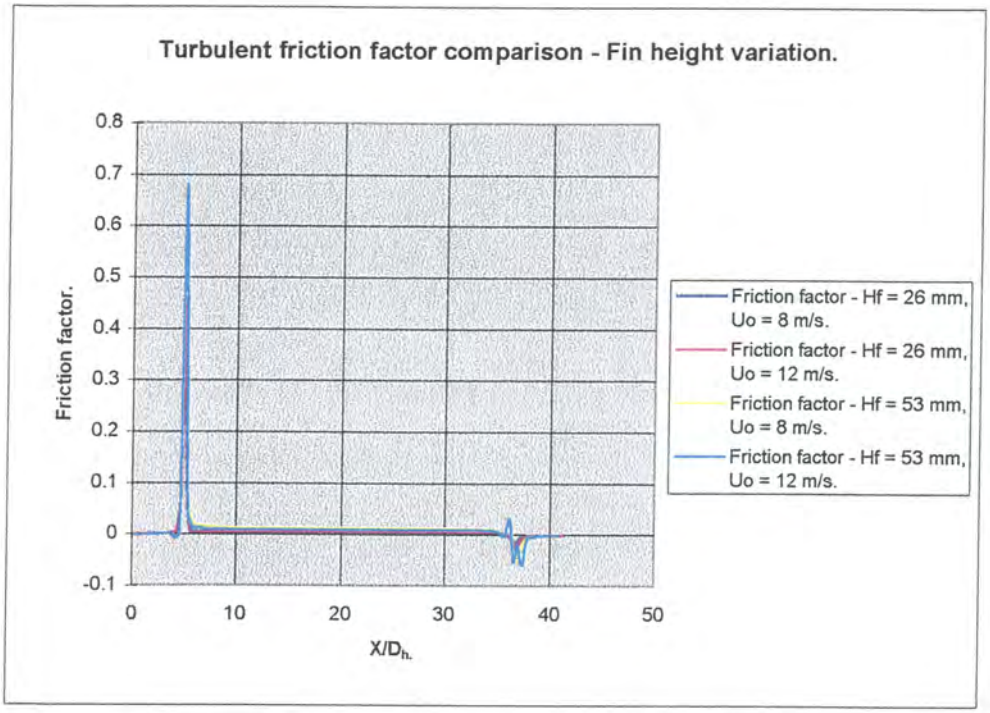

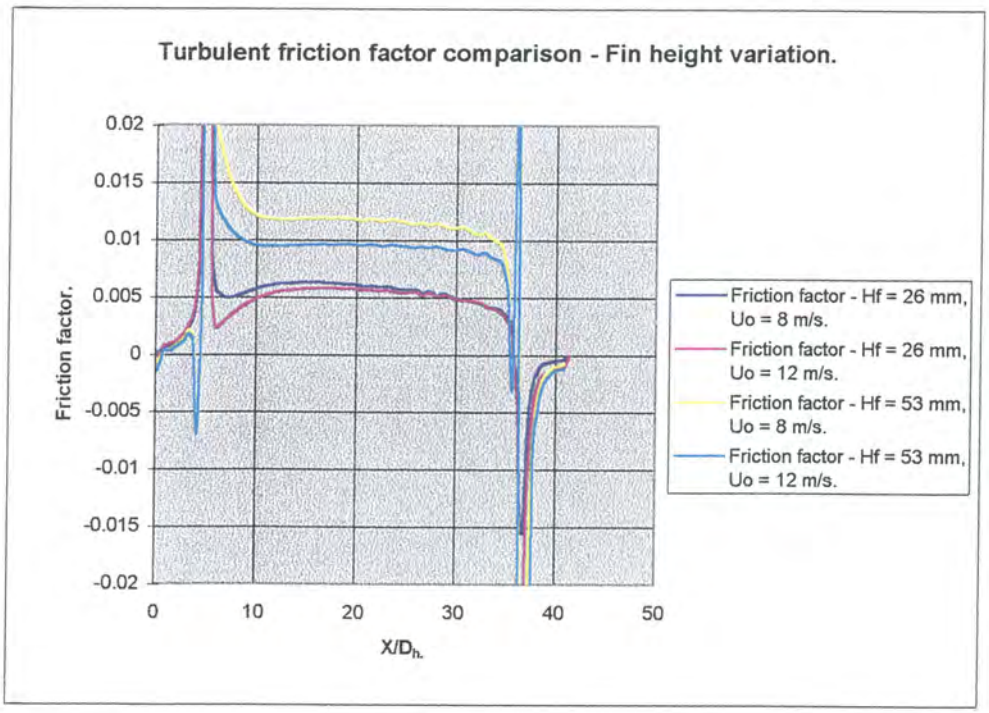

HEAT SINK FIN GAP VARIATION.

Geometric parameters:

Hf = 53 mm
t = 1.27 mm.
s = 2.4 & 3.6 mm.
Hb = 38 mm.
Uo = 1 & 4 m/s - Laminar flow.
Uo = 8 & 12 m/s - Turbulent flow.

Laminar flow comparison.

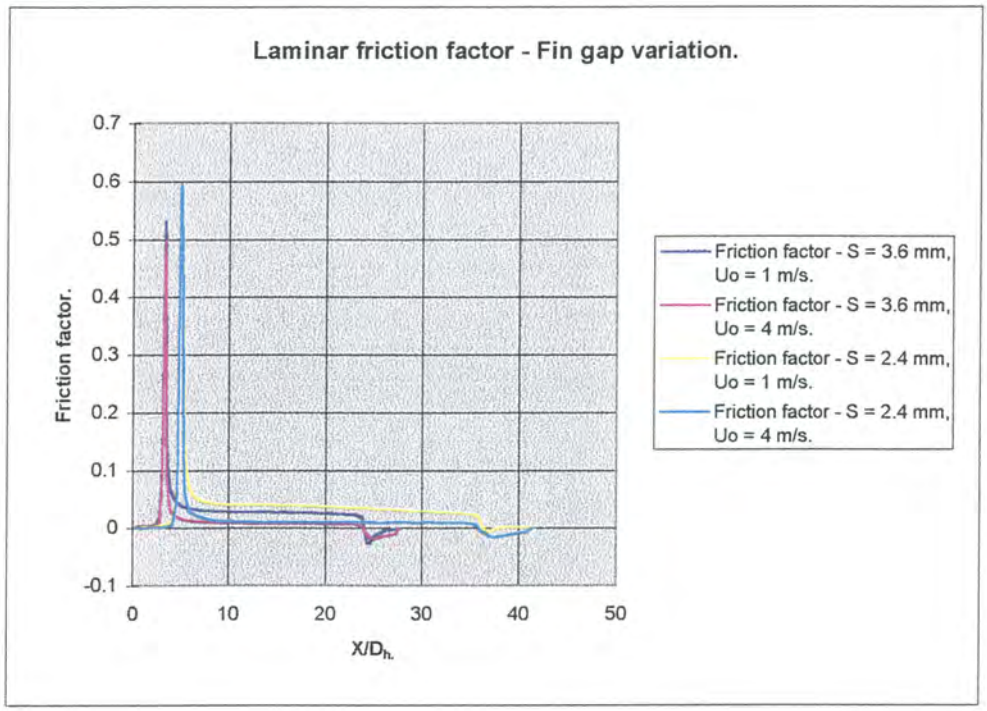

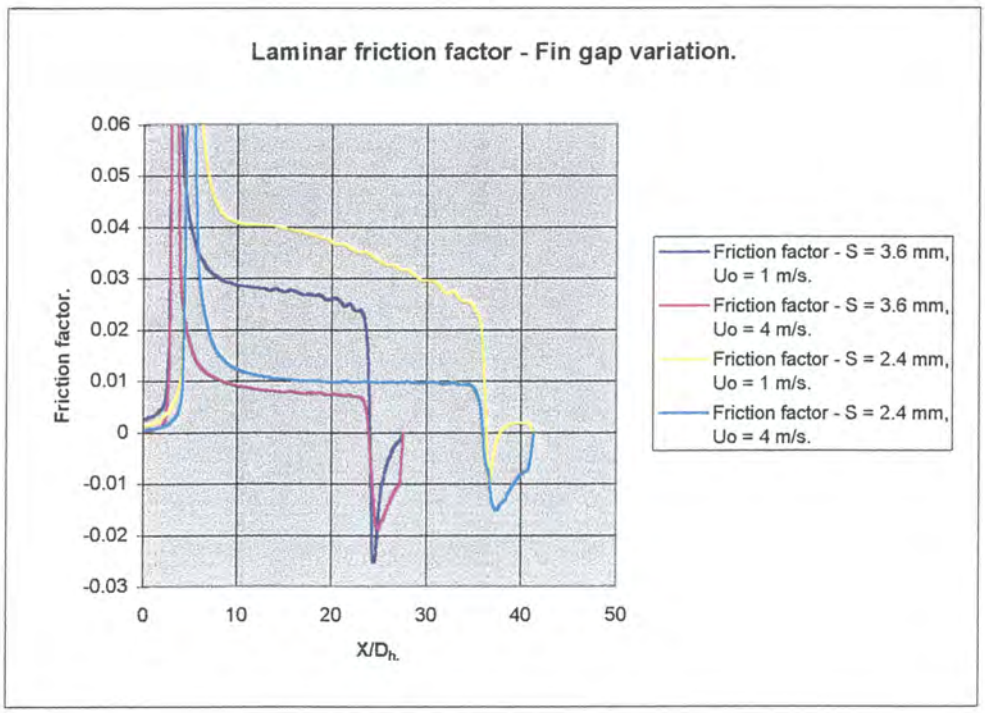

Turbulent flow comparison.

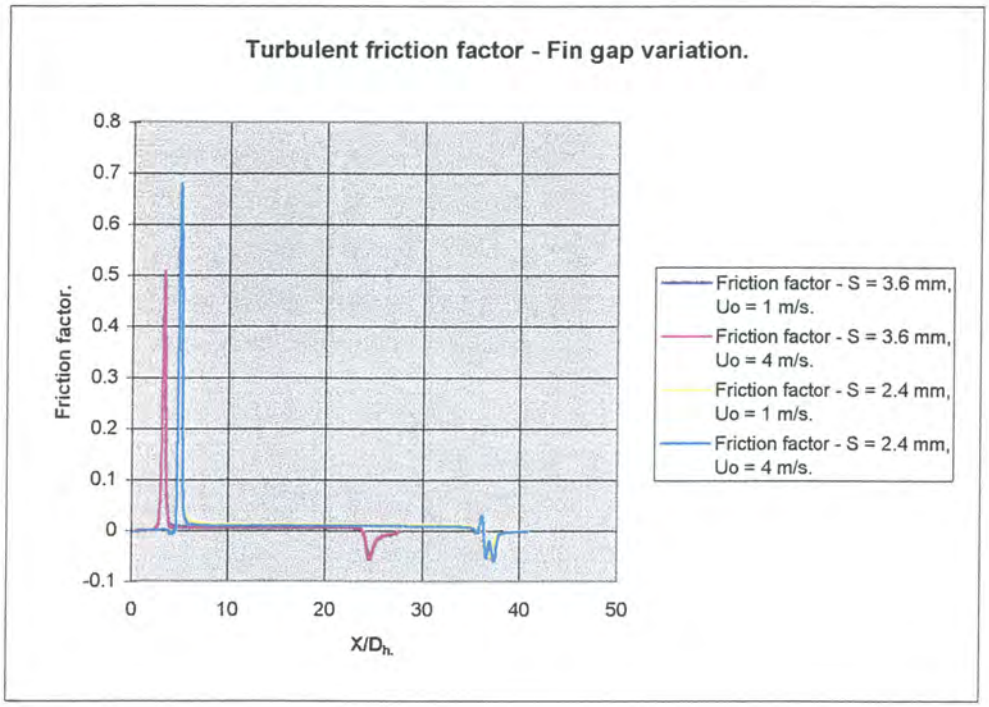

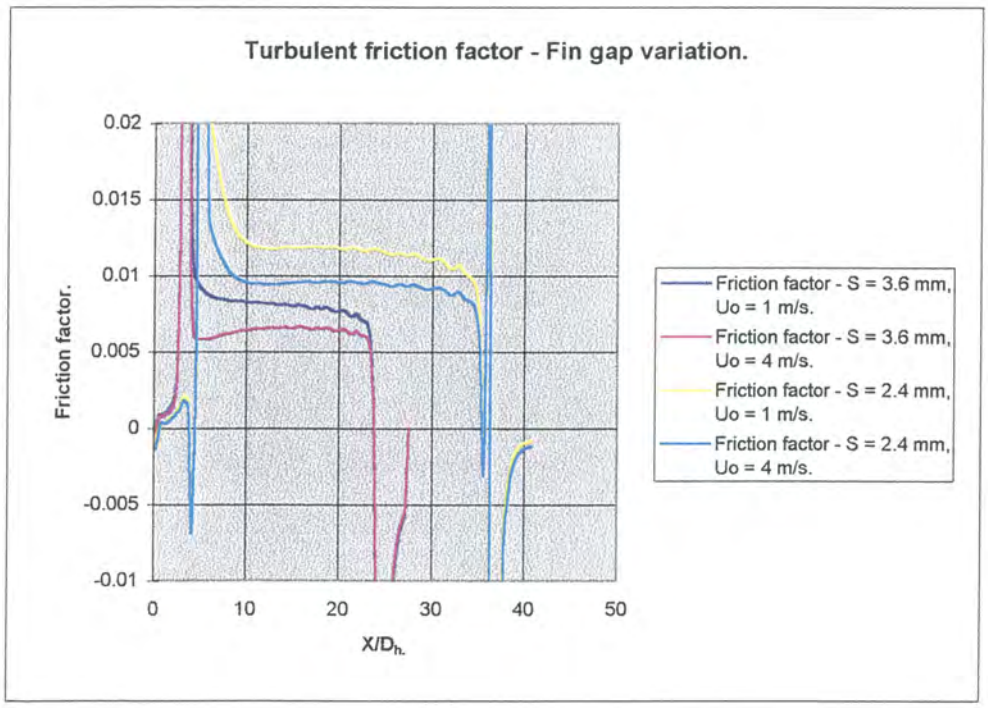

HEAT SINK REYNOLDS NUMBER VARIATION.

Geometric parameters:

Hf = 53 mm
t = 1.27 mm.
s = 2.4 mm.
Hb = 38 mm.
Uo = 1 & 4 m/s - Laminar flow.
Uo = 8 & 12 m/s - Turbulent flow.

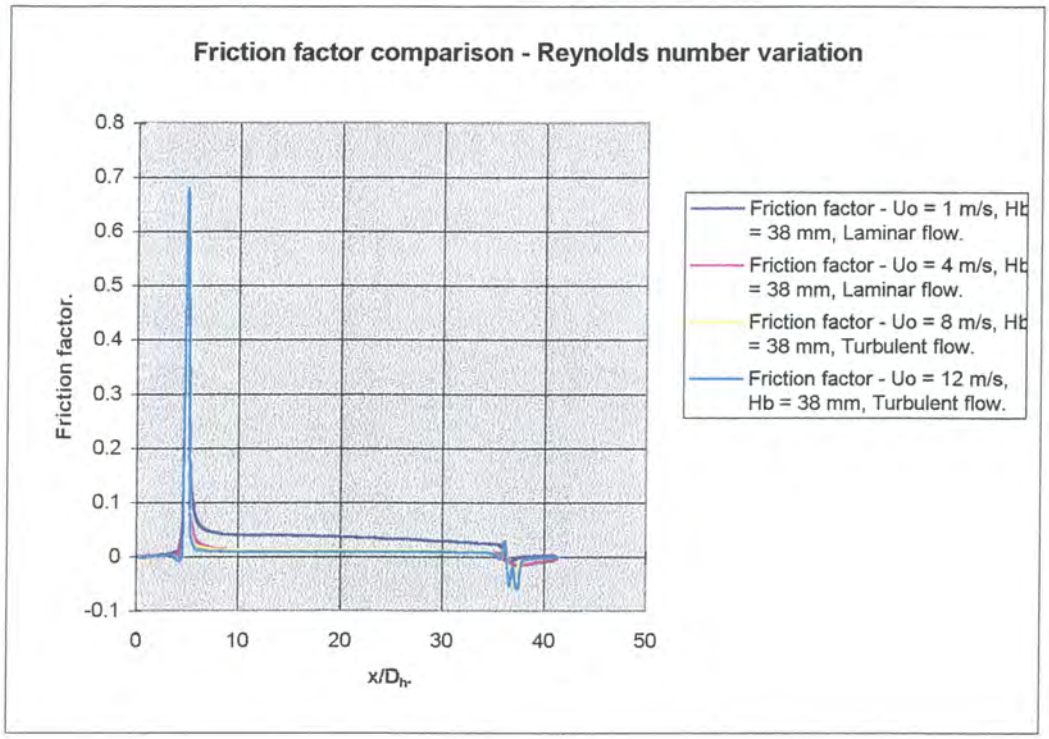

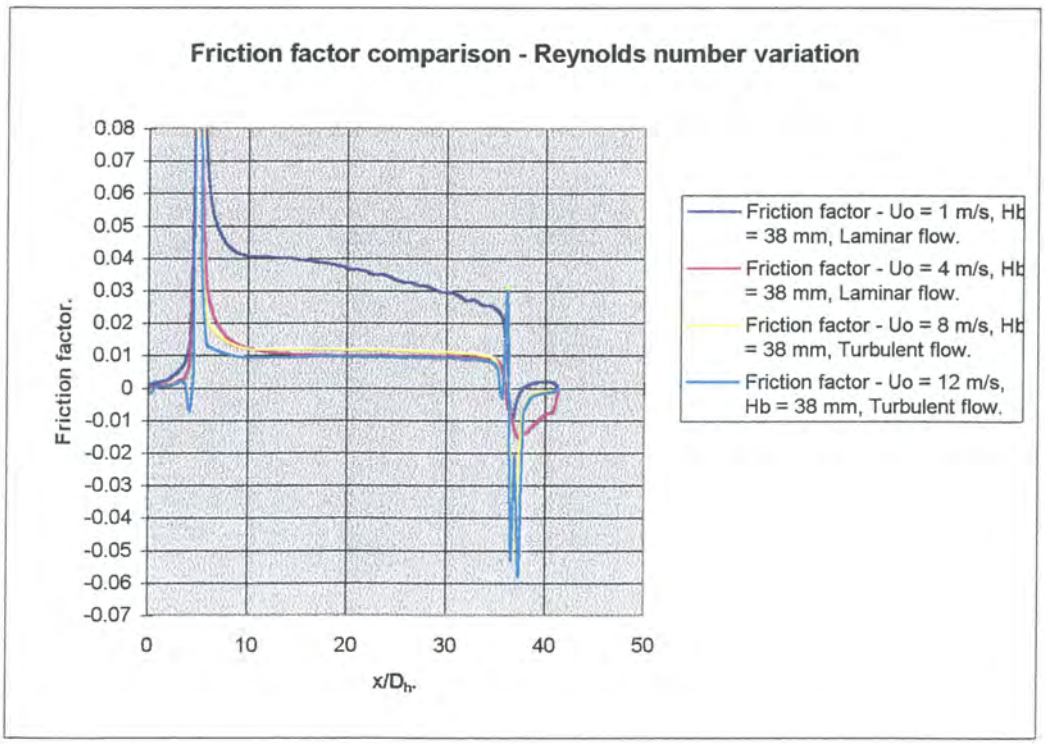

HEAT SINK LENGTH VARIATION.

Geometric parameters:

Hf = 20 mm
t = 5 mm.
s = 5 mm.
Hb = 25 mm.
Uo = 1 m/s - Laminar flow.
Uo = 8 m/s - Turbulent flow.

Laminar flow comparison.

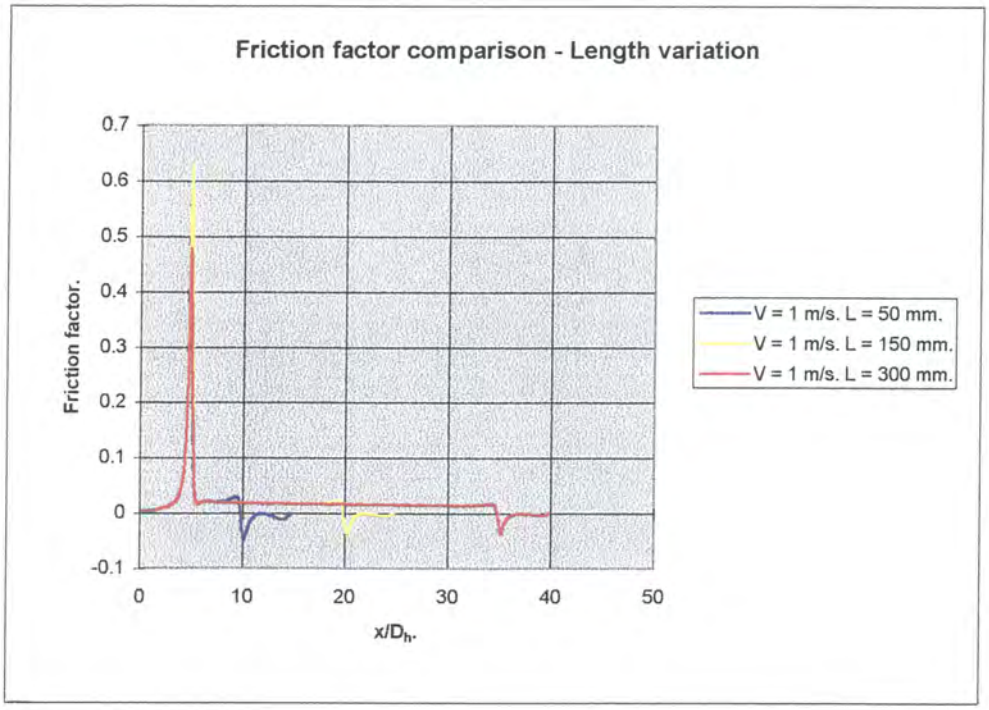

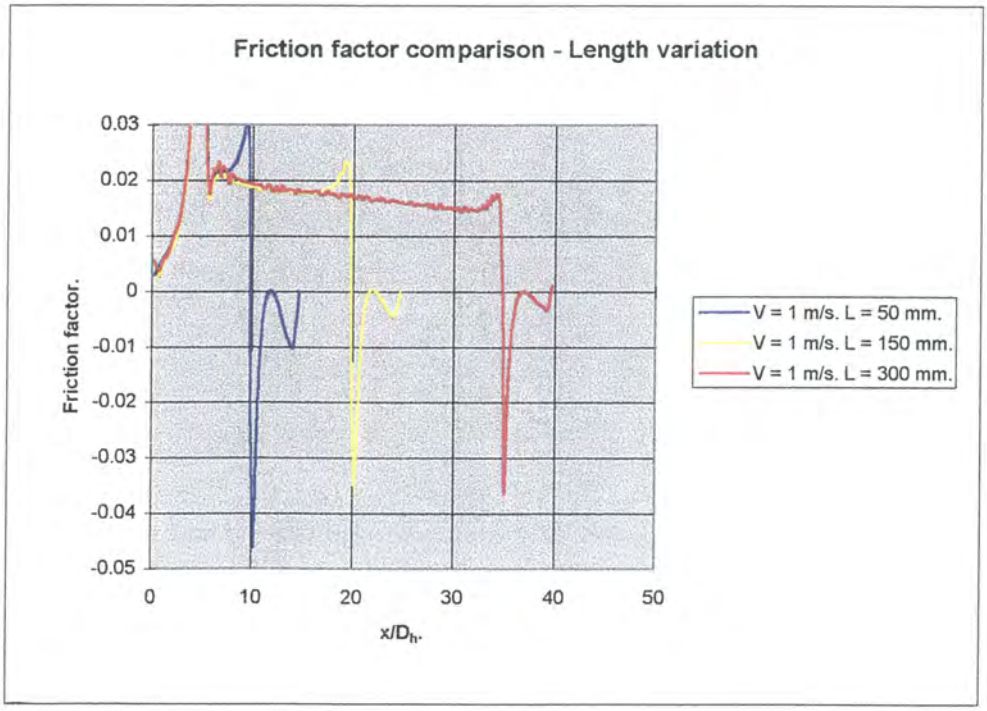

Turbulent flow comparison.

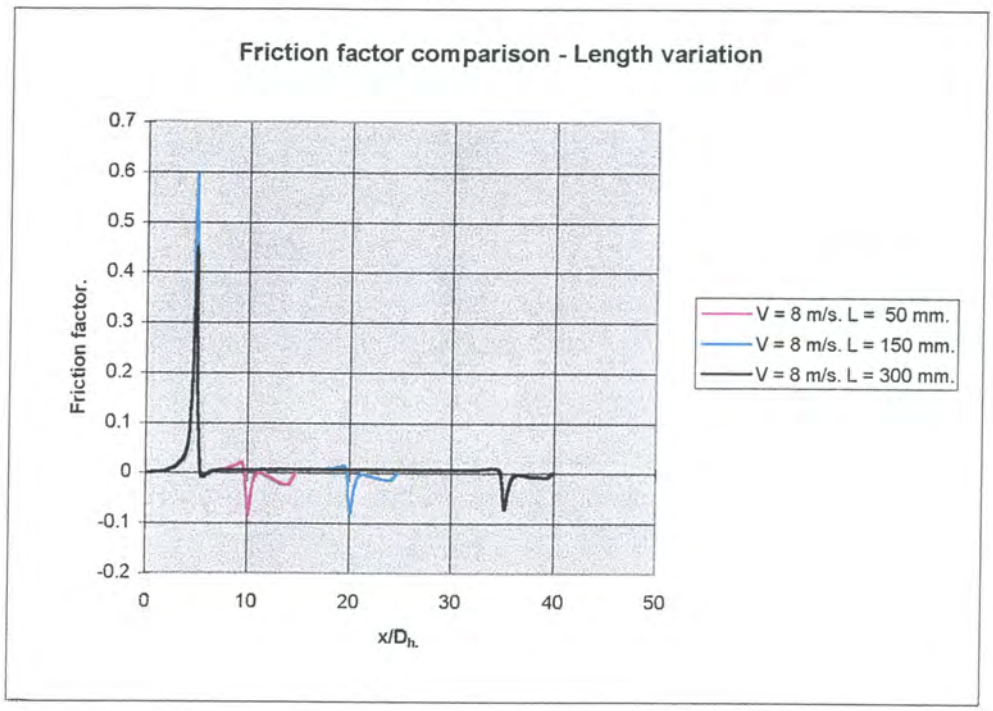

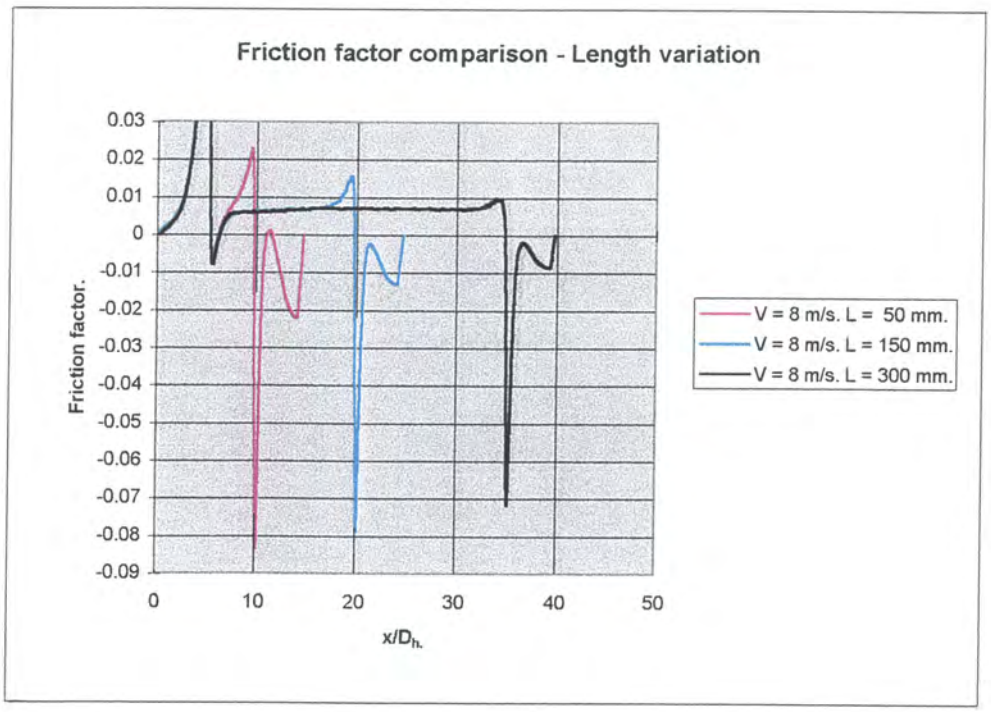

APPENDIX C

TABLED CFD AND COMPACT MODEL RESULTS

TABLED CFD AND COMPACT MODEL RESULTS.

Heat sink 1

Velocity - Uo [m/s]	Predicted pressure loss - CFD ΔP [Pa]	QFIN ΔP [Pa]	Prediction variance - QFIN %	New model ΔP [Pa]	Prediction variance - New model %
1	3.8	3.28	13.68	3.84	1.05
4	24.6	25.2	2.44	28.77	16.95
8	85.4	74.97	12.21	90.99	6.54
12	162.9	148.6	8.78	176.79	8.52
Average variance			9.27		8.26

Heat sink 2.

ocity - Uo [m/s]	Predicted pressure loss - CFD ΔP [Pa]	QFIN ΔP [Pa]	Prediction variance - QFIN %	New model ΔP [Pa]	Prediction variance - New model %
1	1.7	1.04	38.82	1.38	18.30
4	12.9	10.93	15.27	11.95	7.30
8	42.6	34.8	18.31	41.41	2.80
12	94.65	70.2	25.83	89.9	4.97
e variance			24.5		8.34

nk 3.

Velocity - Uo [m/s]	Predicted pressure loss - CFD ΔP [Pa]	QFIN ΔP [Pa]	Prediction variance - QFIN %	New model ΔP [Pa]	Prediction variance - New model %
1	1.86	1.5	19.35	1.91	2.68
4	12.7	12.5	1.57	15.39	21.20
8	43.1	40.3	6.50	50	16.00
12	83.4	81.5	2.28	104.5	25.30
Average variance			7.4		16.2

Heat sink 4.

Velocity - Uo [m/s]	Predicted pressure loss - CFD ΔP [Pa]	QFIN ΔP [Pa]	Prediction variance - QFIN %	New model ΔP [Pa]	Prediction variance - New model %
1	1.32	0.96	27.27	1.44	9.10
4	13.1	9.42	28.09	13.73	4.80
8	44.2	31.96	27.69	47.2	6.70
12	94.6	66.1	30.13	101.2	6.97
Average variance			28.3		6.9

Heat sink 5.

ocity - Uo [m/s]	Predicted pressure loss - CFD ΔP [Pa]	QFIN ΔP [Pa]	Prediction variance - QFIN %	New model ΔP [Pa]	Prediction variance - New model %
1	0.48	0.41	14.58	0.52	8.30
4	4.6	4	13.04	5.81	26.30
8	13.4	13.2	1.49	13.77	2.76
12	24.8	26.8	8.06	27.13	9.40
e variance			9.2		11.67

ink 6.

Velocity - Uo [m/s]	Predicted pressure loss - CFD ΔP [Pa]	QFIN ΔP [Pa]	Prediction variance - QFIN %	New model ΔP [Pa]	Prediction variance - New model %
1	9.7	9.2	5.15	9.56	1.44
4	58.1	50.3	13.43	51.7	11.02
8	209	143.7	31.24	139	33.49
12	394	277	29.70	265	32.74
Average variance			19.9		19.8

APPENDIX D

DETAIL MATLAB PROGRAMMING STRATEGY OF NEW COMPACT MODEL

As mentioned the computer program MATLAB was used for programming purposes throughout the course of the study.

The programming details are provided in the attached software in plain *.m files. In order to operate copy the following files to the MATLAB\BIN directory:

- byp_a.m
- byp_b.m
- byp_main.m

In the MATLAB operating window simply type "byp_main" in order to activate. The program will prompt you for heat sink details, after which it will calculate and display the following variables:

- Heat sink pressure loss.
- Heat sink average interfin velocity.
- Heat sink average tip bypass velocity.
- Plot of predicted heat sink interfin velocity distribution in normalised format..

Due to legal requirements programming details of the program QFIN may not be released, although having been used extensively in the study.